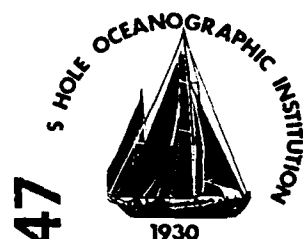WHOI-88-12

Woods Hole Oceanographic Institution
Massachusetts Institute of Technology

Joint Program
in Oceanography
and
Oceanographic Engineering

DOCTORAL DISSERTATION

Exact Reconstruction of Ocean Bottom Velocity Profiles from Monochromatic Scattering Data

by

Andre A. Merab

January 1987

Exact Reconstruction of Ocean Bottom Velocity Profiles from Monochromatic Scattering Data

by

Andre A. Merab

Woods Hole Oceanographic Institution
Woods Hole, Massachusetts 02543

and

The Massachusetts Institute of Technology
Cambridge, Massachusetts 02139

January 1987

Doctoral Dissertation

Approved for Distribution:

Albert J. Williams 3rd, Chairman
Department of Ocean Engineering

Charles D. Hollister
Dean of Graduate Students

EXACT RECONSTRUCTION OF OCEAN BOTTOM VELOCITY PROFILES FROM MONOCHROMATIC SCATTERING DATA

by

ANDRE A. MERAB
S.M., Massachusetts Institute of Technology, 1979

SUBMITTED IN PARTIAL FULFILLMENT OF THE REQUIREMENTS
FOR THE DEGREE OF DOCTOR OF SCIENCE

at the

MASSACHUSETTS INSTITUTE OF TECHNOLOGY
and the
WOODS HOLE OCEANOGRAPHIC INSTITUTION

January 1987
©Andre A. Merab, 1987

Signature of Author _____
Department of Electrical Engineering, Massachusetts
Institute of Technology and the Joint Program in
Oceanography/Ocean Engineering, Massachusetts
Institute of Technology/Woods Hole Oceanographic
Institution.

Certified by _____
George V. Frisk, Thesis Supervisor

Accepted by _____
George V. Frisk, Chairman, MIT/WHOI Joint Committee
for Oceanographic Engineering

Exact Reconstruction of Ocean Bottom Velocity Profiles
from Monochromatic Scattering Data

Andre A. Merab

Submitted in partial fulfillment of the requirements
for the Degree of Doctor of Science

at the

MASSACHUSETTS INSTITUTE OF TECHNOLOGY
and the
WOODS HOLE OCEANOGRAPHIC INSTITUTION

January 1987

ABSTRACT

This thesis presents the theoretical and computational
underpinnings of a novel approach to the determination of the
acoustic parameters of the ocean bottom using a monochromatic
source. The problem is shown to be equivalent to that of the
reconstruction of the potential in a Schrödinger equation
from the knowledge of the plane-wave reflection coefficient
as a function of vertical wavenumber, $r(k_z)$ for all real
positive k_z. First, the reflection coefficient is shown to
decay asymptotically at least as fast as $(1/k_z^2)$ for large k_z
and is therefore integrable. The Gelfand-Levitan inversion
procedure is extended to include the case of basement
velocity higher than the velocity of sound in water. The
neglect of bound states is shown to be justified in both
clayey silt and silty clay at the 220 Hz frequency of
operation.

Three methods for the numerical solution of the integral
equation are investigated. The first one is an "Improved
Born approximation" wherein the solution is given as a series
expansion the first term of which is the Born approximation
while the second term represents a substantial and yet easy
to implement improvement over Born.

The two other methods are based on a discretization of
the Gelfand-Levitan integral equation, and both avoid a
matrix inversion: one by employing a recursive procedure,
and the other by coupling the Gelfand-Levitan equation with a
partial differential equation. Bounds are obtained on errors
in the solution due either to discretization or to data inac-
curacy. These methods are tested on synthetic data obtained
from known geoacoustic models of the ocean bottom. Results

are found to be very accurate particularly at the top of the sediment layer with resolution of less than the wavelength of the acoustic source in the water. Several effects are investigated, such as sampling, attenuation, and noise. Also examined is the gradual restriction of the reflection coefficient to a finite range of vertical wavenumbers and the consequent progressive deterioration of the reconstruction.

The analysis shows how to reconstruct velocity profiles in the presence of density variation when the experiment is conducted at two frequencies.

Our results provide a good understanding of the issues involved in conducting a monochromatic deep ocean bottom experiment and constitute a promising technique for processing the experimental data when it becomes available.

ACKNOWLEDGEMENTS

TABLE OF CONTENTS

TABLE OF CONTENTS (Concluded)

LIST OF FIGURES

LIST OF TABLES

CHAPTER I

BACKGROUND

> It is a rare person whose pulse is
> not stirred by the dramatic sight of
> the restless surface of the sea.
> The chaotic sea surface is a
> limitless source of inspiration to
> poet, painter and musician alike.
> But what lies beneath this churning
> surface? How can we probe the
> depths of the sea?
>
> C. Clay & H. Medwin

1.1 Background

The sea floor begins at the water-sediment interface,

overlies the sedimentary layer, and beneath it, the oceanic

crust. The study of the ocean bottom has been, until

recently, the province of the marine geologist seeking to

probe the oceanic crust, and to unravel the secrets of its

structure and evolution. The marine geologist has now been

joined by the underwater acoustician studying the transmis-

sion of low frequency sound through the ocean; It has become

clear in light of underwater sound propagation experiments

carried out at the various Oceanographic Institutions[1] that

long range low frequency sound transmission is affected by

the nature of the ocean bottom, and hence, that acoustic wave

propagation models - to characterize sonar performance, for

instance - should include a detailed representation of the

bottom, the geoacoustic model. In practice, one posits a "reasonable" ocean bottom model, and then one proceeds to solve the propagation problem at hand, (the "Direct" problem). Here, the opposite perspective is adopted: Since the ocean bottom affects acoustic wave propagation, would it not be possible to learn something about the bottom from that interaction? (The "Inverse" problem.)

The answer to this question is being sought in the context of an original, single frequency, deep ocean bottom interaction experiment designed by G. Frisk and his colleagues of the Woods Hole Oceanographic Institution, and performed in the Hatteras Abyssal Plain[2],[3] and at other locations[4]. The monochromatic character of the Frisk method sets it apart from currently used techniques using explosive (or impulse-like) wide-band sources. The Frisk experiment started off as a heuristic approach.

This thesis presents the theoretical basis and numerical analysis of the monochromatic experiment based on an extension of the Gelfand-Levitan theory of quantum scattering. We succeeded in applying a numerical solution to the exact inverse method which distinguishes this solution method from the currently used approximate or trial and error inverse methods.

1.2 The Experiment

The geometry of the experiment is best explained with reference to Fig. 1. In brief, a drifting vessel tows a 220 Hz pulsed CW source. Hydrophones moored close to the bottom record the resulting pressure, both amplitude and phase (via coherent quadrature demodulation), as the ship opens range.

The pulsing of the 220 Hz source, turning it on for 4 sec every 14 sec, allows for steady state conditions to be attained before any reflections from the ocean surface can reach the receivers. Note that a 14 second duty cycle signifies that the acoustic field is sampled spatially once every half wavelength.

The source aperture is small enough compared to the wavelength (7 m) to be considered an omnidirectional point source. The recorded complex pressure is therefore the field due to the reflections of a spherical wave off the bottom. The information is translated via a Hankel transform, into the plane wave reflection coefficient at a single frequency (220 Hz) for all angles of incidence, both real and complex[5]. The critical point to observe is that for a monochromatic plane wave incident on a flat layered bottom, the reflection coefficient is a function of the angle of incidence. At a given angle of incidence, the magnitude and phase of the reflection coefficient depend on the acoustic
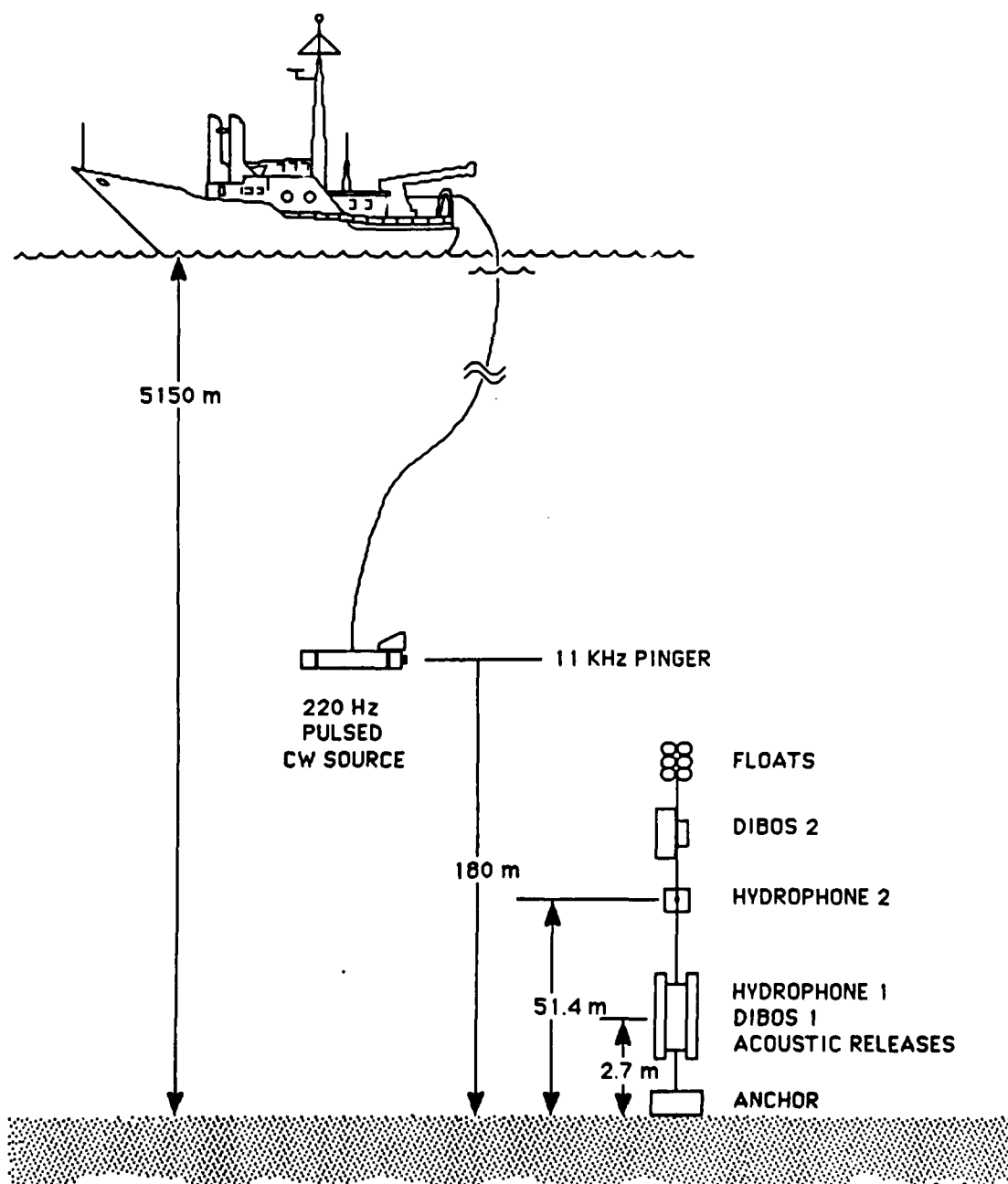
Fig. 1 Experimental Configuration (after Frisk et al.[2])

Labels in figure:
5150 m
220 Hz PULSED CW SOURCE
11 KHz PINGER
FLOATS
DIBOS 2
HYDROPHONE 2
180 m
HYDROPHONE 1
DIBOS 1
ACOUSTIC RELEASES
51.4 m
2.7 m
ANCHOR

properties of the bottom sediments. That naturally leads to the ocean bottom inverse problem: Can the sediment acoustic parameters, velocity and density, be reconstructed from the plane wave reflection data at a single frequency for all angles of incidence? The thesis aims to elucidate that questions.

1.3 Experimental Data

The relationship between the experimental data and the plane wave reflection coefficient has been studied numerically by Frisk et al[3] and Mook[6]. Before beginning our analysis, it is useful here to take a quick look at the underlying theory relating the reflections of spherical waves from a point source, as in the Frisk experiment, to the plane wave reflection as in our model.

The measurements yield the pressure field due to a point source above the bottom half space. Because of the cylindrical symmetry of the problem, the reflected pressure field can be written as a superposition of plane waves

$$P_R(r,z) = \int_0^\infty \frac{1}{\sqrt{k_0^2 - k_r^2}} \Gamma(k_r) e^{i\sqrt{k_0^2 - k_r^2}(z+z_0)} J_0(k_r r) k_r dk_r$$

(1.1)

where k_r is the horizontal wavenumber, and $\Gamma(k_r)$ is the corresponding reflection coefficient.

-11-

This Sommerfeld integral is a Hankel transform which can be inverted to obtain the reflection coefficient

$$\Gamma(k_r) = -i\sqrt{k_0^2 - k_r^2} \; e^{-i\sqrt{k_0^2 - k_r^2}|z+z_0|} \int_0^{\infty} P_R(r)J_0(k_r r)dr$$

(1.2)

Note that $\Gamma(k_r)$ is a function of horizontal wavenumber while the required input to the inverse procedure is the reflection coefficient as a function of the vertical wavenumber $r(k_z)$. The two are of course related by the dispersion relation

$$k_z^2 = k_0^2 - k_r^2$$

(1.3)

Given $\Gamma(kr)$ for real k_r, one can readily generate $r(k_z)$ for $0 < k_z < k_0$. It is more difficult to obtain $r(k_z)$ for the full range $0 < k_z < \infty$ since $k_0 < k_z < \infty$ correspond to $\Gamma(k_r)$ for imaginary k_r. One approach has been suggested by Stickler[7] and involves the use of a theorem by Van Winter to generate $r(k_z)$ on a ray in the complex plane given its value on the real axis segment $0 < k_z < k_0$. The effect of limiting $r(k_z)$ to real angles $(0 < k_z < k_0)$ on the inversion for the unknown potential $V(z)$ will be discussed in Chapter VI.

1.4 The Model

A number of assumptions are implicit in the "exact" inverse procedure detailed in the following chapters.

(a) The ocean is assumed homogeneous, and acoustically transparent. In particular, the depth variation of the velocity of sound propagation is neglected. That is a reasonable assumption at the great depth (5 km) in which the experiment is conducted.

(b) The ocean bottom is assumed to have no horizontal structure, the velocity variation is therefore solely a function of depth. That is a severe restriction imposed by all "exact" inversion formalisms developed to date. Surprisingly, horizontal stratification describes adequately vast areas of the deep ocean floor known as Abyssal plains: These are widespread in the Atlantic and Indian Oceans and in the marginal seas.

The early deep ocean bottom interaction experiments were conducted in the Hatteras Abyssal Plain. This nearly level plain lies at the base of the East Coast Continental rise, and is 1000 km long by 150-300 km wide. Its thick (> 1 km) sediments were formed by the smooth accumulation of turbidites over the rough basement resulting in one of the flattest areas on earth with slopes of less than 1 m/km.

(c) The ocean bottom has been traditionally treated as a fluid in problems involving bottom reflection. In the deep ocean bottom interaction experiments, the acoustic source generates compressional (P) waves in the water, which upon propagation in the bottom, a vertically heterogeneous medium, may be converted to shear (SV) waves. The conversion to shear waves will occur discretely at layer interfaces and continuously, where velocity gradients occur. Fryer had shown in one of his papers[8] that coupling for continuously varying elastic parameters is negligible at frequencies above 20 Hz. Vidmar and Foreman[9] estimated that gradient-induced coupling should be expected in marine sediment at frequencies up to 3 Hz. Another paper by Fryer[10] established that this coupling is extremely small above 1 Hz, regardless of sediment thickness. The most important effect of coupling appears to be the conversion of shear to compressional motion at the sediment basement interface. Note, that although these results are based on a continuously varying structure (approximated by homogeneous layers), they do provide for the sharp discontinuity in elastic parameters at the sediment basement interface. These results do justify the neglect of shear wave effects at the 220 Hz frequency selected for the experiments that have already been conducted, and at the lower frequencies envisaged by the Frisk group for future experiments.

1.5 Overview of the Thesis

In Chapter II, we begin with a mathematical statement of the inverse problem and represent it as a scattering problem for the Schrödinger equation. We conclude the chapter with a review of the relevant literature.

The input to the inverse procedure, the plane-wave reflection coefficient, and particularly its asymptotic behavior for large vertical wavenumbers are the subject of Chapter III.

Chapter IV presents an extension of the Gelfand-Levitan inversion method to the case of non-zero terminal potential. It is this formulation that permits us an exact solution of the inverse problem so that what remains is the numerical solution of the integral equation characterizing the solution.

The derivation presented in Chapter IV is followed in Chapter V by a discussion of three numerical methods to solve the Gelfand-Levitan integral equation: An improved Born approximation and two finite-difference methods.

The numerical methods outlined in Chapter V were tested on various postulated acoustic profiles using synthetically generated reflection coefficients. The representative numerical results, the impact of sampling, finite angle aperture, density, loss and noise are discussed in Chapter VI.

Chapter VII comprises the conclusion and suggestions for future work.

CHAPTER II

PROBLEM FORMULATION AND REVIEW OF PAST WORK

The determination of the acoustic properties of the ocean bottom from the monochromatic plane wave reflection coefficient at all angles of incidence is now shown to be related to a class of inverse problems in quantum scattering theory where an unknown potential in Schrödinger's equation is sought from scattering data. The first part of the chapter casts the problem into mathematical form based on the assumptions set forth in Chapter I. This is followed by a review of the relevant inverse problem literature.

2.1 Problem Formulation

(a) Acoustic Wave Equation

In acoustics, the pressure gradient gives rise to an acceleration of mass density ρ according to

$$\rho \frac{\partial \vec{v}}{\partial t} = - \nabla p \tag{2.1}$$

where p is acoustic pressure and $\vec{v}$ is particle velocity. Mass conservation, together with a constitutive relation (Hooke's law), yields:

$$\frac{\partial p}{\partial t} = - \rho c^2 \nabla \cdot \vec{v} \tag{2.2}$$

in which c is sound velocity in the medium.

Fourier transforming the time dependence in the funda-
mental equations (2.1) and (2.2), $[\frac{\partial \omega}{\partial t} \rightarrow -i\omega]$, and
combining the resulting time-independent equations leads to
the acoustic wave equation:

$$\rho(z)\nabla \cdot \left(\frac{1}{\rho(z)} \nabla p(x,z)\right) + k_o^2 n^2(z)\, p(x,z) = 0 \qquad (2.3)$$

with $k_o = \frac{\omega}{c_o}$ and index of refraction $n(z) = \frac{c_o}{c(z)}$. In the
derivation of equation (2.3), the acoustic medium has been
assumed to be vertically inhomogeneous (or horizontally
stratified). In other words, the material properties are a
function of depth (z) only.

The neglect of density variations reduces equation (2.3)
to the Helmholtz equation for the pressure,

$$\nabla^2 p(x,z) + k_o^2 n^2(z)\, p(x,z) = 0 . \qquad (2.4)$$

The equation (2.4) constitutes the starting point of this
study.

Note: In the presence of smooth density variations, the
acoustic equation (2.3) can also be reduced to the
Helmholtz equation through the change of variable[11]

-17-

$$P = p/\sqrt{\rho} \ . \qquad \text{It follows that,}$$

$$\nabla^2 P + k_o^2 n'^2 (z) P = 0 \qquad\qquad (2.5)$$

with

$$n'^2 = n^2 + k_o^{-2} \left(\frac{1}{2\rho} \nabla^2 \rho - \frac{3}{4} \left(\frac{1}{\rho} \nabla \rho \right)^2 \right) \ .$$

(b) <u>Mapping the Seabed Below a Homogeneous Ocean</u>

The specific problem of interest is mapping the seabed below a homogenous ocean. The starting point is again the acoustic wave equation (2.4):

$$\nabla^2 p(x,z) + k_o^2 n^2(z) \ p(x,z) = 0 \qquad\qquad (2.6)$$

for the configuration shown in Fig. 2. Let

$$n^2(z) = 1 + \mu^2(z) \ .$$

Since the medium is homogeneous in x, the spatial variables can be separated by assuming that:

$$p(x,z,k) = u(z,k) \ e^{i(k_o \sin\theta)x} \qquad\qquad (2.7)$$

Note that $k_o \sin\theta \equiv k_x$, the horizontal wavenumber (cf. Fig. 3).

c_0

$\mathbf{l}$ θ $r(\theta)$

x

$c(z)$

c_1

$k = \dfrac{\omega}{c_0} \; ; \;$ water wavenumber $\quad z \quad t$
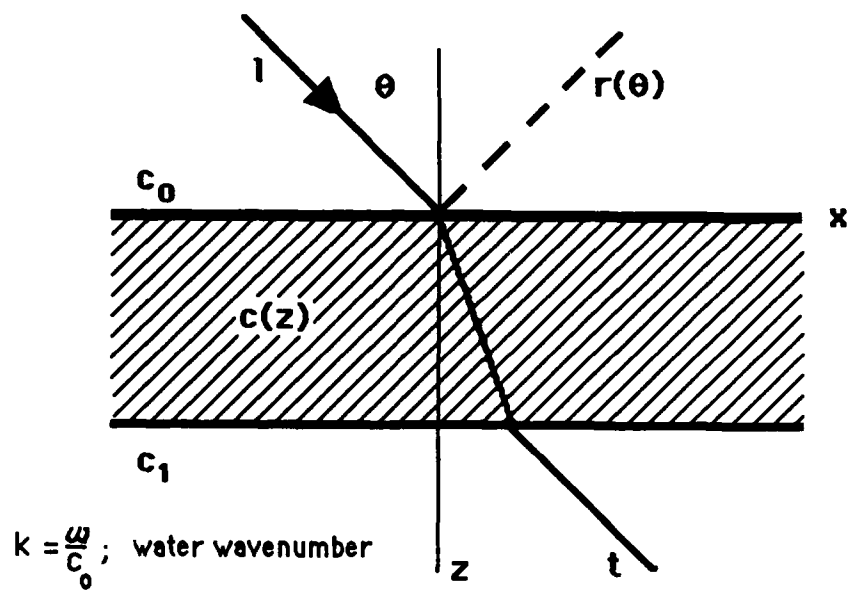
Fig. 2 Schematic Illustration of the Scattering Problem
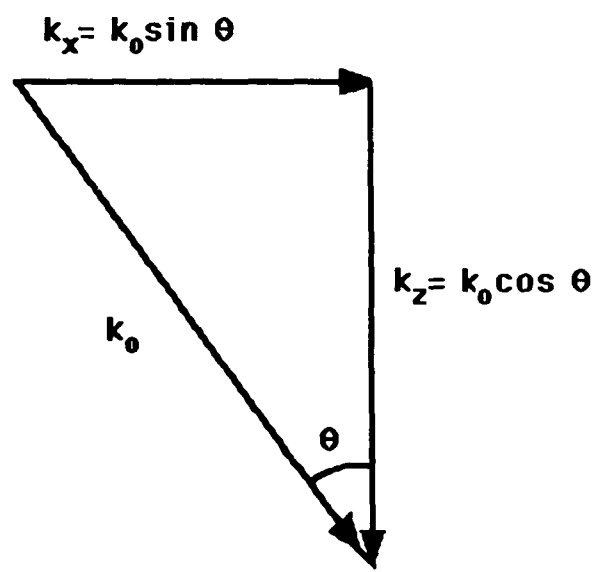
Fig. 3 Wavenumber Decomposition

Substituting from (2.7) for $p(x,z)$ into wave equation (2.6), one obtains an equation for the z variation of pressure, $u(z)$:

$$[\frac{d^2}{dz^2} + (k_o^2 - k_o^2 \sin^2\theta) + k_o^2 \mu^2(z)]u = 0 \qquad (2.8)$$

or

$$\frac{d^2u}{dz^2} + [k_o^2 \cos^2\theta + k_o^2 \mu^2(z)]u = 0 \qquad (2.9)$$

this is similar to the time-independent Schrödinger equation. Equation (2.9) can be written in the familiar form:

$$\frac{d^2u}{dz^2}(z,E) + [E - V(z)]\ u(z,E) = 0 \qquad (2.10)$$

with the identifications:

k_z $= k_o\cos\theta$, the vertical wavenumber is "momentum".

E $= k_o^2\cos^2\theta$ is the "energy".

$V(z)$ $= k_o^2\mu^2(z)$ is the "potential".

A few remarks are in order:

- The vertical wavenumber, k_z, becomes imaginary for $k_x > k_o$.

-21-

- As k_z ranges on $[k_o, \infty]$, k_x becomes pure imaginary.

- The energy $E = k_o^2 \cos^2 \theta$ is always real. For k_z real, E is positive.

- The potential $V(z) = k_o^2(1 - n^2(z))$ is in general positive except, possibly, for a low velocity layer at the ocean bottom interface.

By analogy with quantum mechanics, one can draw a "potential well" diagram (cf. Fig. 4).

The Schrödinger equation (eq. 2.10) has associated with it two asymptotic boundary conditions:

$$u(z) \sim \frac{e^{ik_z z}}{\sqrt{2\pi}} + r(p)\frac{e^{-ik_z z}}{\sqrt{2\pi}} \qquad z \to -\infty$$

$$(2.11)$$

$$u(z) \sim t(p)\frac{e^{ik_z z}}{\sqrt{2\pi}} \qquad z \to \infty$$

where $r(k_z)$ and $t(k_z)$ are identified as reflection and transmission coefficients respectively.

The problem that was proposed in the introduction has now been cast into an equivalent quantum mechanical problem:

-22-
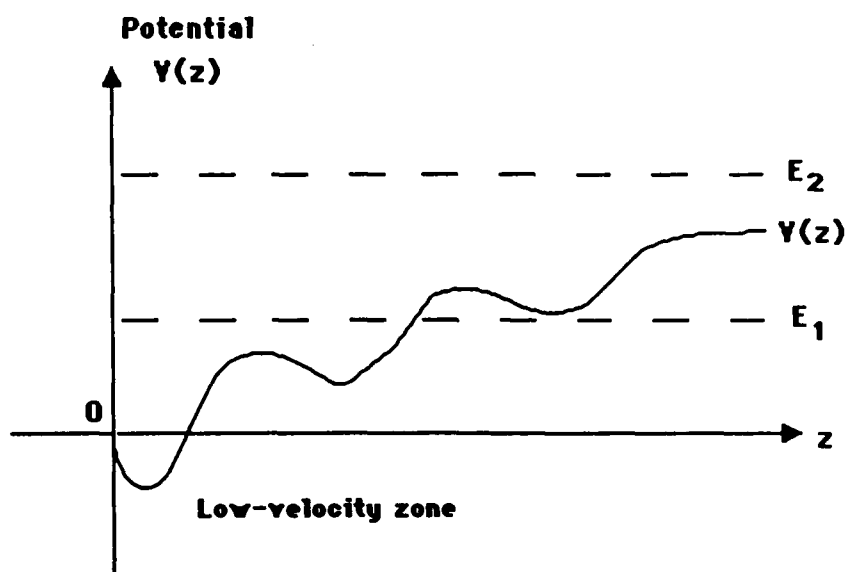
Fig.4 Scattering Potential- Energy Diagram
(E_1, E_2 represent possible Energy levels)

Given $r(k_z)$, the reflection coefficient, as a function of vertical wavenumber k_z, obtain the scattering potential $V(z)$ in equation (2.10).

2.2 Survey of Inverse Methods

2.2.1 Introduction

Much of the background methodology relevant to our problem is found in the geophysical literature. An excellent review of the field is provided by Newton[12,13].

The seismic inverse problem for horizontal layered media of infinite depth consists in determining the vertical structure of the acoustic medium (specified usually by impedance, or, in more detail, by density and velocity) from reflection measurements. But for a few exceptions, most of the previous analyses have been confined to excitation with an impulsive pressure signal (δ-function) and probing at normal incidence. The Fourier transform of a δ-function is essentially flat in frequency domain. What is observed with such an excitation is, therefore, the time trace of the resulting medium response or its Fourier transform. Because of the assumed horizontally layered structure of the medium, and the vertical direction of the signal, acoustic properties of the medium change only with depth and thus the problem is one-dimensional.

In what follows, we present a review of that past inverse problem work that is relevant in several different respects. First, the discussion of the Gelfand-Levitan approach is particularly relevant because this is our basic approach in this thesis adapted to the Frisk experiment.

Next, the discussion of prior work on single frequency excitation, launched at non-normal incidence presents the state of the problem before we addressed it.

The Deift and Trubowitz method is described because Stickler, having been briefed on our work, adapted the Deift and Trubowitz method to the Frisk experiment and was able to devise an alternate approach to its analysis.

The discussion of the Schur algorithm reviews the analysis by Yaqle and Levy of probing with an impulsive excitation also at non-normal incidence. We comment on why Yaqle and Levy dismissed the Gelfand-Levitan approach as inferior to the Schur algorithm although we have in fact, successfully adapted Gelfand-Levitan to the solution of the monochromatic, non-normal incidence problem.

The Riccati equation method is discussed although it was not used. We considered this approach and believe it to be promising, but this method was not fully explored.

2.2.2 The Gelfand-Levitan Approach

The problem that was proposed at the end of Section (2.1), the reconstruction of the potential of a Schrödinger equation from the reflection coefficient, is related to a classic problem of quantum scattering theory: How to reconstruct a Sturm-Liouville differential equation from its spectral function. The problem was solved in a celebrated paper by Gelfand and Levitan [14] who, since they were discussing the radial wave equation, were interested only in a solution on the half-line $0 < r < \infty$ (standing-wave problem). Subsequent developments (e.g., (15)) led to formulations on the full line $-\infty < z < \infty$ in terms of such readily measured quantities as the phase shift or reflection coefficient (traveling-wave problem). An excellent distillation of these ideas is to be found in the papers of Faddeyev [16], while a more general survey of the field of inverse scattering has been carried out more recently by Chadan and Sabatier [17]. The interrelation between the different approaches and their time-domain interpretation has been presented by Burridge [8]. A detailed theoretical presentation and extension of the Gelfand-Levitan theory and its application to our problem will be taken up in Chapter IV.

The exploitation of the Gelfand-Levitan formalism outside of quantum mechanics was first taken up by Kay [19] and Moses and deRidder [20] to solve problems in electromagnetics

-26-

such as the characterization of transmission lines and dielectrics from scattering data. The possibility of mono-chromatic probing is mentioned briefly but not pursued. An interesting by-product of this research is the theoretical construction of dielectrics which are reflectionless at all frequencies.

The Gelfand-Levitan approach was introduced into the field of seismic exploration by Ware and Aki[21]. They presented an analytic approach to the inverse scattering problem for elastic wave propagation in a stratified medium when the medium is probed with impulsive plane waves at normal incidence. The analytic solution was obtained by transforming the equation of motion in a stratified elastic medium for plane waves at normal incidence into a one-dimensional Schrödinger equation. The potential of the resulting Schrödinger equation depends only on the impedance of the medium as a function of travel time. No ambiguity arises owing to the bound state solutions of the Schrödinger equation. Ware and Aki went on to establish a discrete analogy of the continuous solution showing again that the impedance of the medium could be recovered as a result of probing at normal incidence when the medium consists of a homogeneous half-space of impedance $\rho_0 c_0$ in contact with a sequence of n homogeneous layers of impedance $\rho_1 c_1, \rho_2 c_2, \ldots, \rho_n c_n$ and terminates with a homogeneous half-space of impedance $\rho_{n+1} c_{n+1}$. The sequence of n homogeneous layers which have

thickness Δn_i and which are chosen such that travel time through each layer is a constant,

$$\Delta n_i / c_i = \Delta t = constant$$

constitutes what is known as a Goupillaud layered medium.

An elegant solution of the inversion of a Goupillaud medium has been given by Claerbout[22] using z-transforms. Ware and Aki showed the equivalence of the Goupillaud solution and of the discretized version of their continuous solution. They had promised a second paper dealing with the inverse scattering problem for plane waves at non-normal incidence. Such a paper was, however, never published. Although Ware had obtained in his thesis some partial results at non-normal incidence prior to the publication of the Ware and Aki paper, the approach in the thesis was too cumbersome and in fact had hit an unsurmountable wall at and above the critical angle: the reflection coefficient tends to one as $\omega \to \infty$ and therefore fails to meet an integrability criterion required in the application of the Gelfand-Levitan algorithm.

The question arises as to how our approach, a monochromatic experiment at all angles of incidence, relates to the Ware and Aki experiment of an impulsive broadband source at one angle of incidence? The vertical wavenumbers generated in Ware and Aki (normal incidence) $k_z = \frac{\omega}{c_o}$ (for $0 < \omega < \infty$). Cover the range from 0 to ∞ as the frequency is swept. One

can see from Fig. 5 that in our experiment $k_z = k_0\cos\theta$ (for $0 < \cos\theta < \infty$) formally covers the same range of values of k_z although the experiment is monochromatic. There is, however, a fundamental difference between the two approaches in that, as we prove in Chapter III, the reflection response in our monochromatic experiment is integrable and in fact goes to zero as k_z goes to infinity at least as fast as $(1/k_z^2)$. It should be noted that Ware and Aki did not run any computer simulations of their algorithm, and were therefore unaware of its numerical performance (in fact, the Gelfand-Levitan approach was widely held at the time to be numerically unstable).

Inspired by the Ware and Aki approach, a number of researchers particularly Ahn, Jordan, and Kritikos[23,24,25] applied the Gelfand-Levitan algorithm to the analytical problem of the reconstruction of dielectric functions and electron density profiles. Their work is an analytical attempt to solve the problem when a dielectric medium is probed with impulses at normal incidence. Most of their effort was applied to the closed-form solution of the Gelfand-Levitan equation. Such a solution is possible when the reflection coefficient can be represented as a rational function of wavenumber. Although the approximation of the reflection coefficient by rational functions has not yet received any practical application, the availability of such closed-form solutions provided us with valuable canonical examples against which to check numerical inversion results.
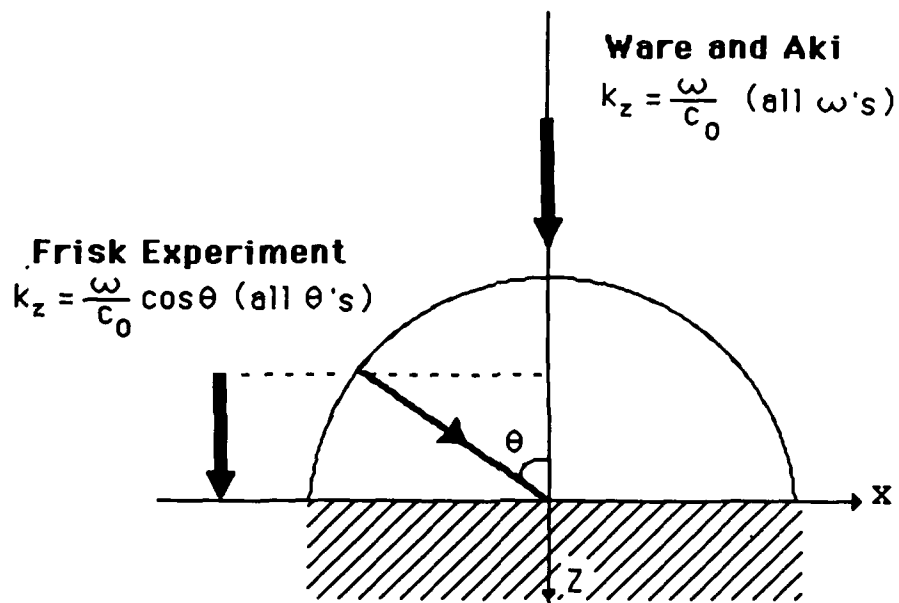
Fig. 5 Generation of Vertical Wavenumbers in the Ware and Aki Method and in the Frisk Experiment

More recently, Berryman and Greene[26] have addressed some long-standing questions regarding the general applicability of the Goupillaud method. They demonstrated the equivalence of the Goupillaud method of inversion and of the Marchenko method[15] for the Schrödinger equation for models with arbitrary layer thicknesses (i.e., continuous impedance variation). When the reflection coefficients are correctly interpreted, in the continuum limit, both methods will reconstruct the same impedance except, possibly, for the values at a finite number of jump points in any finite span of travel time. As part of this work, Berryman and Greene presented a fast $(O(N^2))$ recursive algorithm analogous to the Levinson procedure for the inversion of a Toeplitz matrix. We were able to adapt this algorithm and use it in our numerical computations.

During our research, we became aware of an unpublished report by Jacobs and Stolt[27] which demonstrates four different coordinate transformations which convert the laterally homogeneous acoustic wave equation of the Schrödinger form. One of the transformations takes frequency ω to be a fixed parameter which infers our monochromatic condition. However, Jacobs and Stolt use a slightly different potential function than the one chosen in this thesis. Their effort to verify the Gelfand-Levitan algorithm is similar to the one presented earlier by Moses and deRidder[20]. In discussing the Gelfand-Levitan algorithm,

they make the important assertion that the algorithm holds even for the case of dissimilar end potentials. We have presented, independently, a rigorous proof of that assertion in Chapter IV.

The method of Carroll and Santosa[28] was used by Santosa[29] to solve the inverse problem for an impulsive source at normal incidence. Although the method is similar to the Gelfand-Levitan approach, it is not based on the Schrödinger equation but rather on the equation

$$\hat{v}'' + \omega^2 \hat{v} = q(y)\hat{v}' \qquad (2.12)$$

where $\hat{v}$ is the Fourier transform of the shear displacement and $q(y)$ is related to the change in the impedance $A(y)$ by

$$q(y) = - \frac{A'(y)}{A(y)} \quad . \qquad (2.13)$$

The measured response $q(t) = \delta(t, x = 0)$ is transformed into the spectral density $G(\omega)$

$$G(\omega) = \frac{-2\omega}{\pi} \int_0^\infty q(t)\exp(i\omega t)dt \quad . \qquad (2.14)$$

The Gelfand-Levitan type equation that is to be solved is then

$$T(y,z) + K(y,z) - \int_0^y K(y,\eta)T_\eta(\eta,z)d\eta = 0 \ , \quad z < y$$

(2.15)

where $T(y,z)$ is given by

$$T(y,z) = \int_0^\infty \frac{\sin \omega z}{\omega} \cos\omega y \left[G(\omega) - \frac{2}{\pi} \right] d\omega$$

(2.16)

and the impedance profile is recovered from $K(y,x)$ through

$$\sigma(y) = - \frac{2[K(y,y)]'}{[1 - K(y,y)]} \ .$$

(2.17)

The major difference from the standard Gelfand-Levitan procedure is that in (2.15) the kernel T is differentiated with respect to η.

Santosa[30] refined the method to give it a time-domain meaning by applying it to problems in which the response data are given for a finite time. The representation obtained is similar to that in the Gopinath-Sondhi equation[31]. Santosa demonstrated the method to be stable both theoretically and numerically on a window type profile. Reconstruction errors

-33-

at depth are attributed to errors in the reflection data and to the first order discretization errors committed in the approximation of an integral by a sum.

Coen has extended in one of his papers[32] the work of Ware and Aki so as to recover both the density and compressibility profiles of a layered fluid from the plane wave reflection coefficient at two precritical angles of incidence, and at all frequencies.

In another paper[33], Coen applied the Ware and Aki method to recover the three elastic profiles of a layered half-space from three reflection coefficients. First the shear modulus and density profiles are determined from reflection coefficient data for oblique incidence SH plane waves given at two angles of incidence and for all frequencies. Once the density and shear modulus have been obtained, a further experiment using the reflection coefficient due to an impulsive normally incident P-wave permits the retrieval of the P-wave velocity and hence of the Lamé profile. The limitation in Coen's work, as in Ware and Aki's, is that the potential $V(\zeta)$ satisfy the integrability condition.

$$\int_0^\infty (1 + |\zeta|)|V(\zeta)|d\zeta < \infty \qquad (2.18)$$

which would be very restrictive in practice. One result we demonstrate in our work is that the Gelfand-Levitan algorithm still applies to the fundamental case when $V(\zeta)$ tends to a non-zero finite value at infinity in violation of the above integrability condition.

In a third paper[34], Coen addresses the problem of common source point surface data wherein a source is placed on the free surface of a plane stratified half-space and the vertical component of velocity or of acceleration is measured on the free surface. After solving the impulsive source problem, Coen discusses the monochromatic source problem. His approach is deceptively similar to the one we present in this thesis as both approaches transform the original problem into a one-dimensional Schrödinger equation and then proceed to use the Gelfand-Levitan integral equation to solve the inverse problem. However, the problem in the two approaches is posed in a different way and the steps towards the solution are dissimilar.

It is useful here to run through Coen's method so as to point out the difficulty he encounters and which does not arise in our approach (a constant density is assumed).

The Hankel transform of the pressure field

$$\phi(\zeta,z,\omega) = \int\limits_{0}^{\infty} \int\limits_{0}^{\infty} p(r,z,t)rJ_0(r,\zeta)e^{-i\omega t}drdt$$

(2.19)

satisfies the Schrödinger equation

$$(\frac{\partial^2}{\partial z^2} - k^2)\phi(k,z,\omega) = Q(z,\omega)\phi(k,z,\omega) \ .$$

(2.20)

where $Q(z,\omega)$ is the potential

$$Q(z,\omega) = \frac{\omega^2}{c_o^2}(1 - \frac{c_o^2}{c^2})$$

(2.21)

and k is related to the horizontal wavenumber ζ through

$$\zeta = \sqrt{k^2 + \frac{\omega^2}{c_o^2}} \ .$$

(2.22)

The Schrödinger equation is accompanied by two initial conditions

$$\phi\big|_{z=0} = 1 \quad , \quad \phi'\big|_{z=0} = -\frac{1}{q(\xi,\omega)} \qquad (2.23)$$

where

$$q(\xi,\omega) = -\frac{1}{\rho(0)d(\xi,\omega)} \qquad (2.24)$$

and $d(\zeta,\omega)$ is the Hankel transform of the vertical component of particle acceleration at the surface $z = 0$.

Coen's scheme proceeds from an input function $r(k,\omega)$

$$r(k,\omega) = \frac{1 - kq(k,\omega)}{1 + kq(k,\omega)} \qquad (2.25)$$

given for all real positive k values and requires the computation of $R(z,\omega)$ where

$$r(k,\omega) = \int_0^\infty R(z,\omega)e^{-kz}dz \quad . \qquad (2.26)$$

The Gelfand-Levitan equation

$$A(z,y,\omega) = R(z+y,\omega) + \int_{-z}^{z} A(z,x,\omega)R(y+x)dy \quad |y| < z$$

(2.27)

is then solved for A(z,y) which in turn yields the potential

$$O(z) = 2 \frac{d}{dz} A(z,z) \quad , \quad z > 0 \; .$$

(2.28)

The difficulty with the whole procedure stems from the second step, namely the computation of R(z) from r(k). That involves an inverse Laplace transform which is numerically inherently unstable. Our method, on the other hand, starts off from the Schrödinger equation for the field (rather than for its Hankel transform) with the associated plane wave reflection coefficient as a function of vertical wavenumber. The Laplace transform of Coen's approach is replaced by a Fourier transform which does not present any numerical difficulties. It is to be noted that the known numerical instability of the Laplace transform has led some researchers, notably Santosa and Symes[42] to dismiss the Gelfand-Levitan approach to the solution of the inverse problem. We believe that our approach to the inverse problem could lead to a positive reassessment of the Gelfand-Levitan inverse method.

2.2.3 Single Frequency, Non-Normal Incidence

Very few researchers other than Coen have considered the single frequency non-normal incidence case. One exception is Mittra and Schaubert[35] who used a method different from ours. Their approach is a spectral domain method of probing stratified, lossless, dielectric media using an alternative to the Marchenko formulation and resulting in a Fredholm equation of the second kind which is solved through the use of rational basis functions. They noted that accurate inversions can be obtained if data is provided for $k_z \gg k_o$. The Mittra and Schaubert examples all have zero terminal potentials, and although the results are good in general, the inaccuracies are interestingly larger near the origin with higher frequencies "seeming to give better resolution."[35]

Another example of the prior single frequency, non-normal incidence analysis is provided by the work of Roger[36]. Roger sought to determine the index profile of a dielectric plate backed by a perfectly conducting plane. That last fact complicates the problem, since the potential is always negative and bound states due to surface waves might exist. Roger starts from a nonlinear integral equation which he linearizes to obtain a Fredholm equation of the first kind whose solution constitutes an ill-posed problem (in the sense of Hadamard). Roger solves this equation by using the Tikhonov regularization method. The method fails when the permittivity $\epsilon(z)$ exceeds a constant by more than 20% and also when the layer is thicker than 1.5λ.

2.2.4 The Deift and Trubowitz Method

Deift and Trubowitz[37] introduced the trace method for
determining the potential in one-dimensional scattering
problems for the Schrödinger equation. The trace method
requires as data the reflection coefficient, while the method
we adopted requires the Fourier transform of the reflection
coefficient. Furthermore, the trace method requires the
solution of a nonlinear differential equation while the
Gelfand-Levitan (or Marchenko) equation that we use is a
linear integral equation.

Stickler visited us in Woods Hole and became interested
in adapting the Deift and Trubowitz trace method to our
problem. He took the same input, i.e., the measurement of
the pressure field as a function of range, where both the
real and imaginary parts of the pressure field are needed.
After the reflection coefficient $R(k)$ is derived by using the
same approach as ours, he then introduces an auxiliary
potential, $\tilde{q}(z)$, which is determined by using the trace
formula methods of Deift and Trubowitz. Stickler[7] defines
the auxiliary potential, $\tilde{q}(z)$ by

$$\tilde{q}(z) = q(z) - \frac{\sqrt{\rho}}{2} \left(\frac{\rho'}{\rho^{3/2}}\right)' \tag{2.29}$$

where primes denote derivatives with respect to z. The auxi-
liary potential, $\tilde{q}(z)$, can be determined from the Deift and
Trubowitz trace formula

$$\tilde{q}(z) = -\frac{4}{\pi} \int_0^\infty k \operatorname{Im}[R(k)u_2^2(z,-k)]dk \quad . \tag{2.30}$$

The Jost function $u_2(z,k)$ in (2.30) is determined by solving

$$-u_2'' + \tilde{q}(z)\, u_2 = k^2 u_2 \tag{2.31}$$

with the boundary condition

$$u_2 \sim e^{-ikz}, \quad z \to \infty \quad . \tag{2.32}$$

Deift and Trubowitz have shown that the usual iteration
scheme for solving two coupled nonlinear integral equations
such as (2.13) and (2.14) converges. In our case, instead of
(2.13) and (2.14), we solve for $\tilde{q}(z)$ using a Gelfand-Levitan
linear integral equation.

Stickler presented two numerical examples[7] of applying
the Deift and Trubowitz algorithm on a twice continuous
function (in Chapter VI we apply our method to one of his
examples and refer to it as the "Stickler's Profile"). Since
Stickler generated the reflection coefficient from the solu-
tion of a Riccati equation, he had control over the local
tolerance for the determination of the reflection coeffi-
cient. As in the Gelfand-Levitan method, the results are
excellent for $z/L \ll 1$, but deteriorate gradually with depth
($z/L > 1$). Stickler attributes the degradation of his method

to the lack of accuracy of the local reflection coefficients generated via the Riccati equation.

When we compare Stickler's numerical results to ours, we observe the general similarity of his results to the ones described in this thesis. This similarity should not be too surprising in view of the close relationship between the two methods (see further discussion in Chapter IV). We have no data to assess the computational efficiency of Stickler's method versus ours.

2.2.5 Schur Algorithm

Yagle and Levy[38,39] have adopted an algorithm which reconstructs the unknown acoustic medium layer by layer (layer stripping procedure). The method is analogous to the downward continuation method, in that successive up and down-going waves are measured at the surface. The first reflection of the impulse yields information about the medium immediately beneath the surface (at depth Δ). This information is used to update the waves at depth Δ which then becomes the new reference surface. The procedure is successively repeated until the depth of interest is reached. The Schur algorithm applies to the study of the two component system of coupled differential equations

$$q_{1x}(x,t) + q_{1t}(x,t) = - r(x) \, q_2(x,t)$$

$$q_{2x}(x,t) - q_{2t}(x,t) = - r(x) \, q_1(x,t) \qquad (2.33)$$

where the subscripts x and t denote derivatives with respect to x and t, and r(x), the reflectivity function, provides a coupling between the downgoing wave $q_1(x,t)$ and the upgoing wave $q_2(x,t)$ (unit velocity).

Yagle and Levy begin their derivation with the set of equations arising after an initial impulse excitation $\delta(t)$, so that $q_1(x,t)$ and $q_2(x,t)$ can be written as

$$q_1(x,t) = \delta(t-u) + \tilde{q}_1(x,t) \, u_{-1}(t-u)$$

$$q_2(x,t) = \tilde{q}_2(x,t) \, u_{-1}(t-u) \, ,$$

(2.34)

in which causality has been used (no waves exist for t < u). From (2.33) and (2.34) Yagle and Levy derive

$$r(x) = 2q_2(u,x)$$

(2.35)

The equations (2.33) and (2.35) constitute the continuous parameter fast Cholesky recursion where $q_1(x,t)$ and $q_2(x,t)$ are updated to yield r(x) from equation (2.35).

At this point, the application of the Schur method entails taking the Fourier transforms of the system in (2.33). Denoting the transform of q by $\hat{q}$, we get:

$$\hat{q}_{1x} = - i\omega\hat{q}_1(x,\omega) - r(x) \, \hat{q}_2(x,\omega)$$

(2.36)

$$\hat{q}_{2x} = - r(x) \, \hat{q}_1(x,\omega) + i\omega\hat{q}_2(x,\omega) \, .$$

Yagle and Levy thus find a reflection coefficient

$$\hat{R}(x,w) = \frac{\hat{q}_2(x,\omega)}{\hat{q}_1(x,\omega)} \qquad (2.37)$$

which obeys a Riccati equation

$$\hat{R}_x = 2i\omega\hat{R}(x,\omega) + r(x)\left(\hat{R}(x,\omega)^2 - 1\right) \qquad (2.38)$$

with

$$r(x) = \lim_{\omega \to \infty} \left[2iw\,\hat{R}(x,\omega)\right] \; . \qquad (2.39)$$

Equations (2.36), (2.37), and (2.38) constitute the Schur algorithm, while (2.38) and (2.39) represent a continuous parameter dynamic deconvolution algorithm. It is to be noted that the discretized Schur algorithm is similar to the fast recursion procedure of Berryman and Greene.

Yagle and Levy assert in the concluding section of their paper that their Schur algorithm is computationally superior to the Gelfand-Levitan algorithm as used by Coen. This observation may be true of the Gelfand-Levitan procedure for impulsive sources at non-normal incidence as presented by Ware and Aki[21] and by Coen[33], but it certainly does not apply to our approach. Yagle and Levy's main objection to Gelfand-Levitan is that the boundedness of the potential

-44-

$$\int_0^\infty (1 + |\tau|)|V(\tau)|d\tau < \infty \qquad (2.40)$$

may not be satisfied at non-normal incidence. However, we show in Chapter IV, that the Gelfand-Levitan algorithm can in fact be applied even for a non-zero end potential which would render the integral in (2.40) infinite. Moreover, the Frisk experiment studied here is performed at a single frequency and not with an impulsive excitation. We have shown that the monochromatic reflection coefficient as a function of vertical wave number is integrable so that the negative comment of Yagle and Levy does not apply to our work.

Although not stated in their paper, the application of the Schur algorithm to the inverse problem in a layered acoustic medium involves implicitly approximations similar to those inherent in the Claerbout's migration method. Although the Schur algorithm constitutes an improvement over migration in so far as the downgoing wave strength is modified by the upgoing wave strength it is still an approximation. Indeed, in some of our earlier unpublished work, we succeeded in improving the Claerbout migration method precisely by introducing the coupling between the reflected and the downgoing wave. By contrast, our Gelfand-Levitan approach is not an approximation and except for numerical computation represents an exact formulation of the problem.

2.2.6   Riccati Equation Method

One method which we considered upon Stickler's suggestion and which appears to have considerable potential is based on the Riccati equation. Reflectivity as a function of travel time τ obeys the Riccati equation[12]

$$\frac{dr}{d\tau} = - 2i\omega r - \gamma(\tau)(1 - r^2) \qquad (2.41)$$

with boundary condition $r(\omega,\infty) = 0$ in which

$$\gamma(\tau) = \frac{1}{Z} \frac{dZ}{d\tau} \qquad (2.42)$$

where the acoustic impedance has been defined by

$$Z(\tau) = \sqrt{\frac{\omega}{k_z}} \, \rho \qquad (2.43)$$

The inverse problem is here that of reconstructing $Z(z)$ from surface observations of r. To get $Z(z)$ from $Z(\tau)$ involves further assumptions. We can formulate the problem equivalently by writing

$$r(\omega,\tau) = \int_{\tau}^{\infty} d\tau' \, \gamma(\tau')e^{[2i\omega(\tau'-\tau)]}(1-r^2(\omega,\tau)) \qquad (2.44)$$

while at the surface, the reflection amplitude is

$$r(\omega,o) = \int_{0}^{\infty} d\tau\gamma(\tau)e^{(i\omega\tau)}(1-r^2(\omega,\tau)) \qquad (2.45)$$

The last two equations can be regarded as a nonlinear mapping of $r(\omega,0)$, given as a function of ω, into $\gamma(\tau)$. The aim of such an approach would be to reconstruct $\gamma(\tau)$ from $r(\omega,0)$. Although the existence of a complete solution to the above problem has not yet been demonstrated, an approximation can be derived. An inverse Fourier transform of (2.28) yields

$$r(t) = \frac{1}{\pi} \int_{-\infty}^{\infty} d\omega e^{-(2i\omega\tau)} r(\omega,0)$$

$$+ \frac{1}{\pi} \int_{-\infty}^{\infty} d\omega \int_{0}^{\infty} d\tau' \alpha(\tau') r^2(\omega,\tau') \; xe^{[2i\omega(\tau'-\tau)]}.$$

$$(2.46)$$

The first approximation to the solution is the Born series term, namely

$$\gamma_1(\tau) = \frac{1}{\pi} \int_{-\infty}^{\infty} d\omega \; r(\omega,0) e^{-2i\omega\tau} \qquad (2.47)$$

which resembles the first term of our own result. The convergence of the iteration series solution has not yet been established, but the approach as formulated by Nilsen and Gjevik[40] appears promising.

It is useful here to note that a Riccati equation still applies in the presence of density discontinuities. The equation obeyed by the pressure p is

$$\rho(\rho^{-1}p')' + (k^2 - V)p = 0 \quad , \quad (2.48)$$

where V is the potential.

The reflection coefficient may be obtained at the surface from the continuity of pressure and vertical velocity.

$$R(k)\big|_{z=0} = \frac{\rho^{-1}p' - ikp}{-ik} \quad . \quad (2.49)$$

The ratio of vertical velocity to pressure, i.e., the admittance,

$$u = \frac{\rho^{-1}p'}{p} \quad (2.50)$$

is continuous even in the presence of material discontinuities, as it is the ratio of two continuous quantities. The admittance u obeys a Riccati equation,

$$u' = -Q - \rho u^2 \tag{2.51}$$

in which $Q = \frac{1}{\rho}(k^2 - V)$

Note that $u(z=0) = ik\frac{(1 - R)}{1 + R}$

Let $u(z) = ik\frac{(1 - W(z))}{1 + W(z)}$

It follows that $W(0) = R(k)\big|_{z=0}$, and $W(z)$ itself obeys a Riccati equation

$$2ikW' - 2W(Q + \rho k^2) + W^{-2}(\rho k^2 - Q) = (\Omega - \rho k^2)$$

$$\tag{2.52}$$

which can be used to generate the reflection coefficient in the direct problem or to use an iterative procedure for the inverse problem. We did not pursue this approach further but it merits further study.

We have covered here those papers that were most relevant to the work that follows. It should be noted, how-

ever, that there are a number of other interesting inverse methods that have not been included in this review. Particularly noteworthy are the papers by Moses[41], Gopinath and Sondhi[31], Santosa and Symes[42] and others[43,44]. Also of interest is additional literature on the approximate inverse methods[55-57]. Special mention should be made of methods based on the Born approximation which originated with the seminal work of Cohen and Bleistein[45-54].

THE REFLECTION COEFFICIENT

3.1 Introduction

The plane-wave reflection coefficient as a function of vertical wavenumber $r(k_z)$ is central to the inversion procedure we adopted to solve the inverse problem. Its symmetry property is shown to follow from the integral equation representation of the field. We then derive its asymptotic behavior for large k_z by induction and show that $r(k_z)$ is integrable, and hence is an acceptable input to the inverse method presented in Chapter IV.

3.2 Definition and Properties of the Reflection Coefficient

Consider the problem of a plane wave

$$\psi_i(z) = e^{ik_z z}$$

incident from $z = -\infty$ onto a half-space extending from $z = 0$ to $z = +\infty$. The half space is characterized by a potential $V(z)$. $V(z)$ is all that is needed to describe the scattering of the incident wave $\psi_i(z)$ by the acoustic half space:

$$\psi(z) = e^{ik_z z} + \int_{-\infty}^{\infty} G(z,z')\, V(z')\, \psi(z')dz' \qquad -\infty < z < \infty$$

$$(3.1)$$

where the Green's function $G(z,z')$ is determined by

$$G(z,z') = \frac{e^{ik_z|z-z'|}}{2ik_z} \qquad (3.2)$$

It follows that as $z \to -\infty$,

$$\psi(z) = e^{ik_z z} + e^{-ik_z z} \int_{-\infty}^{\infty} \frac{e^{ik_z z'}}{2ik_z} V(z') \; \psi(z')dz' \qquad (3.3)$$

and the coefficient of $e^{ik_z z}$ can be identified as the reflection coefficient.

$$r(k_z) = \frac{1}{2ik_z} \int_{-\infty}^{\infty} e^{+ik_z z'} V(z') \; \psi(z')dz' \qquad (3.4)$$

The integral representation of the reflection coefficient allows a simple derivation of the symmetry properties of $r(k_z)$ in the complex plane.

From (3.4)

$$r(-k_z) = -\frac{1}{2ik_z} \int_{-\infty}^{\infty} e^{-ik_z z'} V(z') \; \psi(z', -k_z) \; dz' \qquad (3.5)$$

But, for a real potential $V(z)$ and for real k_z, Schrodinger's equation shows that when $\psi(z',k_z)$ is a solution, so is $\psi(z', -k_z)$. Moreover, $\psi(z', -k_z) = \psi^*(z',k_z)$ which implies

- 52 -

$$r(-k_z) = r^*(k_z) \qquad\qquad (3.6)$$

The result can be extended to the complex plane through the use of the Schwartz reflection principle,

$$r(-k_z^*) = r^*(k_z) \qquad\qquad (3.7)$$

in any region of analyticity connected with the real k_z axis. (This constitutes the analytic continuation of $r(k_z)$).

Now, the Gelfand-Levitan algorithm requires knowledge of $r(k_z)$ for all real k_z. However, the symmetry property expressed in (equation 3.6) demonstrates that knowledge of $r(k_z)$ on the half-line of $0 < k_z < \infty$ is sufficient.

Note that when the vertical wavenumber $k_z = k_0 \cos\Theta$ is real and larger than the water wavenumber k_0, the angle of incidence becomes imaginary. That can be verified by requiring that $\cos\Theta = \cos(\Theta_r + i\Theta_i)$ be real. And since

$$\cos(\Theta_r + i\Theta_i) = \cos\Theta_r \cosh\Theta_i - i \sin\Theta_r \sinh\Theta_i$$

it follows that $\Theta_r = 0$ and $k_z = k_0 \cosh\Theta_i$ for $k_0 < k_z < \infty$. The mapping between the k_z-plane and the Θ-plane is drawn in Figure 6.
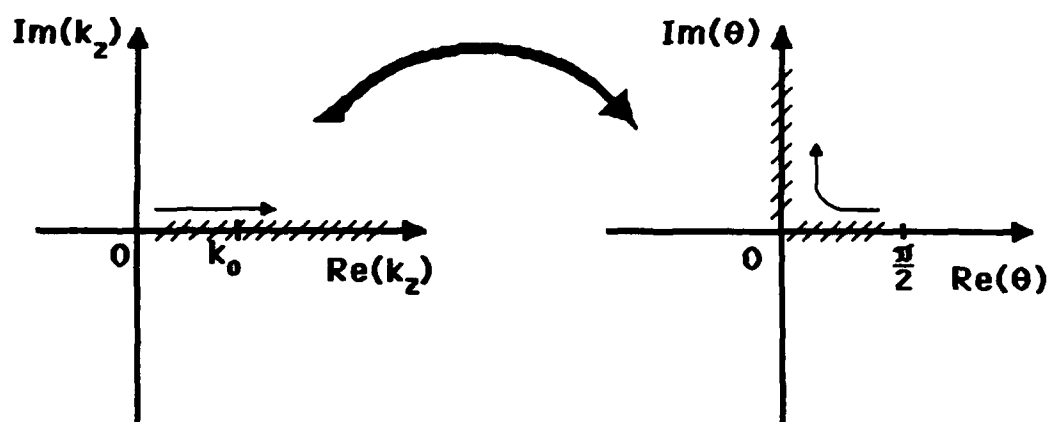
Fig. 6 Mapping from the k_z-Plane into the θ-Plane

3.3 Asymptotic Behavior of the Plane Wave Reflection Coefficient

The input to both the Gelfand-Levitan algorithm and to the Born approximation is the Fourier transform of the reflection coefficient

$$R(z) = \int_{-\infty}^{\infty} r(k_z) \, e^{ik_z z} \, dk_z$$

The properties of $r(k_z)$ as $k_z \to \infty$ are studied for two simple cases and then generalized.

(a) Half space

The reflection coefficient is given by

$$r(k_z) = \frac{Z_1 - Z}{Z_1 + Z} \tag{3.8}$$

where the impedance $Z = \rho c / \cos\theta$ or

$$Z = \frac{\rho \omega_0}{k_z} \tag{3.9}$$

Therefore,

$$r(k_z) = \frac{k_z - k_{z1}}{k_z + k_{z1}} \tag{3.10}$$

And since k_x is continuous,

$$k_{z1}^2 = (k_1^2 - k_0^2) + k_z^2 \tag{3.11}$$

and

$$r(k_z) = \frac{k_z - \sqrt{(k_1^2 - k_0^2) + k_z^2}}{k_z + \sqrt{(k_1^2 - k_0^2) + k_z^2}} \tag{3.12}$$

As $k_z \to \infty$

$$r(k_z) \sim \frac{k_z - k_z(1 + \frac{1}{2k_z^2}(k_1^2 - k_0^2))}{k_z + k_z(1 + \frac{1}{2k_z^2}(k_1^2 - k_0^2)} \tag{3.13}$$

$$= -\frac{1}{4}(k_1^2 - k_0^2)/k_z^2$$

Hence,

$$r(k_z) \xrightarrow[k_z \to \infty]{} 0 \text{ as } (1/k_z^2)$$

When density variations are considered,

$$r(k_z) = \frac{m\cos\Theta - n\cos\Theta_1}{m\cos\Theta + n\cos\Theta_1} \tag{3.15}$$

- 56 -

where $m = \rho_1/\rho$ and $n = k_1/k_0$

$$r(k_z) = \frac{mk_z - k_{z1}}{mk_z + k_{z1}}$$

As $k_z \to \infty$

$$r(k_z) \sim (\frac{m-1}{m+1}) + (k_1^2 - k_0^2)/2k_z^2 \qquad (3.17)$$

which still decays as $(1/k_z^2)$, but tends to a finite limit $(\frac{m-1}{m+1})$ as $k_z \to \infty$

Therefore, the Fourier transform of $r(k_z)$ involves generalized functions,

$$F(r(k_z)) = (\frac{m-1}{m+1})\delta(z) + \text{(analytic function)} \qquad (3.18)$$

(b)   One Layer Case (cf. Figure 7).

The reflection coefficient at the (0 - 1) interface is

$$r(k_z) = \frac{(\frac{z_1 - z_0}{z_1 + z_0}) + (\frac{z_2 - z_1}{z_2 + z_1}) e^{2ik_{1z}d}}{1 + (\frac{z_1 - z_0}{z_1 + z_0})(\frac{z_2 - z_1}{z_2 + z_1}) e^{2ik_{1z}d}}$$
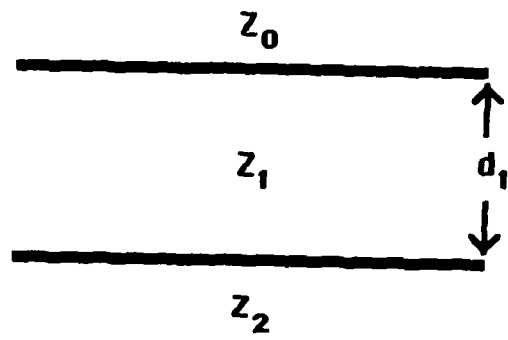
$$(3.19)$$

- 57 -

Fig. 7   One Layer Case

The analysis of the terms within parentheses is identical to the analysis carried out in the previous section. One can conclude immediately that

$$r(k_z) \xrightarrow[k_z \to \infty]{} [(k_1^2 - k_0^2) + (k_2^2 - k_1^2) e^{2ik_z d}]/4k_z^2$$

$$\longrightarrow 0 \text{ as } (1/k_z^2) \tag{3.20}$$

Note:

The delta function potential

$$V(z) = A\delta(z) \tag{3.21}$$

can be considered as a limiting case of the one-layer problem. It has associated with it a reflection coefficient[20]

$$r(k_z) = - i \frac{A}{2k_z + iA} \tag{3.22}$$

which goes to zero as $k_z \to \infty$, but only as $(1/k_z)$ in apparent violation of the result just derived. The reason is that in a delta function potential, $V(z) \to \infty$ which implies $(k_0^2 - k_1^2) \to \infty$, invalidating the binomial approximation to the square root used in section (a). However, the formulation of the acoustic problem requires $V(z) \le k_0^2$ which is finite (as long as the frequency ω_0 is finite). Therefore,

delta-like potentials do not arise and the binomial
approximation is valid.

(c)   General Case

The expression for $r(k_z)$ given in the previous
section can be rewritten in the general form

$$r(k_z) = \frac{R_{01} + R_{12}\, e^{2ik_{1z}d_1}}{1 + R_{01}R_{12}e^{2ik_{1z}d_1}} \tag{3.23}$$

$$= \frac{1}{R_{01}} + \frac{[1 - (1/R_{01})^2]\, e^{-2ik_{1z}d_1}}{(\frac{1}{R_{01}})\, e^{-2ik_{1z}d_1} + R_{12}} \tag{3.24}$$

The reflection coefficient can be readily generalized
to include stratified media (58)

$$R = \frac{1}{R_{01}} + \left/ \frac{[1 - 1/R_{01})^2]\, e^{-2ik_{1z}d_1}}{(\frac{1}{R_{01}})\, e^{-i2k_{1z}d_1}} \right.$$

$$+ \frac{1}{R_{12}} + \left/ \frac{[1 - (1/R_{12}^2)]e^{-i2k_{2z}(d_2-d_1)}}{(\frac{1}{R_{12}})e^{-i2k_{2z}(d_2-d_1)}} \right. + \ldots$$

$$+ \frac{1}{R_{(n-1)n}} + \left/ \frac{[1 - (1/R^2_{(n-1)n})]e^{-i2k_{nz}(d_n-d_{n-1})}}{[1/R_{n-1)n}]e^{-i2k_{nz}(d_n - d_{n-1})}} \right.$$

$$+ R_{n+1} \tag{3.25}$$

The continued fraction representation of (equation 3.25) indicates that the partial reflection coefficient $R_{12}(k_z)$ in (equation 5.23) could represent the reflection coefficient due to a complicated medium rather than to a simple homogeneous half space.

The asymptotic behavior of $r(k_z)$ is deduced in a two step process. Assume the configuration of Figure 8 with $R_1(k_z) \rightarrow (\frac{\alpha}{k_z^2})$ as $k_z \rightarrow \infty$

Adding a new interface to the set-up (Figure 9) and using equation (5.24),

$$r(k_z) \rightarrow \frac{k_z^2}{\beta} + \frac{(1 - k_z^4/\beta^2)\, e^{-i2k_z d_1}}{\frac{k_z^2}{\beta}\, e^{-2ik_z d_i} + \frac{\alpha}{k_z^2}}$$

$$\rightarrow \frac{k_z^2}{\beta} + (\frac{\beta}{k_z^2} - \frac{k_z^2}{\beta})\, (1 - \frac{\beta\alpha}{k_z^4}\, e^{2ik_z d_1}$$

$$+ \frac{\beta^2\alpha^2}{k_z^8}\, e^{4ik_z d_1} + \ldots)$$

$$\tag{3.26}$$

Therefore,

$$r(k_z) \xrightarrow[k_z \rightarrow \infty]{} 0 \text{ as } (1/k_z^2) \tag{3.27}$$
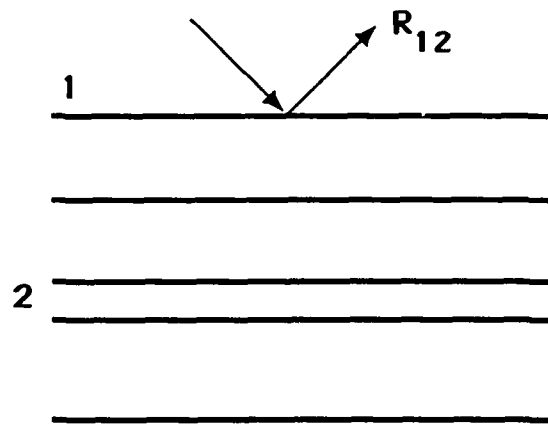
Fig. 8 Stack of Isovelocity Layers
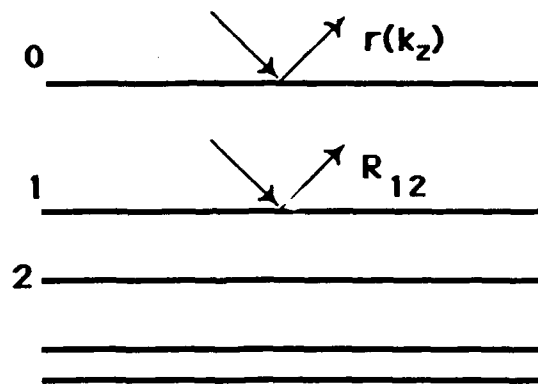
Fig.9 Adding a Top Layer to the Stack in Fig.8

The argument just presented is, in fact, the last step in a proof by induction of the proposition that $r(k_z) \to 0$ as $(1/k_z^2)$ in the presence of a homogeneous half space. The proposition was proved true for one or two interfaces was assumed true for an arbitrary number of interfaces and was shown to hold for one more interface. This result should be contrasted with the corresponding situation in the Ware and Aki experiment; For angles of incidence greater than critical, they were confronted with the fact that $r(\omega) \to 1$, as $\omega \to \infty$, and could not proceed with the Gelfand-Levitan inversion procedure.

CHAPTER IV

THE ONE-DIMENSIONAL INVERSE PROBLEM

This chapter presents the derivation of our approach to
the one-dimensional inverse problem. The results yield the
methodology underlying the numerical computations described
in Chapter V. The derivation exploits the equivalence
between the acoustic problem and the corresponding quantum
scattering problem as presented in Chapter II. A major dif-
ference between the two is the boundary conditions. Whereas
in quantum mechanics, the unknown slab is surrounded by
isovelocity space (zero end potential), in the acoustics
problem, as applied to the ocean bottom, differing velocities
have to be accommodated above and below the slab (non-zero
end potential). The solution to the inverse problem detailed
in this chapter consists of an extension of Faddeev's
method[16] for deriving the scattering matrix in the case of
zero end potential (or integrable potential) to the case of
non-zero end potential which is representative of the reflec-
tions from the bottom of the ocean. We are able to solve the
problem analytically, in part, because of its one-dimensional
modeling. Our technique is related to that applied by
Stickler to a similar scattering problem.

4.1 Introduction

The determination of the potential $V(z)$ in the Schrödinger equation

$$\frac{d^2\psi}{dz^2} + \left[p^2 - V(z)\right]\psi(z) = 0 \quad . \tag{4.1}$$

from scattering data such as the reflection coefficient constitutes the one-dimensional inverse problem.

Two scattering solutions of the Schrödinger equation are defined by their asymptotic behavior (p is the vertical wavenumber also referred to as k_z):

$$\psi_1(z,p) = \begin{cases} e^{ipz} + s_{12}(p)\, e^{-ipz} & \text{as} \quad z \to -\infty \\ s_{11}(p)e^{ipz} & z \to +\infty \end{cases} \tag{4.2}$$

$$\psi_2(z,p) = \begin{cases} e^{-ipz} + s_{21}(p)e^{ipz} & \text{as} \quad z \to +\infty \\ s_{22}(p)\, e^{-ipz} & z \to -\infty \quad . \end{cases} \tag{4.3}$$

The matrix of coefficients

$$\begin{pmatrix} s_{11}(p) & s_{12}(p) \\ s_{21}(p) & s_{22}(p) \end{pmatrix}$$

is known as the S matrix of the Schrödinger equation. The element $s_{12}(p)$ corresponds to the plane wave reflection coefficient determined in the WHOI experiment.

Faddeev[16B] has shown that $s_{12}(p)$ may determine all the elements of the S matrix and hence is sufficient to obtain the scattering potential $V(z)$. However, these results have an important practical restriction, namely, that the end potential tends to zero; i.e., $V(z) \rightarrow 0$ as $z \rightarrow \pm\infty$. They are reviewed in the first part of this chapter.

In the second part of the chapter, we present an extension of the theory to include the geophysically significant case of a finite end potential, $V(z) \rightarrow V_1$ as $z \rightarrow \infty$. Finally, an appropriate choice of source frequency is shown to eliminate trapped modes.

4.2 Properties of the Solution of the Schrödinger Equation ($V_1=0$)

Two fundamental solutions of the Schrödinger equation are introduced,

$$u_1(z,p) \sim e^{ipz} \quad \text{as} \quad z \rightarrow +\infty \tag{4.4}$$

$$u_2(z,p) \sim e^{-ipz} \quad \text{as} \quad z \rightarrow -\infty \tag{4.5}$$

The method of variation of parameters leads to a representation of $u_1(z,k)$ and $u_2(z,k)$ as solutions of Volterra equations of the second kind[16]

$$u_1(z,p) = e^{ipz} - \int_z^\infty \frac{\sin p(z-z')}{p} V(z)u_1(z',p)dz' \qquad (4.6)$$

$$u_2(z,p) = e^{-ipz} + \int_{-\infty}^z \frac{\sin p(z-z')}{p} V(z)u_2(z',p)dz' . \qquad (4.7)$$

But, since the Schrödinger equation is symmetrical in p, $u_1(z,-p)$ and $u_2(z,-p)$ are also solutions of (eq. 4.1). The solution pairs $[u_1(z,p), u_1(z,-p)]$ and $[u_2(z,p), u_2(z,-p)]$ are linearly independent since their Wronskians obtained from their asymptotic form (eqs. 4.4, 4.5)

$$W(u_1, u_1^*) = 2ip$$
$$W(u_2, u_2^*) = -2ip$$
$$(4.8)$$

are non-zero for $p \neq 0$.

Now, any solution of the Schrödinger equation can be written as a linear combination of two independent solutions. In particular,

$$u_1(z,p) = u_2(z,p)c_{22}(p) + u_2(z,-p)c_{21}(p) \qquad (4.9)$$

$$u_2(z,p) = u_1(z,p)c_{11}(p) + u_1(z,-p)c_{12}(p) \quad . \qquad (4.10)$$

The next section examines some properties of the coefficients $c_{ij}(k)$ which will later be shown to be closely related to the elements of the S matrix.

4.2.1   Properties of the Coefficients $c_{ij}(p)$

The coefficients $c_{ij}(p)$ can be expressed as Wronskians by "taking Wronskians" of both sides in equations (4.9 and 4.10). For instance, from (equation 4.9)

$$W\bigl(u_1(z,p),u_2(z,p)\bigr) = W[u_1,u_1]c_{11}(p)$$
$$+ W[u_1(z,p),u_1(z,-p)]c_{12}(p). \qquad (4.11)$$

We know, however, that in (4.11)

$$W[u_1,u_1] = 0 \qquad \text{(linearly dependent functions)}$$

and

$$W[u_1(z,p),u_1(z,-p)] = 2ip \qquad (cf., eq. 4.8) . \qquad (4.12)$$

It follows that

$$c_{12}(p) = \frac{1}{2ip} W[u_1(z,p), u_2(z,p)] \quad . \qquad (4.13)$$

One can show similarly that

$$c_{21}(p) = c_{12}(p) \qquad (4.14)$$

$$c_{11}(p) = -c_{22}(-p) = \frac{1}{2ik} W[u_2(z,-p),u_1(z,p)] \qquad (4.15)$$

Using the values of c_{ij} expressed in this form, and substituting eq. 4.9 into eq. 4.10, one gets the compatibility relations,

$$c_{11}(p)c_{22}(p) + c_{21}(p)c_{12}(-p) = 1$$

$$|c_{12}(p)|^2 - |c_{11}(p)|^2 = 1 \quad . \qquad (4.16)$$

and,

$$c_{12}(p)c_{22}(p) + c_{11}(-p)c_{21}(p) = 0 \quad . \tag{4.17}$$

The asymptotic form of $u_2(z,k)$ in (eq. 4.7) for $z \to \infty$,

$$u_2(z,p) = e^{-ipz}\left[1 - \frac{1}{2ip}\int_{-\infty}^{\infty} e^{ipz'}V(z')u_2(z')dz'\right]$$

$$+ \frac{e^{ipz}}{2ip}\int_{-\infty}^{\infty} e^{-ipz'}V(z')u_2(z')dz' \tag{4.18}$$

leads by comparison with (eq. 4.9) to the identifications:

$$c_{12}(p) = 1 - \frac{1}{2ip}\int_{-\infty}^{\infty} e^{ipz'}V(z')u_2(z')dz' \tag{4.19}$$

$$c_{11}(p) = \frac{1}{2ip}\int_{-\infty}^{\infty} e^{-ipz'}V(z')u_2(z')dz' \quad . \tag{4.20}$$

Using the previous estimates for u_2 in eq. 4.5 and the Riemann-Lebesgue theorem, it can be seen, that for large p, $c_{12}(p)-1$ is $o(1/p)$ and $c_{11}(p)$ is $o(\frac{1}{p})$.[*] Moreover, $c_{12}(p)$ is analytic in the upper half plane, does not vanish on the real p axis, and has only a finite number of simple zeros on the imaginary axis.

4.2.2 Properties of the $s_{ij}(k)$ Coefficients

One is now ready to return to the original scattering problem and its associated S matrix.

$\psi_1(z,p)$, the solution of the scattering problem of interest, can be written in terms of the linearly independent solutions $u_2(z,p)$ and $u_2(z,-p)$

$$\psi_1(z,p) = u_2(z,-p) + s_{12}(p)u_2(z,p) \qquad (4.21)$$

$$= s_{11}(p)u_1(z,p) \quad . \qquad (4.22)$$

---

[*] The order symbol o( ) is defined as follows:

$$f(\epsilon) = o[q(\epsilon)] \text{ as } \epsilon \to 0$$

$$\text{if} \quad \lim_{\epsilon \to 0} \frac{f(\epsilon)}{q(\epsilon)} = 0$$

Writing out $u_1(z,p)$ in terms of $u_2(z,\pm p)$ as given in eq. 4.10, one obtains the compatibility relations

$$s_{11}(p) = \frac{1}{c_{21}(p)}$$

$$s_{12}(p) = \frac{c_{22}(p)}{c_{21}(p)} \; .$$

(4.23)

Carrying out the same operation on $\psi_2(z,k)$, one obtains

$$s_{22}(p) = \frac{1}{c_{12}(p)}$$

$$s_{21}(p) = \frac{c_{11}(p)}{c_{12}(p)} \; .$$

(4.24)

From the asymptotic behavior of the Jost functions c_{ij} one can deduce the asymptotics of the S matrix[*]

$$s_{11}(p) = s_{22}(p) = 1 + O(1/p)$$

$$s_{12}(p) \text{ and } s_{21}(p) = O(1/p)$$

(4.25)

---

[*] The order symbol $O(\ )$ is defined as follows:

$$f(\epsilon) = O[g(\epsilon)] \text{ as } \epsilon \to 0$$

$$\text{if } \lim_{\epsilon \to 0} \frac{f(\epsilon)}{g(\epsilon)} = A \; , \; 0 < |A| < \infty$$

It can be seen from eq. 4.24,   4.16 and eq. 4.17 that the
S matrix is unitary,

$$|s_{11}|^2 + |s_{12}|^2 = |s_{22}|^2 + |s_{21}|^2 = 1 \quad , \qquad (4.26)$$

implying conservation of energy, and that since $s_{ij}(-p) = s^*_{ij}(p)$,

$$s_{11}s^*_{21} + s_{12}s^*_{22} = 0 \quad . \qquad (4.27)$$

The coefficients $s_{ij}(p)$ are continuous for real
p, $s_{11}(p)$ being analytic in the upper half plane except for
poles on the imaginary axis (corresponding to the zeros of
$c_{12}(p)$). Conditions (4.26) and (4.27) allow one to recon-
struct the scattering matrix from a knowledge of the reflec-
tion coefficient $s_{12}(p)$. In what follows, $s_{12}(p)$ is
identified with the plane wave reflection coefficient $r(k_z)$
and $s_{11}(p)$ with the transmission coefficient $t(k_z)$. Substi-
tuting c_{21} by $(1/t)$ and c_{22} by (r/t) in (eq. 4.10), it
follows that

$$t(p)u_1(z,p) = r(p)u_2(z,p) + u_2(z,-p) \quad . \qquad (4.28)$$

The above equation is the basis for the derivation of
the Gelfand-Levitan inversion method that has been obtained
for a potential $V(z) \to 0$ as $z \to \pm\infty$. Such a potential arises

in the study of dielectric slabs by electromagnetic probing.
In the earth, however, the velocity $c(z)$ tends to a value c_1
larger than the surface velocity c_0. Correspondingly, the
potential $V(z)$ tends to a positive constant V_1,

$$
\begin{aligned}
V_1 &= k_0^2 \left(1 - \frac{c_0^2}{c_1^2}\right) \\
&= k_0^2 - k_1^2 \quad .
\end{aligned}
$$

(4.29)

Therefore the Gelfand-Levitan inversion does not really
apply, and a scattering solution is needed that allows a non-
zero end potential. In the next section, we present our
approach to this problem.

4.3 Non Zero Final Potential

To accommodate to a non-zero V_1, we now consider the
fundamental solution of the Schrödinger equation $u_1(z,p)$
defined asymptotically as

$$
u_1(z,p) \sim e^{ip'z} \qquad z \to \infty
$$

(4.30)

where

$$
p' = \sqrt{p^2 - V_1} \quad .
$$

We assume $\text{Im}p' > 0$, in order to satisfy the radiation condition at ∞. The Volterra integral equation representation of $u_1(z,p)$ in eq. 4.6 is modified to

$$u_1(z,p) = e^{ip'z} - \int_z^\infty \frac{\sin p'(z-z')}{p'}[V(z)-V_1]u_1(z',p)dz' \qquad (4.31)$$

while the integral equation representation of $u_2(z,p)$ is unchanged

$$u_2(z,p) = e^{-ipz} + \int_{-\infty}^z \frac{\sin p(z-z')}{p} V(z)u_2(z',p)dz' \quad . \qquad (4.32)$$

4.3.1 Asymptotic Behavior

The key observations to be made relative to eq. 4.31 is that since $u_1(z,p)$ is the solution of a Volterra equation of the second kind with square integrable kernel, the method of successive approximation will converge. That observation has in fact been applied by D. Stickler[7] in connection with the Deift-Trubowitz inversion procedure; thus, we have

$$u_1(z,p) = \left[1 - \frac{V(z)-V_1}{(2ip)^2}\right] e^{ipz - \frac{iV_1}{2p}z - \frac{1}{2ip}\int_z^\infty (V(z')-V_1)dz'} + \text{H.O.T.}^*$$
$$(\text{Im}p > 0)$$

$$(4.33)$$

---

* H.O.T. stands for higher order terms

from which the transmission coefficient t(p) can be deduced

$$t(p) = \left(1 - \frac{V_1}{(2ip)^2}\right) e^{i\frac{V_1 z_0}{2p} + \frac{1}{2ip}\int_{-\infty}^{z_0} V(z')dz' + \frac{1}{2ip}\int_{z_0}^{\infty}(V(z')-V_1)dz'} + \text{H.O.T.}$$

$$(4.34)$$

where z_0 is arbitrary.

Similarly, $(\text{Im} p > 0)$

$$u_2(z,p) = \left(1 - \frac{V(z)}{(2ip)^2}\right) e^{-ipz - \frac{1}{2ip}\int_{-\infty}^{z} V(z')dz'} + \text{H.O.T.} \qquad (4.35)$$

4.3.2 Inversion Procedure

We are now ready to present the inversion procedure for $V_1 > 0$. Note that the basic relation (eq. 4.28) still holds for $V_1 > 0$,

$$t(p)u_1(z,p) = r(p)u_2(z,p) + u_2(z,-p) \qquad (4.36)$$

Following Faddeev's[16] case of $V = 0$, for the case of $V_1 > 0$, a function $h(z,p) = u_2(z,p)e^{ipz}$ is introduced. The expression for $u_2(z,p)$ (eq. 4.35) shows that $h(z,p)-1$ is analytic in the upper half plane and $\text{Im}(p) > 0$ and $\to 0$ as $|p| \to \infty$. We thus obtain $(\varepsilon \to 0+)$

$$h(z,p)-1 = \frac{1}{2\pi i} \int_{-\infty}^{\infty} \frac{h(z,p')-1}{p'-p-i\varepsilon} \quad , \tag{4.37}$$

or using (eq. 4.36)

$$h(z,p)-1 = \frac{1}{2\pi i} \int_{-\infty}^{\infty} dp' \frac{t(p')u_1(z,p')e^{-ip'z}-1}{p'+p+i\varepsilon}$$

$$- \frac{1}{2\pi i} \int_{-\infty}^{\infty} \frac{r(p')u_2(z,p')e^{-ip'z}}{p'+p+i\varepsilon} dp' \tag{4.38}$$

The first integral in (eq. 4.38) is zero since

$$t(p)u_1(z,p)e^{-ipz}-1= - \frac{V(z)}{(2ip)^2} e^{\frac{1}{2ip}\int_{-\infty}^{z} V(z')dz'} + \text{H.O.T.} \tag{4.39}$$

thus

$$h(z,p) - 1 = - \frac{1}{2\pi i} \int_{-\infty}^{\infty} \frac{r(p')u_2(z,p')e^{-ip'z}}{p'+p+i\varepsilon} dp' \quad . \tag{4.38a}$$

Comparing eqs. (4.37) and (4.38a), we can express $u_2(z,p')$ in the Levin representation[17],

$$u_2(z,p) = e^{-ipz} + \int_{-\infty}^{z} K(z,z')e^{ipz'}dz' \tag{4.40}$$

in which the kernel of the integral does not depend on p; i.e.,

$$K(z,y) = - \frac{1}{2\pi} \int_{-\infty}^{\infty} r(p)u_2(z,p)e^{-ipy}dp \quad . \tag{4.41}$$

Inserting (eq. 4.40) into (eq. 4.41) results in the Gelfand-Levitan type equation

$$K(z,y) + R(z+y) + \int_{-\infty}^{z} R(z'+y)K(z,z')dz' = 0 \atop y < z \tag{4.42}$$

where $R(z)$ is the Fourier transform of $r(p)$

$$R(z) = \frac{1}{2\pi} \int_{-\infty}^{\infty} r(p)e^{-ipz}dp \quad . \tag{4.43}$$

When (eq. 4.41) is substituted into the Schrödinger equation, it is found that $K(z,y)$ satisfies a partial differential equation

$$\frac{\partial^2 K}{\partial z^2} - \frac{\partial^2 K^2}{\partial y^2} - V(z)K = 0 \tag{4.44}$$

subject to the boundary conditions

$$K(z, -\infty) = 0 \tag{4.45}$$

$$V(z) = 2\frac{dK}{dz}(z,z) \quad .$$

The solution of R(z) in eq. 4.43 consists, in general, of both a continuous and a discrete part. The discrete part applies in the presence of trapped modes. In that case, additional information is required to construct R(z)

$$R(z) = \frac{1}{2\pi} \int_{-\infty}^{\infty} r(p)e^{-ipz}dp + \sum_i m_i e^{-ip_i z} . \qquad (4.47)$$

where the p_i's are the poles of $r(p)$ on the positive imaginary axis.

The choice of the constant normalization coefficients m_i is dictated by the requirement that $V(z) = 0$ for $z < 0$. This can be seen by examining the Gelfand-Levitan equation (4.42),

$$K(z,y) + R(z + y) + \int_{-\infty}^{z} R(z' + y) K(z,z')dz' = 0. \qquad (4.48)$$
$$y < z$$

We note that $R(z) = 0$ for $z < 0$ insures that $K(z,y)$, and hence that $V(z) = 2 \frac{dK}{dz}(z,z)$ are all zero for $z < 0$. The choice of m_i in (eq. 4.47) is therefore dictated by the requirement $R(z) = 0$ for $z < 0$. Now, the integral in (eq. 4.47) is for $z < 0$,

$$\frac{1}{2\pi} \int_{-\infty}^{\infty} r(p)e^{-ipz}dp = i \sum_i b_i e^{-p_i z} \qquad (4.49)$$

where the b_i's are the residues at the poles p_i of $r(p)$. Substituting for the value of the integral in (eq. 4.47), and imposing $R(z) = 0$ for $z < 0$ yields $m_i = -ib_i$.

In principle, in order to solve for R(z), an additional measurement would be required to obtain the residues b_i. However, the next section demonstrates that, in the presence of slow velocity layers in the sediment, the frequency can be selected low enough to eliminate the trapped modes (or bound states of the Schrödinger equation), and thus the continuous part of the solution for R(z) will suffice.

4.4 Bound States

The potential diagram (Fig. 3) indicates that bound states may occur due to the presence of a low velocity zone near the water sediment interface. Bound states are square integrable solutions of Schrödinger's equation and, as will be shown later, present considerable difficulty in the inversion procedure. The number of bound states M was obtained by Bargmann[59]

$$M < \int_0^\infty z \left| V_-(z) \right| dz < M + 1 \qquad (4.50)$$

where $V_-(z)$ is the negative portion of the potential for z > 0. It is clear that the number of bound states is determined by the width of the low velocity zone (prescribed by the geology) and by the depth of the potential well which is a function of the frequency at which the experiment is conducted.

To eliminate bound states, we impose the condition:

$$\int_0^\infty z|V_-(z)|dz < 1 \quad . \tag{4.51}$$

Now,

$$\int_0^\infty z|V_-(z)|dz < \frac{1}{2}\ell^2|V_-(z)|_{max} \tag{4.52}$$

where ℓ is the width of the well and $|V_-(z)|_{max}$ its maximum depth:

$$|V_-(z)|_{max} = \left|\frac{\omega^2}{c_0^2}\left(1 - \frac{c_0^2}{c_{min}^2}\right)\right| \tag{4.53}$$

The condition expressed by eq. (4.12) is satisfied when

$$\left(\frac{\ell\omega}{c_0}\right) \quad \left|1 - \frac{c_0^2}{c_{min}^2}\right| < \sqrt{2} \tag{4.54}$$

In particular, for $\dfrac{\ell\omega}{c_{min}} < \sqrt{2}$, there will be no trapped modes. This simplified condition is a refinement of Stickler's result that $\left(\frac{\ell\omega}{c_0}\right)$ should be sufficiently small (4.50). We have found that either of the two simplified conditions is too restrictive in practice and one should use our full equation (4.54). Hamilton has studied the characteristics of surface sound channels in marine sediments[60]. The velocity ratio $R = (c_{min}/c_0)$ ranges from 0.984 for pelagic clay to 0.99 for terrigeneous sediments, while the height of the channel depends on the velocity gradient a

$$\ell = c_0(1 - R)/a \quad . \tag{4.55}$$

Therefore, for $R \sim 1$, the condition of zero bound states (eq. 4.54) can be written

$$\omega < a(1 - R)^{-3/2} \quad . \tag{4.56}$$

A marked improvement in the bound obtains if a linear velocity profile

$$c(z) = az + c_{min} \tag{4.57}$$

with

$$c(\ell) = c_0$$

is assumed in the condition of zero bound states (eq. 4.51). The corresponding potential is then

$$V(z) = -k_0^2 \left(1 - \frac{c_0^2}{\left(az + c_{min} \right)^2} \right) \quad \text{for} \quad 0 < z < \ell \tag{4.58}$$

Substituting this $V(z)$ into eq. 4.51 and integrating by parts yields

$$- \frac{\omega^2}{a^2} \left[(1-R) + \frac{1}{2} (1-R)^2 + \ln R \right] < 1 \quad . \tag{4.59}$$

For $R \sim 1$,

$$- \ln R \approx (1-R) + \frac{1}{2} (1-R)^2 + \frac{1}{3} (1-R)^3 \tag{4.60}$$

Therefore,

$$\omega < a\sqrt{3} \; (1-R)^{-3/2} \tag{4.61}$$

Table I presents the upper bound on the probing frequency with the condition of zero bound states for representative values* of a and R in the abyssal plain environment[60]. The current frequency of operation[2], 220 Hz, is low enough to eliminate the bound states in clayey silt and silty clay. It is assumed that for operations in clay sediments, an acoustic source will be available at about half the current frequency which would be sufficient to do away with the possible bound states.

---

* The velocity gradient (a) can assume values over a wider range than shown in Table I. For instance, Frisk et al.,[4] have inferred from experimental data that (a) ranged for $0.5s^{-1}$ to $2.9s^{-1}$ at three locations in the Icelandic Basin.

Table I: Upper bound on the probing frequency for
the condition of zero bound states as a
function of velocity ratio, R, and
velocity gradient, a.

R a	Clayey Silt 0.999	Silty Clay 0.99	Clay 0.984
$1s^{-1}$	8.7 kHz	275 Hz	136 Hz
$1.2s^{-1}$	10.4 kHz	330 Hz	162 Hz
$1.3s^{-1}$	11.3 kHz	358 kHz	176 Hz

CHAPTER V

NUMERICAL SOLUTION OF THE GELFAND-LEVITAN EQUATION

5.1   Introduction

The Gelfand-Levitan Equation

$$R(z+y) + K(z,y) + \int_{-\infty}^{z} K(z,z') \, R(y+z') \, dz' = 0$$

$$(5.1)$$

is a Fredholm equation of the second kind in the variable y
with z regarded as a parameter.   The object of this chapter is
to present three methods of computing $K(z,z)$ and hence to
reconstruct the potential $V(z)$.

5.2   Series Expansion

A parameter λ is introduced in the Gelfand-Levitan
equation

$$R(z+y) + K(z,y) + \lambda \int_{-y}^{z} K(z,z') \, R(y+z') dz' \qquad (5.2)$$

and a solution is sought by a method of successive approxima-
tions.   The solution is written as a power series in λ

$$K(z,y) = K_0(z,y) + \lambda K_1(z,y) + \lambda^2 K_2(z,y) + \ldots$$

$$(5.3)$$

Integrating term by term and equating coefficients of equal power of λ one gets

$$K_O(z,y) = -R(z+y) \tag{5.4}$$

$$K_1(z,y) = - \int_{-y}^{z} R(y+z') \, K_O(z,z')dz' \tag{5.5}$$

and in general

$$K_n(z,y) = - \int_{-y}^{z} R(y+z') \, K_{n-1}(z,z')dz' \tag{5.6}$$

The theory of Volterra integral equations of the second kind demonstrates that the series is convergent for all λ when the norm of R,

$$||R|| = \int_{-z}^{z} R^2(z+y)dy \tag{5.7}$$

exists.[61] But, Parseval's identity indicates that $||R||$ is always finite since

$$||R|| \leqslant \int_{-\infty}^{\infty} R^2(y)dy = \frac{1}{2\pi} \int_{-\infty}^{\infty} |b(p)|^2 dp \tag{5.8}$$

Hence, $b(p)$, given $|b(p)| \leqslant 1$ and $b(p) \xrightarrow[p \to \infty]{} (1/p^2)$, is square integrable.

- 87 -

The $K_n(z,y)$ are bounded by

$$|K_n(z,y)| < ||R||^2 \sqrt{\frac{AB^{(n-1)}}{(n-1)!}} \qquad (5.9)$$

where $A = \int_{-y}^{z} R^2(y+z')dz'$ and $B = \int_{-y}^{z} \int_{-y}^{z} dy'dy'' R^2(y'+y'')$

5.2.1 The Potential

The expansion of $K(z,y)$ yields a corresponding expansion for the potential $V(z) = 2 \frac{dK(z,z)}{dz}$,

$$V(z) = V^{(0)} + V^{(1)} + V^{(2)} + \ldots \qquad (5.10)$$

where,

$$V^{(0)} = 2 \frac{dK_o}{dz}(z,z) = -2 \frac{dR}{dz}(2z) \qquad (5.11)$$

$$V^{(1)} = 2 \frac{dK_1}{dz}(z,z) = 4R^2 (2z) \qquad (5.12)$$

The computation of $V^{(2)}$ is more involved and is presented here for reference purposes

$$K_2(z,y) = \int_{-y}^{z} \int_{-z'}^{z} R(y+z') \ R(z'+z'') \ R(z+z'')dz''dz'$$

$$(5.13)$$

which can be written

$$K_2(z,y) = \int_{-z'}^{z} dz' \; \Phi(z,z') \qquad (5.14)$$

where

$$\Phi(z,z') = \int_{-z'}^{z} R(z+z') \; R(z'+z'') \; R(z+z'') \; dz'' \qquad (5.15)$$

Therefore,

$$\frac{dK_2}{dz}(z,z) = \Phi(z,z) + \phi(z,-z) + \int_{-z}^{z} dz' \; \frac{\partial \Phi}{\partial z}(z,z')$$

$$(5.16)$$

But,

$$\phi(z,-z) = 0 \qquad (5.17)$$

and

$$\Phi(z,z) = R(2z) \int_{0}^{2z} R^2(z')dz' \qquad (5.18)$$

$$\frac{\partial \Phi}{\partial z}(z,z') = R(2z) \; R^2(z+z') + R(z+z') \int_{-z'}^{z} \frac{\partial}{\partial z}(R(z+z'')) R(z'+z'')dz''$$

$$(5.19)$$

Finally,

$$V^{(2)}(z) = 4R(2z) \int_0^{2z} R^2(z')dz' +$$

$$+ 2 \int_{-z}^{z} \int_{-z'}^{z} R(z+z') \ R(z'+z'') \ \frac{\partial R}{\partial z}(z+z')dz''dz' \tag{5.20}$$

$V^{(2)}(z)$ displays the global character of the higher order

terms (which become increasingly unwieldy).

To summarize, the following approximation will be used

$$\hat{V}(z) = -2\frac{dR}{dz}(2z) + 4R^2(2z) \tag{5.21}$$

5.2.2 Connection with Other Formulations

To first order,

$$\hat{V}(z) = -2\frac{dR}{dz}(2z) \tag{5.22}$$

which can be written in terms of the reflection coefficient

$b(p)$

$$\hat{V}(z) = \frac{2i}{\pi} \int_{-\infty}^{\infty} pb(p)e^{-i2pz}dp. \tag{5.23}$$

Recall the expression for the reflection coefficient

$$b(p) = \frac{1}{2ip} \int_{-\infty}^{\infty} e^{ipz'} V(z') \; \Phi(z')dz' \qquad (5.24)$$

The Born approximation $\Phi(z') \simeq e^{ipz'}$ results in

$$b(p) \simeq \frac{1}{2ip} \int_{-\infty}^{\infty} V(z') e^{2ipz'} dz' \qquad (5.25)$$

Taking a Fourier transform of both sides leads to

$$V(z) = \frac{2i}{\pi} \int_{-\infty}^{\infty} pb(p) e^{-2ipz} dp \qquad (5.26)$$

That is the result obtained by Cohen and Bleistein (45). The first order approximation to $V(z)$ in the Gelfand-Levitan formulation is therefore the Born approximation.

Stickler's inverse procedure entails the solution of the coupled equations

$$\begin{cases} -u''_z - \tilde{q}(z)u_2 = p^2 u_2 \\[2ex] \tilde{q}(z) = \frac{2i}{\pi} \int_{-\infty}^{\infty} pb(p) \; u_2^2(z,p) \, dp \end{cases} \qquad (5.27)$$

The auxiliary potential $\tilde{q}(z)$ is identical to $V(z)$ and $u_2(z,p)$ is the solution that satisfies $u_2(z,p) = e^{-ipz}$, $z \to -\infty$. To first order assume $u_2(z,p) = e^{-izp}$ and obtain once again,

$$\tilde{q}(z) = \frac{2i}{\pi} \int_{-\infty}^{\infty} pb(p)e^{-2ipz}dp \qquad (5.28)$$

5.2.3 Algorithm

The first step is, of course, the computation of the Fourier transform of the data,

$$R(z) = \frac{1}{2\pi} \int_{-\infty}^{\infty} b(p)e^{-ipz}dp, \qquad (5.29)$$

followed by a straightforward computation of

$$\hat{V}(z) = -2\frac{dR}{dz}(2z) + 4R^2(2z) \qquad (5.30)$$

Observe that determining the potential at depth z requires data at depth $2z$. The truncation of the series leads to a deterioration of the estimate of $V(z)$ with depth. In particular, since $b(p)$ is integrable, $R(z)$ tends to zero as $z \to \infty$ (Riemann-Lebesgue theorem) and it follows that $\hat{V}(z) \to 0$ at depth even when the potential $V(z)$ tends to a non-zero final potential V_f.

- 92 -

5.3   Uniqueness of the Solution

Suppose there were two solutions of the Gelfand-Levitan equation, $K(z,y)$ and $K'(z,y)$

$$K(z,y) + R(z+y) + \int_{-y}^{z} K(z,z')\, R(y+z')\, dz' = 0$$

$$K'(z,y) + R(z+y) + \int_{-y}^{z} K'(z,z')\, R(y+z')\, dz' = 0 \qquad (5.31)$$

Then $\hat{K}(z,y) = K(z,y) - K'(z,y)$ satisfies a homogeneous Volterra equation of the second kind

$$\hat{K}(z,y) = \int_{-y}^{z} \hat{K}(z,z')\, R(y+z')\, dz' \qquad (5.32)$$

Since $R(z)$ is square integrable (cf. Ch.III), it follows [61] that this equation has only the trivial solution $\hat{K}(z,y) = 0$ and therefore the solution of the Gelfand-Levitan equation is unique.

5.4   Finite Difference Methods

The natural way to solve the Gelfand-Levitan equation is to discretize it by converting the integral into a sum

$$K(n,m) + R(n+m) + h \sum_{i=-m}^{n} w_i K(n,i)\, R(m+i) = 0 \qquad (5.33)$$

where w_i are the weights in an appropriate quadrature formula. For the trapezoidal rule, w_i is $\frac{1}{2}$ at the end points and 1 in between

$$K(n,m) + R(n+m) + h \sum_{i=-m}^{n} K(n,i) R(i+m)$$

$$- \tfrac{1}{2}h(R(0)K + R(n+m) K(n,n)) = 0 \qquad (5.34)$$

and since $R(0) = 0$

$$K(n,m) + h \sum_{i=1-m}^{n} K(n,i) R(i+m) + R(n+m)[1 - \tfrac{h}{2}(n,n)] = 0$$

$$(5.35)$$

To solve for $K(n,n)$, one has to solve the Ware and Aki (21) type matrix equation,

$$(I + h\hat{R})K = b \qquad (5.36)$$

$(I + h\hat{R})$ can be inverted by Gauss elimination. A more efficient algorithm has been presented by Berryman and Greene (26) who put the equation in the form:

$$\mathbf{I} + h \begin{bmatrix} & & R_1 \\ & & R_1 R_2 \\ & & \cdot \\ & & \cdot \\ & & \cdot \\ R_1 R_2 \ldots R_{2n} & & \end{bmatrix} \begin{bmatrix} hk(n, -n+1) \\ \cdot \\ \cdot \\ \cdot \\ hk(n,n-1) \\ 1+hk(n,n) \end{bmatrix} = \begin{bmatrix} 0 \\ \cdot \\ \cdot \\ \cdot \\ 0 \\ 1 \end{bmatrix}$$

$$(5.37)$$

where $k(n,m) = \dfrac{K(n,m)}{1-\frac{h}{2}K(n,n)}$ (5.38)

To obtain the potential at depth $n - \frac{1}{2}$,

$$q_{n-\frac{1}{2}} = \frac{2}{h}[K(n,n) - K(n-1,\ n-1)] \qquad (5.39)$$

one needs to invert a $(2n-2) \times (2n-2)$ matrix for $K(n-1,n-1)$ followed by the inversion of a $(2n) \times (2n)$ matrix for $K(n,n)$. In fact, since the object is to reconstruct the potential down to depth nh, a succession of matrices of increasing size have to be inverted. The Berryman and Greene algorithm is similar to the Levinson algorithm for the inversion of Toeplitz matrices (22). The method proceeds by recursion; given the solution of the $(2n-1) \times (2n-1)$ system, the solution of the $(2n) \times (2n)$ system is generated by using the recursion formulae:

$$\begin{bmatrix} f_i(2n) \\ g_i(2n) \end{bmatrix} = \begin{bmatrix} 1 & r_n \\ r_n & 1 \end{bmatrix} = \begin{bmatrix} f_i(2n-1) \\ g_i(2n-1) \end{bmatrix} \qquad (5.40)$$

The vectors $f(2n-1)$ and $g(2n-1)$ are defined by

$$h \begin{bmatrix} & & R_1 \\ & & R_1R_2 \\ & & \cdot \\ & & \cdot \\ & & \cdot \\ R_1 \ldots R_{2n-1} \end{bmatrix} \begin{bmatrix} f_{2n-1}(2n-1) \\ \cdot \\ \cdot \\ \cdot \\ f_1(2n-1) \\ f_0(2n-1) \end{bmatrix} = \begin{bmatrix} f_{2n-1}(2n-1) \\ \cdot \\ \cdot \\ \cdot \\ g_1(2n-1) \\ g_0(2n-1) \end{bmatrix}$$

$$(5.41)$$

and

$$h \begin{bmatrix} & & R_1 \\ & & R_1R_2 \\ & & \cdot \\ & & \cdot \\ & & \cdot \\ R_1 \ldots R_{2n-1} \end{bmatrix} \begin{bmatrix} g_{2n-1}(2n-1) \\ \cdot \\ \cdot \\ \cdot \\ g_0(2n-1) \end{bmatrix} = \begin{bmatrix} f_{2n-1}(2n-1) \\ \cdot \\ \cdot \\ f_1(2n-1) \\ f_0(2n-1)-Q_{2n-1} \end{bmatrix}$$

$$(5.42)$$

where $Q_{2n} = Q_{2n-1}(1-r_n{}^2)$

and $\quad r_{2n} = h \sum\limits_{i=0}^{2n-1} f_i(2n-1) \, R_{2n+1-i}/Q_{2n-1}$

The recursion starts with $f_0(0) = 1$ and $g_0(0) = \Delta R_1$

The solution is then,

$$K(n,n) = \frac{2}{h} \frac{1 - Q_{2n-1}(1 + r_{2n})}{1 + Q_{2n-1}(1 + r_{2n})} \qquad (5.43)$$

Berryman and Greene have suggested smoothing R(z) to obtain R(n) (26).

$$R(n) = \frac{1}{h} \int_{n-1}^{n} R(z)dz \qquad (5.44)$$

which would allow for delta functions in R(z).

5.5 Coupled Equations Method

A method to bypass the matrix inversion has been suggested by Kritikos, Jaggard and Ge who were interested in determining the dielectric permittivity of a slab from reflection measurements at normal incidence. The algorithm was tested numerically on reflection coefficients that could be represented by two and three pole Butterworth filters. The scheme uses in conjunction with the Gelfand-Levitan equation, the hyperbolic partial differential equation satisfied by K(z,y) (cf. Eq. (4.44)).

$$\frac{\partial^2 K}{\partial z^2}(z,y) - \frac{\partial^2 K}{\partial y^2}(z,y) - 2K(z,y)\frac{dK(z,z)}{dz} = 0$$

$$(5.45)$$

For simplicity, a change or coordinates is introduced

$$\begin{bmatrix} \xi \\ \eta \end{bmatrix} = \frac{1}{2} \begin{bmatrix} 1 & 1 \\ 1 & -1 \end{bmatrix} \begin{bmatrix} z \\ y \end{bmatrix} \qquad (5.46)$$

and the equations are discretized:

Gelfand-Levitan: $K_{m,n} + 2h \sum\limits_{i=2}^{m-1} K_{i+n-1,m-i+1} R_{2i-1}$

$$+ (1 + hK_{m+n-1,1}) R_{2m-1} = 0$$

$$(5.47)$$

PDE: $\quad K_{m+1,n+1} = K_{m,n+1} + K_{m+1,n} + 2h[(K_{m+1,1} - K_{m,1})-1]K_{m,n}$

$$(5.48)$$

The potential is obtained through

$$V_{m-1/2} = \frac{2}{h} (K_{m,1} - K_{m-1,1}) \qquad (5.49)$$

The point of the method is that $K_{m,1}$ can be computed directly from the Gelfand-Levitan equation without a matrix inversion since the terms within the sum can be generated via the PDE.

5.5.1 Analysis of Stability

Although it has not been possible to study the stability of the coupled system of equations, a simplified

- 98 -

analysis of the PDE may be of interest.

Let $K_{m,n} = W^m e^{ikn}$ be a Fourier component and
assume that

$$2h(K_{m+1,1} - K_{m,1}) = h^2 V_m \qquad (5.50)$$

is known. The PDE becomes

$$W^{m+1} e^{ik} = W^m e^{ik} + W^{m+1} + (h^2 V_m - 1) \qquad (5.51)$$

The amplification factor is therefore

$$\left| \frac{W^{m+1}}{W^m} \right| = \left| 1 + \frac{h^2 V_m}{e^{ik} - 1} \right| \qquad (5.52)$$

which is larger than 1 for arbitrarily small step size h or
potential V_m as $k \rightarrow 0$.

5.6   Error Estimates

5.6.1 Discretization Errors

The discretization of the Gelfand Levitan equation
is accompanied by an error $\varepsilon_{n,m}$,

$$K(n,m) + R(n+m) + h \sum_{i=-m}^{n} w_i K(n,i) R(m+i) + \varepsilon_{n,m} = 0$$

$$(5.53)$$

For the trapezoidal rule, $\quad \varepsilon = -\dfrac{h^2}{12} (KR)' \Big|_{-y}^{z}$

The equation that is actually solved is

$$\hat{K}(n,m) + R(n+m) + h \sum_{i=-m}^{n} w_i \hat{K}(n,i) \, R(m+i) = 0$$

$$(5.54)$$

Or, in matrix notation (see equation 5.37).

$$(I + hR)\hat{K} = b \tag{5.55}$$

rather than

$$(I + hR)K = b - \varepsilon \tag{5.56}$$

It follows that

$$(I + hR)(\hat{K} - K) = \varepsilon \tag{5.57}$$

For a nonsingular matrix $(I + hR)$,

$$\hat{K} - K = (I + hR)^{-1} \varepsilon \tag{5.58}$$

Taking norms,

$$||\hat{K} - K|| \leq ||(I + hR)^{-1}|| \cdot ||\varepsilon|| \tag{5.59}$$

Assuming that $||hR|| < 1$, where the norm is such that $||I|| = 1$,

$$||(I + hR)^{-1}|| \leq \frac{1}{1 - h||R||} \qquad (5.60)$$

Therefore,

$$||\hat{K} - K|| \leq \frac{\varepsilon}{1 - h||R||} \qquad (5.61)$$

Using the ∞ norm, $||\varepsilon||_{\infty} = \max |\varepsilon_i|$ and $||R||_{\infty} = \sum_{i=1}^{2n} |R(i)|$ (which also equals $||R||_i$, the absolute column sum of column (2n)).

$$||\hat{K} - K|| \leq \frac{\max |\varepsilon|}{1 - h \sum_{i=1}^{2n} |R(i)|} \qquad (5.62)$$

Since $|\varepsilon|$ is $O(h^2)$ for the trapezoidal rule, the approximate solution $\hat{K}$ converges to the exact solution K as $h \rightarrow 0$. Note that the denominator in (equation 5.62) decreases with increasing depth, hence raising the bound on $||\hat{K} - K||$.

5.6.2 Data Errors

Errors in the plane wave reflection coefficient $r(kz)$ and in its Fourier transform $R(z)$, mean that one is solving for $\hat{K}(n,m)$ in the Gelfand-Levitan equation:

$$\hat{K}(n,m) + \hat{R}(n+m) + h \sum_{i=-m}^{n} w_i \hat{K}(n,i) \hat{R}(m+i) = 0$$

$$(5.63)$$

Or in matrix notation,

$$(I + h\hat{R})\hat{K} = \hat{b} \qquad (5.64)$$

which can be written,

$$(I + hR + h\delta R)(K + \delta K) = (b + \delta b) \qquad (5.65)$$

where $\hat{R} = R + \delta R$, and $\hat{K} = K + \delta K$.

It follows that

$$\delta K = (I + (I + hR)^{-1} h\delta R)^{-1} (I + hR)^{-1} (\delta b - Kh\delta R)$$

$$(5.66)$$

Hence,

$$||\delta K|| \leq ||(I + hr)^{-1}|| \cdot ||(I + (I + hR)^{-1} h\delta R)^{-1}||$$

$$\cdot (||\delta b|| + h||\delta R|| \cdot ||K||)$$

$$(5.67)$$

or,

$$||\delta K|| \leq \frac{1}{1 - h(||R|| + ||\delta R||)} (||\delta b|| + h||K|| \cdot ||\delta R||)$$

$$(5.68)$$

As the errors in R(z) increase, the bound on $\|\delta K\|$ also increases. Moreover, it is clear that as depth increases $\|R\|_\infty = \sum\limits_{i=1}^{2n} |R(i)|$ also increases raising the bound on the relative error $\|\delta K\|/\|K\|$.

5.6.3 Errors in the Potential

The discrete version of the potential yields:

$$|\delta V(n)| \leq \frac{2}{h} (|\delta K(n,n)| + |\delta K(n-1,\ n-1)|) \qquad (5.69)$$

In the absence of data error δR, $|\delta V(n)| \to 0$ as the sampling interval $h \to 0$ since the quadrature error ε is $O(h^2)$ (see equation 5-62).

CHAPTER VI

NUMERICAL RESULTS

The derivation of the plane-wave reflection coefficient from pressure measurements for the setup of the Frisk experiment was the subject of Mook's thesis[64]. Unfortunately, the attempt by Mook to apply his technique to one set of experimental data yielded reflection coefficients higher than one; such a result is not consistent with physical requirements ($|R| < 1$). It is not yet clear whether Mook's problem lay with improper modeling of the experimental setup, with the imprecision of the data, or with the numerical techniques used to extract the reflection coefficient from the data. It should be noted, however, that the experimental data have yielded, via trial and error methods, excellent models for the acoustic parameters of the seabed[4]. This was done by assuming a seabed model, computing the pressure field and matching it up to the observations.

The starting point in our analysis is a layered model of the acoustic profile to be recovered. From this exactly known model, a plane-wave reflection coefficient is generated. The reflection coefficient is what would have been computed from Mook's method, or subsequent improvements to it, for the Frisk experiment on this particular layered seabed. The reflection coefficient is then Fourier trans-

formed via an FFT to provide the input to the Gelfand-Levitan integral equation in accordance with the theory developed in Chapter IV. The particular case of two half-spaces in contact (step discontinuity) yields a reflection coefficient which can be Fourier transformed analytically. Closed-form solutions for the Born and Improved Born approximations to the inverse solution are also obtained for that case.

More generally, the Gelfand-Levitan equation is solved numerically to yield the potential and velocity profiles.

We have concentrated our efforts on the study of the Gelfand-Levitan inverse method using synthetic data for which the correct answer is known. The comparison of the reconstructed profile with the known original profile allows us to assess the impacts of limited aperture, frequency, profile, noise, density and path loss on the accuracy of the numerical schemes described in Chapter V.

6.1 Generation of the Reflection Coefficient

The first step in the evaluation of our approach is the generation of the reflection coefficient. With the exception of the simplest cases, the plane-wave reflection coefficient must be generated numerically. The method used is based on the Thomson-Haskell propagator matrix approach used by Mook[64], with one modification. The plane-wave reflection coefficient is obtained as a function of the vertical wave-

number ($R(k_z)$) rather than as a function of the horizontal

wavenumber ($R(k_x)$). There are two essential elements of the

propagator matrix approach: (a) dividing the acoustic

profile into homogeneous layers, and (b) selecting variables

that are continuous across interfaces. The latter is accom-

plished by choosing the pressure $P(z)$ and vertical component

of velocity $U(z)$. Within an isovelocity layer, the field can

be decomposed into up and down going waves,

$$P(z) = P_+ e^{ik_z z} + P_- e^{-ik_z z} \qquad (6.1)$$

where k_z denotes the vertical wavenumber within the homogene-

ous layer. Unlike $P(z)$, P_+ and P_- are discontinuous at an

interface. The normal component of velocity $U(z)$ is related

to $P(z)$ through one of the time-harmonic "telegraph"

equations:

$$\frac{\partial P}{\partial z} = i\omega\rho U \qquad (6.2)$$

which yields,

$$U(z) = Y_n \left[P_+ e^{ik_z z} - P_- e^{-ik_z z} \right] \quad . \qquad (6.3)$$

Where $Y_n = k_{z_n}/\omega\rho_n$ is the admittance of the homogeneous

layer n. In matrix form, equations (6.2) and (6.3) become:

$$
\begin{bmatrix} P(z) \\ U(z) \end{bmatrix} = \begin{bmatrix} e^{ik_z z} & e^{-ik_z z} \\ Y_n e^{ik_z z} & -Y_n e^{-ik_z z} \end{bmatrix} \begin{bmatrix} P_+ \\ P_- \end{bmatrix} \qquad (6.4)
$$

When $P(z)$ and $U(z)$ are known at point z_1 of the layer, one can deduce the up and down going components P_+ and P_- by inverting the matrix in (6.4)

$$
\begin{bmatrix} P_+ \\ P_- \end{bmatrix} = \begin{bmatrix} e^{ik_z z_1} & e^{-ik_z z_1} \\ -Y_n e^{-ik_z z_1} & -Y_n e^{-ik_z z_1} \end{bmatrix}^{-1} \begin{bmatrix} P(z_1) \\ U(z_1) \end{bmatrix} \qquad (6.5)
$$

(Within a homogeneous layer P_+ and P_- are, of course, constants.) One can then determine $P(z)$ and $U(z)$ at another point, say z_2, within the layer by substituting (6.5) into the right-hand side of (6.4):

$$
\begin{bmatrix} P(z_1) \\ U(z_1) \end{bmatrix} = \begin{bmatrix} \cos k_z(z_1 - z_2) & \frac{i}{Y_n} \sin k_z(z_1 - z_2) \\ iY \sin k_z(z_1 - z_2) & \cos k_z(z_1 - z_2) \end{bmatrix} \begin{bmatrix} P(z_2) \\ U(z_2) \end{bmatrix}
$$

$$(6.6)$$

or, introducing the propagator matrix Φ

$$\begin{bmatrix} P(z_1) \\ \\ U(z_1) \end{bmatrix} = \Phi_1(z_2 - z_1) \begin{bmatrix} P(z_2) \\ \\ U(z_2) \end{bmatrix} . \qquad (6.7)$$

One can now proceed from one layer to another by integration,

$$\begin{bmatrix} P(z_0) \\ \\ U(z_0) \end{bmatrix} = \underbrace{\Phi_1 \ \Phi_2 \cdots \Phi_n}_{\Phi} \begin{bmatrix} P(z_n) \\ \\ U(z_n) \end{bmatrix} \qquad (6.8)$$

Where the Φ_i's depend on the parameters of the material making up the respective layers. Mook[64] has found that the computations can be improved by modifying (6.8) to

$$\begin{bmatrix} P(z_0) \\ \\ Y_0 U(z_0) \end{bmatrix} = \prod_{i=1}^{n} \begin{bmatrix} a_i & b_i \\ \zeta_i \ b_i & \zeta_i \ a_i \end{bmatrix} \begin{bmatrix} P(z_n) \\ \\ Y_n U(z_n) \end{bmatrix} \qquad (6.9)$$

in which

$$\prod_{i=1}^{n} \begin{bmatrix} a_i & b_i \\ \zeta_i \ b_i & \zeta_i \ a_i \end{bmatrix} = \begin{bmatrix} \phi_{11} & \phi_{12} \\ \phi_{21} & \phi_{22} \end{bmatrix} \qquad (6.9a)$$

.

and where

$$\zeta_i \;=\; \frac{Y_{n-1}}{Y_n} \quad \text{is a normalized admittance}$$

$$a_i \;=\; \cos k_{z_i} h_i$$

$$b_i \;=\; -i \sin k_{z_i} h_i$$

$$h_i \;=\; \text{thickness of } i^{th} \text{ layer}$$

$$k_{zi} \;=\; \sqrt{k_n^2 - (k_0^2 - k_{z_0}^2)} \quad .$$

This has the effect of giving the two components $P(z)$ and $YU(z)$ similar scales of magnitude.

Now, the reflection coefficient $R(k_z)$ at the top inter-face is defined as

$$R(k_z) \;=\; \frac{P_{-0}}{P_{+0}} \tag{6.10}$$

Therefore by introducing (6.5) into (6.9) one obtains

$$\begin{bmatrix} P_{+0} \\ P_{-0} \end{bmatrix} \;=\; \frac{1}{2} \begin{bmatrix} 1 & 1 \\ 1 & -1 \end{bmatrix} \begin{bmatrix} \phi_{11} & \phi_{12} \\ \phi_{21} & \phi_{22} \end{bmatrix} \begin{bmatrix} P(z_n) \\ \zeta_n U(z_n) \end{bmatrix} \tag{6.11}$$

To compute the ratio in (6.10), a relation (boundary condition) is needed between $P(z_n)$ and $U(z_n)$. That relation is obtained by noticing that in the $(n + 1)^{st}$ layer, one has only down going waves. Therefore,

$$U_{n+1} = \frac{1}{\zeta_{n+1}} P(z_{n+1}) \qquad (6.12)$$

and, since $P_{n+1} = P(z_n)$, one has

$$\begin{bmatrix} P_{+0} \\ P_{-0} \end{bmatrix} = \frac{1}{2} \begin{bmatrix} \phi_{11} + \phi_{21} & \phi_{12} + \phi_{22} \\ \phi_{11} - \phi_{21} & \phi_{12} - \phi_{22} \end{bmatrix} \begin{bmatrix} 1 \\ \zeta_{n+1} \end{bmatrix} P_{n+1} \qquad (6.13)$$

which yields the reflection coefficient

$$R(k_z) = \frac{P_{-0}}{P_{+0}} = \frac{\phi_{11} - \phi_{21} + \zeta_{N+1}(\phi_{12} - \phi_{22})}{\phi_{11} + \phi_{21} + \zeta_{N+1}(\phi_{12} + \phi_{22})} . \qquad (6.14)$$

Mook[64] has also found it advantageous to scale the layer propagation matrices so that the largest element value in a given layer matrix is 1.

The values of admittance for three terminations are readily identified: hard bottom ($Y_{n+1} = 0$), soft bottom

$(Y_{n+1} = \infty)$, and isovelocity termination $(Y_{n+1} = Y_n)$.
Although of theoretical interest, and of possible applicability to other situations, the soft bottom case has no application in the ocean bottom problem discussed here.

The division of the acoustic profile into homogeneous layers is done in a way akin to quadrature formulae in numerical integration using thinner, closely-spaced, layers in regions of rapid change in the acoustic parameters and thicker, wider-spaced layers in regions of slow change. We have found that the common rule of thumb, ten layers per wavelength, although satisfactory in general, is probably too conservative. We have found that for complicated profiles, where the reflection coefficient was required for a large number of values of k_z, the computation of the plane-wave reflection coefficient constituted the most time-consuming step in modeling the whole inversion procedure. Clearly, this step, is inherent only in our analytical evaluation of the inversion problem; when reflection coefficients are being processed from measurements, this step will be eliminated.

In order to test our inverse procedure, we selected a few representative profiles which are defined as follows:

(a) Half-Space

The half-space profile is defined by a velocity profile $c(z)$,

$$c(z) = c_0 \quad , \quad z < 0$$
$$= c_1 \quad , \quad z > 0$$

The reflection coefficient for this profile and its Fourier transform were obtained analytically in Section (6.2).

(b) Window Profile

Although of no direct application in ocean bottom acoustics, the window profile defined by

$$c(z) = c_0 \quad , \quad z < 0$$
$$= c_1 \quad , \quad 0 < z < L$$
$$= c_0 \quad , \quad z > L$$

is a standard example used to test inverse procedures. The window profile is of particular interest in electromagnetics (dielectric slabs).

(c) Stickler Profile

Stickler[7] chose a twice continuous function to test the Deift-Trubowitz inverse method,

$$c(z) = c_0 \ , \qquad\qquad\qquad\qquad z < 0$$
$$= c_0 + (c_1 - c_0)\left(3\left(\frac{z}{L}\right)^2 - 2\left(\frac{z}{L}\right)^3\right), \quad 0 < z < L$$
$$= c_1 \ , \qquad\qquad\qquad\qquad L < z \ .$$

This profile does not support a trapped mode at any frequency.

Stickler generated the associated reflection coefficient via the Riccati equation, while we used the Thomas-Haskell procedure outlined earlier in this section. An example of the Stickler profile is shown in Fig. 10.

(d) Frisk Profile

This velocity profile is based on the results obtained by Frisk in his deep ocean bottom experiments[4]

$$c(z) = c_0 \ , \qquad\qquad z < 0$$
$$= c_0 - (c_0 - c_1)z \ , \qquad 0 < z \ z \ 1$$
$$= c_1 + \gamma z \ , \qquad\qquad 1 < z < L$$
$$= c_2 \ , \qquad\qquad\qquad z > L$$

Typical parameters used are: $c_0 = 1540$ m/s, $c_1 = 1515$ m/s, $c_2 = 1655$ m/s, $\gamma = .97$, and $L = 145$ m (see Fig. 11).

In spite of the low velocity zone near the ocean-bottom interface, this profile does not support trapped modes at the frequency used for the examples (25 Hz).

Examples of reflection coefficients are shown in the amplitude and phase diagrams of Fig. 18. Note that as we have shown in Chapter III for the uniform density case, the amplitude goes asymptotically to zero as the vertical wave-number goes to infinity.

6.2 Case of a Step Discontinuity in Potential

We have been able to obtain analytically the Fourier transform of the reflection coefficient in the case of a step discontinuity in potential, that is, in the case where the ocean bottom is a homogeneous half-space. ($V(z) = V_0$ for $z > 0$).

The reflection coefficient at a step discontinuity in potential is

$$r(k_z) = \frac{k_z - \sqrt{-V_0 + k_z^2}}{k_z + \sqrt{-V_0 + k_z^2}}$$

$$\text{(6.15)}$$

$$= \frac{[k_z - \sqrt{-V_0 + k_z^2}]^2}{V_0}$$

The Fourier transform of $r(k_z)$ is

$$R(z) = \frac{1}{2\pi} \int_{-\infty}^{\infty} r(k_z) e^{-ik_z z} dk_z$$

$$\text{(6.16)}$$

$$= \frac{i}{2\pi i} \int_{-i\infty}^{i\infty} \frac{(s - \sqrt{V_0 + s^2})^2}{V_0} e^{sz} ds$$

which in this form can be identified as a known inverse Laplace transform[65],

$$R(z) = -\frac{2}{z} J_2 (\sqrt{V_0} z) \qquad \text{(6.17)}$$

Thus, in this particular case, one can proceed to the Gelfand-Levitan procedure with an input which is as accurate as the computation of the Bessel function, and therefore, this approach removes any inaccuracies which may be

-115-

introduced either in the computation of the reflection coefficient or in that of its Fourier transform.

Figs. 12a,b,c represent the reflection coefficient of eq. 6.15 and its Fourier transform for a half-space (eq. 6.17).

As a matter of fact, we have illustrated in Figs. 13 and 14b reconstructions of the step discontinuity using the exact analytical expression (eq. 6.17) for the Fourier transform of the reflection coefficient and the numerically devised transform in accordance with the method discussed in Section 6.1. It can be seen that our reflection coefficient method yields results as accurate as the Bessel function expression.

6.2.1 Approximate Solution of the Gelfand-Levitan Equation for a Step Discontinuity

Continuing with the case of a homogenous half-space, or step discontinuity, the "Improved Born" approximation presented in Chapter V can be now readily obtained in terms of Bessel functions

$$\hat{V}(z) = -2\frac{dR}{dz}(2z) + 4R^2(2z)$$

<div align="right">(6.18)</div>

$$= 4\frac{\sqrt{V_0}}{z} J_1(2\sqrt{V_0}z) - \frac{6}{z^2} J_2(2\sqrt{V_0}z) - \frac{4}{z^2} J_2^2(2\sqrt{V_0}z) \ .$$

<div align="center">Born   Correction Term</div>

<div align="center">Improved Born   .</div>

From the asymptotic behavior of the Bessel functions, we know that,

$$J_1(\zeta) \xrightarrow[\zeta \to \infty]{} \sqrt{\frac{2}{\pi\zeta}} \cos\left(\zeta - \frac{3\pi}{4}\right)$$

and

<div align="right">(6.19)</div>

$$J_2(\zeta) \xrightarrow[\zeta \to \infty]{} \sqrt{\frac{2}{\pi\zeta}} \cos\left(\zeta - \frac{5\pi}{4}\right) \quad .$$

Hence, we can deduce the asymptotic behavior of the reconstructed potential,

$$\hat{V}(z) \xrightarrow[z \to \infty]{} 0 \quad as(z^{-3/2})$$

<div align="right">(6.20)</div>

which recalls the limitation of the Improved Born approximation, already mentioned in Chapter V, that $\hat{V}(z) \xrightarrow[z \to \infty]{} 0$, even in the case of a finite terminal potential.

On the other hand, the asymptotic behavior of the Bessel functions near the origin is

$$J_1(\zeta) \xrightarrow[\zeta \to 0]{} \frac{1}{2}\zeta$$

(6.21)

$$J_2(\zeta) \xrightarrow[\zeta \to 0]{} \frac{1}{8}\zeta^2$$

and therefore, substituting in (6.18) the reconstructed potential $\hat{V}(\zeta)$ tends to the exact potential near the origin,

$$\hat{V}(z) \xrightarrow[z \to 0]{} V_0$$

(6.22)

At the origin, the "Improved Born" correction term is zero, but its contribution to the accuracy of the results becomes progressively more important as z increases.

We illustrate the Improved Born approximation in Fig. 12d along with the Standard Born approximation and the Correction Term. The substantial improvement due to the Correction Term in (6.18) over the standard Born approximation is clearly visible in the half-space case. Moreover, our Improved Born approximation results in a more accurate reconstruction of the acoustic velocity profile to further depth. The other features of the approximation are also visible, i.e., excellent reconstruction near the origin and

deterioration of the reconstructed velocity with depth (the potential $V \to 0$ as $z \to \infty$ means that $c(z) \to c_0$, the water acoustic velocity as $z \to \infty$). The Improved Born is also illustrated in the case of a Stickler profile in Figs. 28 and 29.

6.3 Fourier Transform of the Reflection Coefficient

The Gelfand-Levitan algorithm requires as an input the Fourier transform, $R(z)$, of the reflection coefficient $r(k_z)$,

$$R(z) = \frac{1}{2\pi} \int_{-\infty}^{\infty} r(k_z) e^{-ik_z z} dk_z \qquad (6.23)$$

which requires a knowledge of $r(k_z)$ over the whole line $-\infty < k_z < \infty$. But the symmetry property demonstrated in Chapter III (eq. 3.6),

$$r(-k_z) = r^*(k_z) \qquad (6.24)$$

reduces the requirement to a knowlege of $r(k_z)$ over the half-line $0 < k_z < \infty$. It follows that

$$R(z) = \frac{1}{2\pi} \int_{0}^{\infty} r(k_z) e^{-ik_z z} dk_z + \text{complex conjugate} \qquad (6.25)$$

is real, and therefore all the quantities involved in the Gelfand-Levitan algorithm are also real.

Theoretically, $r(k_z)$ can be calculated for a given acoustic model over the range $0 < k_z < \infty$. In practice, samples of $r(k_z)$ are given over a finite range $a < k_z < b$, and presumably this range is restricted to real angles $0 < k_z < k_0$, where $k_z = 0$ corresponds to grazing incidence and $k_z = k_0$ (the water wavenumber) corresponds to vertical incidence. It is useful to study the behavior of the Fourier transform under different restrictions imposed upon the knowledge of the reflection coefficient such as limited angular aperture and different sampling densities.

6.3.1 Fast Fourier Transform

The computation of the FFT for reflection coefficients $r(k_z)$ computed over $0 < k_z < a$, including the case where $a > k_0$ (corresponding to complex angles of incidence), does not present difficulties. The adopted algorithm uses time decomposition with input bit reversal[66]. In fact, for the acoustic profiles tested, $a = 2$ or 3 k_0 was sufficient as the asymptotic decay of the reflection coefficient with increasing k_z was even more rapid than the $(1/k_z^2)$ derived in Chapter III. The errors in the imaginary part of the FFT, which are of the order of 10^{-8} (single precision), are negligible, and therefore the real part of the FFT and its amplitude are interchangeable on the plotted results.

6.3.2 Limited Angular Aperture

Since it is not practical to have the sampling process cover the entire non-zero portion of $r(k_z)$, it is useful to study the effect of limited angular aperture, i.e., $r(k_z)$ given over the finite range $a < k_z < b$, on $R(z)$, the Fourier transform of $r(k_z)$. The Fourier transform is affected by the nature of $r(k_z)$ and by the degree of truncation.

For N sampling points spaced Δk_z apart, the total sampling interval T covered is $N \cdot \Delta k_z$. This corresponds to an angular aperture of $\alpha = \sin^{-1}\left(\frac{N\Delta k_z}{k_0}\right)$, when $k_z = 0$ is within the known aperture (i.e., $90° > \theta > \cos^{-1}(N\Delta k_z/k_0)$). Note that for $T > k_0$, $\cos(T/k_0) > 1$, and the aperture includes all real angles plus complex angles. Now, the Fourier transform of $r(k_z)$ can be written

$$R(z) = \frac{1}{2\pi} \int_0^T r(k_z) e^{-ik_z z} dk_z + \frac{1}{2\pi} \int_T^\infty r(k_z) e^{-ik_z z} dk_z$$

(6.26)

$$= R_1(z) + R_2(z) \quad .$$

$R_1(z)$ is the part of $R(z)$ that is approximated by the discrete Fourier transform (N samples).

$R_2(z)$ represents the error incurred due to the limited angular aperture. The energy lost in the process,

$$F = \int_T^\infty |R_2(z)|^2 dz \qquad (6.27)$$

can be computed on synthetic examples. Due to the precipitous drop in $r(k_z)$ beyond k_c, the wavenumber corresponding to the critical angle $\theta_c = \sin^{-1}(\frac{c_0}{c_f})$, and due to the asymptotic behavior of $r(k_z)$ for large k_z, it is readily shown on computer simulations that a knowledge of $r(k_z)$ over real angles is adequate for most cases. In fact, there is little change in the reconstructed profile as more angles are included beyond the real ones. On the other hand, as the angular aperture is restricted, the profile reconstruction, via the Gelfand-Levitan method, produces a smoothed out version of the original profile. This low-pass filtering phenomenon is best understood by interpreting the effect of a finite aperture as a low-pass filtering of the original velocity profile. This may be seen from the Born approximation eq. (5.26),

$$\hat{V}(z) = \frac{2i}{\pi} \int_{-\infty}^\infty k_z r(k_z)\, e^{-2ik_z z}\, dk_z$$

where $\hat{V}(z)$ and $k_z r(k_z)$ form a Fourier transform pair; windowing $r(k_z)$ signifies low-pass filtering $\hat{V}(z)$ and therefore yields a smoothed out velocity profile. The Gelfand-Levitan reconstruction can then be interpreted as an unfiltered, faithful reconstruction of the smoothed out original. Severe degradation of the reconstruction is

-122-

observed when the angle of incidence is restricted to $90° > \theta > \theta_c$ (angular aperture $\alpha < (90°-\theta_c)$). This is easily understood, as the critical angle region contributes substantially to the reflection coefficient. A cursory examination of reflection profiles will demonstrate this point.

A series of figures displays the progressive deterioration in profile reconstruction as the angular range is restricted. The evolution from Fig. 19 ($k_{z_{max}} = .512$, complex angle of incidence) to Fig. 20 ($k_{z_{max}} = 0.128$), and Fig. 21 ($k_{z_{max}} = 0.064$, $\theta = 51.13°$) where $k_{z_{max}} > k_{z_{critical}} = 0.0373$ ($\theta_c = 68.5°$) shows that only small changes take place and that these changes are confined for the most part to the velocity drop region near the ocean bottom interface. However, as the angles are further restricted to beyond the critical angle ($k_{z_{max}} < k_{z_{critical}}$) major changes do occur as seen in Fig. 22 ($k_{z_{max}} = .032$, $\theta = 71°$) and Fig. 23 ($k_{z_{max}} = 0.016$, $\theta = 80.9°$). The examination of the impact of limited angular aperture in this case leads us to expect, in practice, a good reconstruction of acoustic velocity profiles from reflection data restricted to real angles ($0 < \theta < 90°$).

6.3.3 Sampling

The sampling rate to be chosen is governed by three competing considerations:

(a) Adequate sampling in the k_z-domain to avoid aliasing in the Fourier transform of $r(k_z)$.

(b) Adequate sampling in the z-domain to obtain a stable and accurate Gelfand-Levitan numerical reconstruction.

(c) Adequate sampling in the z-domain to obtain the necessary resolution in the reconstructed profile.

Each of these points is discussed next.

(a) Aliasing

Since the Fourier transform of the reflection coefficient, as is the rule with spectra of transients, tends to be smooth and approaches zero asymptotically as k_z increases to infinity, the sampling interval Δk_z is chosen so that essentially all, rather than all, the spectral content of the waveform is contained below $1/(2\Delta k_z)$. For a box-like reflection coefficient of width $2 \cdot k_{critical}$ where $k_{critical}$ corresponds to θ_{crit}, the bandwidth is proportional to $1/(2 k_{critical})$ which indicates that an appropriate sampling interval should be a fraction of $k_{critical}$. One should note

-124-

however, that in the context of an actual experiment, the
choice of Δk_z is not as straightforward. The reflection
coefficient $r(k_z)$ is obtained from $r(k_r)$, the reflection
coefficient as a function of horizontal wavenumber k_r,

$$k_r^2 + k_z^2 = k_0^2 \ . \tag{6.28}$$

The sampling interval in k_r is determined by the maximum
distance, D, between source and receiver during the
experiment

$$\Delta k_r = \frac{\pi}{D} \ . \tag{6.29}$$

It is clear that a uniform sampling in k_r does not lead
to a uniform sampling in k_z,

$$\frac{dk_z}{dk_r} = - \tan \theta_{inc} \ , \tag{6.30}$$

which also shows that the problem is particularly severe near
$\theta_{inc} = \pi/2$ (grazing). On the other hand $r(k_z)$ near grazing
is well known, $r(k_z) \approx -1$. A useful way to look at the
problem is to represent the dispersion relation in the
$(k_r - k_z)$ plane which clearly shows the increase in Δk_z as k_r
goes from 0 to k_0.

(b),(c) Sampling in the z-domain

The sampling interval in wavenumber space, Δk_z, is not chosen through aliasing considerations alone. The other consideration is the resulting resolution in the z-domain imposed by the total sampling interval T,

$$\Delta z = \frac{2\pi}{T}$$

where $T = N \, \Delta k_z$

A decrease in Δz can be effected either by a decrease in the sampling interval in the wavenumber domain Δk_z or by an increase in the number of points N. It is easier to resort to the latter method as the reflection coefficient due to its rapid decrease for large vertical wavenumbers can be conveniently padded with zeros. Moreover, the size of Δk_z, which can be varied in a synthetic experiment, is usually fixed in an actual experiment.

An examination of the reconstructions of a half-space of profile, Figs. 14-17, reveals that excellent reconstructions can be achieved for appropriate choices of N and Δz. A window reconstruction is shown in Fig. 24. The main effect of a decrease in Δz is that adequate reconstruction of the acoustic profile is possible to a greater depth. It is also true that for given sampling intervals Δk_z and Δz, an increase in the height of the velocity jump at the seafloor

results in a deterioration of the reconstruction with depth. That is evident for a half-space by comparing Fig. 14b and Fig. 17 and for the Improved Born approximation by analyzing eq. (6.18).

6.4 Frequency Scaling of the Reflection Coefficient

Although the experiment we are analyzing is mono-chromatic, it is important, for a proper choice of operating frequency, to study the behavior of the plane-wave reflection coefficient with frequency. For the simplest acoustic medium, a homogeneous half-space, the reflection coefficient is independent of frequency. As soon as a spatial scale is introduced in the acoustic medium, by inserting a layer for instance, the reflection coefficient becomes frequency dependent. This dependence, which can be expressed through the continued fraction expression of eq. (3.25), is at the heart of the Ware and Aki inverse method. In this section we show that the solution of a high frequency problem is equivalent to the solution of a scaled problem at a lower frequency.

The one-dimensional Schrödinger equation,

$$(\frac{d^2}{dz^2} + k_z^2)\phi(z) = V(z)\phi(z) \tag{6.31}$$

gives rise to the reflection coefficient

$$R(k_z) = \int_{-\infty}^{\infty} \frac{e^{ik_z z'}}{2ik_z} V(z')\phi(z')dz' \tag{6.32}$$

At a different angular frequency $\omega' = \alpha\omega_0$, with corresponding water wavenumber $k' = \alpha k_0$, the Schrödinger equation becomes

$$\left(\frac{d^2}{dz^2} + \alpha^2 k_z^2\right)\phi'(z) = V'(z)\phi'(z) \qquad (6.33)$$

where V' represents the potential at the new frequency ω'. Now, the potential is frequency dependent,

$$V_0(z) = k_0^2(1 - n^2) \qquad (6.34)$$

in which n, the index of refraction is a function of depth z. Therefore,

$$V'(z) = \alpha^2 V_0(z) \qquad (6.35)$$

yields the Schrödinger equation

$$\left(\frac{d^2}{dz^2} + \alpha^2 k_z^2\right)\phi'(z) = \alpha^2 V_0(z)\phi'(z) \quad . \qquad (6.36)$$

The change of variable $z' = \alpha z$ restores the original Schrödinger equation (6.31) albeit with a "stretched" version of the original potential,

$$\left(\frac{d^2}{dz'^2} + k_z^2\right)\phi'(z') = V_0(z'/\alpha)\phi'(z') \quad . \qquad (6.37)$$

The corresponding reflection coefficient is now

$$R'(k_z) = \int_{-\infty}^{\infty} \frac{e^{ik_z z'}}{2ik_z} V_0(z'/\alpha)\phi'(z')dz' \qquad (6.38)$$

The reflection coefficients at the experimental frequencies ω and ω' are therefore identical for a given wavenumber k_z if

$$V_0(z) = V_0(z'/\alpha) \quad . \qquad (6.39)$$

One can therefore conclude that a high frequency experiment ($\omega' > \omega$) is equivalent to a low frequency experiment with a stretched profile ($\alpha > 1$). One can therefore compare the reconstruction of a given profile at two frequencies, say ω and $\omega' = \alpha\omega$, by comparing the reconstruction at a single frequency ω of the given profile with its stretched version (stretch factor α). Now, it is a numerical fact, as seen in previous examples, that profile reconstruction via the Gelfand-Levitan algorithm deteriorates with depth. It is therefore clear, at least for simple profiles, such as a step (half-space) or a window (layer), that a lower experimental frequency entails deeper reconstruction as shown in Fig. 30. That holds for more complicated profiles, and we therefore conclude from a frequency scaling point of view that the lowering of the experimental frequency allows for deeper profile reconstruction without noticeable effects on the reconstruction of the detailed variations of the profile.

6.5 Profile Reconstruction in the Presence of Density Variations

Although the focus of this thesis has been on the reconstruction of the acoustic profile in the presence of velocity variations at a single frequency, it is useful here to show how one can extend the method to the retrieval of the velocity in the presence of density variations and also to recover the density profile.

We have shown in Chapter II (eq. (2.5)) that in the presence of smooth density variations, a change of variables retained the governing Helmholtz and Schrödinger equations with an attending redefinition of the index of refraction to account for variations in the density ρ,

$$n' = n^2 + k_0^{-2}\left(\frac{1}{2\rho} \nabla^2 \rho - \frac{3}{4}\left(\frac{1}{\rho} \nabla\rho\right)^2\right) \quad . \tag{6.40}$$

The density dependent potential to be reconstructed is now,

$$V' = k_0^2 \left(1 - n'^2\right) \tag{6.41}$$

A single frequency experiment can only hope to reconstruct $n'(z)$. To recover $n(z)$ (and therefore the velocity, $c(z)$) and $\rho(z)$ one needs to carry out the experiment at two frequencies ω_1 and ω_2 with water wavenumbers k_0 and k_1, respectively. The associated potentials are then

$$V_1(z) = k_1^2(1 - n_1'^2)$$

and   (6.42)

$$V_2(z) = k_2^2(1 - n_2'^2) \quad .$$

These potentials can be reconstructed by the application of
the Gelfand-Levitan algorithm to the corresponding reflection
coefficients. One can then obtain the difference of the
potentials,

$$V_1 - V_2 = \left(k_1^2 - k_2^2\right)(1 - n^2) \quad ,$$ (6.43)

and therefore retrieve the velocity dependent index of
refraction n(z),

$$n(z) = \frac{(V_1 - V_2)}{k_1^2 - k_2^2} - 1$$ (6.44)

and subsequently reconstruct the acoustic velocity profile,

$$c(z) = \frac{c_0}{n(z)} \quad .$$ (6.45)

One of our numerical computations, was to conduct the
two-frequency procedure on the profile of Figure 10. The
reconstruction of c(z) is shown in Figure 30i. The recon-
struction features in this case of c(z) are similar to the

-131-

constant density case. The density as function of z could in turn be recovered by solving the differential equation (6.40) for $\rho(z)$ given $n(z)$.

Density discontinuities invalidate the asymptotic behavior of the reflection coefficient presented in Chapter III. In fact, the reflection coefficient is generally not integrable, and one has to introduce generalized functions in its Fourier transform. The attending difficulties and their resolution in the Gelfand-Levitan algorithm have not been studied here.

6.6 Acoustic Attenuation

The study of the attenuation of acoustic waves in marine sediments has been studied recently by Rajan and Frisk[67] who proposed a perturbative inverse method for the recovery of the attenuation data from reflection data. Rajan has successfully inverted for the acoustic attenuation profile given the reconstructed velocity profile we had obtained through the Gelfand-Levitan algorithm[68]. Here, we shall look at the effects of intrinsic attenuation on the reconstructed acoustic profile.

Although our formulation of the model of a Frisk experiment does not include attenuation, it is possible to posit a lossy acoustic profile, generate the corresponding reflection coefficient and then run it through the Gelfand-Levitan

algorithm. As expected, for small loss ($\alpha \sim 0.001$-0.005 dB/m), the reflection coefficient, its Fourier transform, and the reconstructed profile are little affected by the perturbation (see Figs. 25a, 25b, 26, 27). As loss increases ($\alpha \sim 0.01$ dB/m), the reconstructed profile deteriorates rapidly. It should be pointed out that the lower values of intrinsic attenuation prevail in the sediments in the abyssal plain at the frequencies of interest (220 Hz). Incidentally, one of the advantages of a monochromatic experiment is that the frequency dispersion law of the intrinsic attenuation, which is difficult to establish experimentally, particularly at low frequencies (< 1 kHz), does not enter into consideration.

6.7 Noise

As demonstrated in Chapter V, the Gelfand-Levitan algorithm is stable, with small errors in the reflection coefficient resulting in small errors in the reconstructed velocity. The numerical experiments we have conducted by adding zero-mean Gaussian stationary noise to the reflection coefficient input support our previous conclusion.

Gaussian noise was added to both the real and imaginary part of the reflection coefficient generated by the method of Section 6.1. The resulting reflection coefficient was submitted to the usual steps involved in the inversion procedure, namely the Fourier transform step followed by the application of the Gelfand-Levitan algorithm.

The signal to noise ratio (SNR) is defined as

$$SNR = 10 \log_{10}\left(\frac{I_s}{I_n}\right)$$

where the signal and noise powers for N discrete points are

$$I_s = \frac{1}{N} \sum_{n=1}^{N} |r_s|^2$$

and

$$I_n = \sigma_n^2 \text{ , the variance of the noise.}$$

As shown in Fig. 31 for a window profile, the perturbation of the reflection coefficient by the addition of zero-mean Gaussian noise ($\sigma = 0.1$) results in a roughly proportional degradation of the reconstructed potential.

The preliminary assessment of the effect of noise leads us to conclude that the Gelfand-Levitan inverse method is stable in the presence of noise. This analysis can be refined in the future by including a more pertinent model for the noise based on Mook's results[64]; Mook has shown that the addition of zero-mean stationary white Gaussian noise to the point source pressure field resulted in a non-stationary variance with the noise power concentrated near the vertical ($k_z = k_0$, the water wavenumber). One should also note that the measured reflection coefficient itself can be regarded

as a non-stationary process with a mean that varies between one near grazing incidence and zero at infinity. That consideration may lead to a more appropriate measure of performance than that of SNR presented here.

CHAPTER VII

CONCLUSION

In this thesis we have examined the theoretical and computational underpinnings of a novel approach to the determination of the acoustic parameters of the oceanic sediment layer. Traditional marine seismic methods, acoustic reflection and refraction measurements, "yield no velocity information in the top of the first sediment layer which is of critical interest for modeling the sea floor for underwater acoustics" (34). That is precisely where the method we have analyzed in the thesis is most accurate. Interval velocity calculations are restricted to layer thicknesses larger than one twelfth the water depth (34), and subsequently the velocity at the sediment interface cannot be determined accurately. In the absence of in situ core measurements of surface velocity V_0, the velocity gradient at the top of the sediment column is also uncertain. The direct inverse method presented here requires only the a priori knowledge of the speed of sound in the water above the sediment layer.

By operating at a single frequency, the effects of dispersion are separated from the propagation process. Moreover, the dispersive characteristics of the medium can be studied by performing the experiment at various frequencies.

A single frequency, steady-state experiment also means
that the measurement relies on amplitudes rather than on
arrival times (explosive methods). While it is true that
time is measured more accurately than acoustic pressure,
arrival times can not always be interpreted correctly due
to multiple reflections. Amplitude, in turn, may be affected
by a host of factors to which arrival time is insensitive
such as loss and diffraction; it is not yet possible to judg⌣
the relative merits of the two methods in the absence of apprc-
priate experitmental data.

Contributions

The determination of the acoustic properties of the
ocean bottom was showr to be equivalent to the reconstruction
of an unknown potential in a Schrodinger equation from the
plane-wave reflection coefficient given at all angles of
incidence (Chapter II).

The pivotal role of the reflection coefficient lead
us to a detailed examination of its properties in Chapter III.
In particular, we showed, by induction, that the reflection
coefficient decays at least as rapidly as $(1/k_z^2)$ and is
therefore integrable.

The derivation of our approach to the direct inversion
method was presented in Chapter IV. The Gelfand-Levitan
method was extended to the case where the acoustic velocities
on either side of a slab are different. That is, of course,
the case in the ocean bottom problem where the acoustic velocity

in the basement is larger than the acoustic velocity in the water. We also showed that the neglect of bound states is justified at the current operating frequency in both clayey silt and in silty clay.

Three methods for the numerical solution of the Gelfand-Levitan integral equation were investigated (Chapter V). The first method we developed is a series expansion of the solution obtained by successive approximations. The first two terms of this expansion represent a substantial improvement over the well known Born approximation.

The other two numerical methods presented in Chapter V are based on the discretization of the Gelfand-Levitan integral equation. They represent two ways to bypass the matrix inversion inherent in a straightforward solution of the discretized equation. We then obtained estimates for the bound on the error in the integral of the potential due to discretization errors and due to errors in the reflection coefficient.

In Chapter VI, we discussed the numerical results obtained from the inversion of synthetic data. By dealing with synthetic data, we insured that the bottom profile was known exactly and that the effectiveness of the method could be studied without any fear of experimental imperfections. We concluded that the Gelfand-Levitan method appears to be very accurate at the top of a sediment column, just where the more usual methods are least accurate. The resolution

obtained is less than the wavelength of the acoustic source in the water. The degradation of the reconstructed velocity profile becomes, however, pronounced if the reflection data is restricted to real angles above critical. Perturbations of data were also studied. Perturbations such as intrinsic loss in the acoustic medium or noise in the data produce perturbations in the reconstructed profile. The inclusion of density variations requires the use of two frequencies and two separate inversions of the Gelfand-Levitan equation.

We were able to gauge the performance of the numerical schemes through the study of the inversion of the acoustic profile for two half-spaces (constant velocity), *for* which we derived the Fourier transform of the reflection coefficient analytically. The improvements wrought by the improved Born method are clear, as are the effects of sampling on the reconstructed profile. The improved Born method represents a fast and easy to implement method of recovering the velocity at the top of the sediment column. The two finite difference methods are more time-consuming but yield an accurate reconstruction of the acoustic profile over greater depth.

Future Work

On the theoretical front, we suggest a thorough investigation of the Gelfand-Levitan method in the presence

of density variations. It may also be useful to incorporate

loss directly into the original formulation. One should also

seek efficient numerical implementations of the Gelfand-

Levitan algorithm that could increase the penetration depth

of the reconstruction. In this respect, we think that the

combination of the Gelfand-Levitan algorithm with a priori

information such as the acoustic properties of the basement

might constitute a promising approach.

On the experimental front, the testing of the Gelfand-

Levitan inverse method on field data should be given priority

to determine its ultimate value. If an actual ocean-based

experiment were precluded at the moment, we would suggest

carrying out a similar electromagnetic experiment on dielectrics

at microwave frequencies.

On the numerical front, one would want to test the

whole experimental scheme, starting from pressure measurements

due to a point source and ending with the Gelfand-Levitan

inversion. Special attention should be paid to the effect

of noise in the recording of pressure on the plane-wave

reflection coefficient and ultimately on the reconstructed

acoustic parameters.

It is remarkable that the Frisk experiment which was conceived on purely intuitive grounds, when modelled theoretically, bears out the expectation that accurate results are achievable. To date, experimental data has been interpreted by time - consuming trial and error procedures. Our mathematical and numerical approach suggests that a more direct inverse method for processing experimental data, requiring no a priori information about the acoustic parameters of the bottom is feasible.
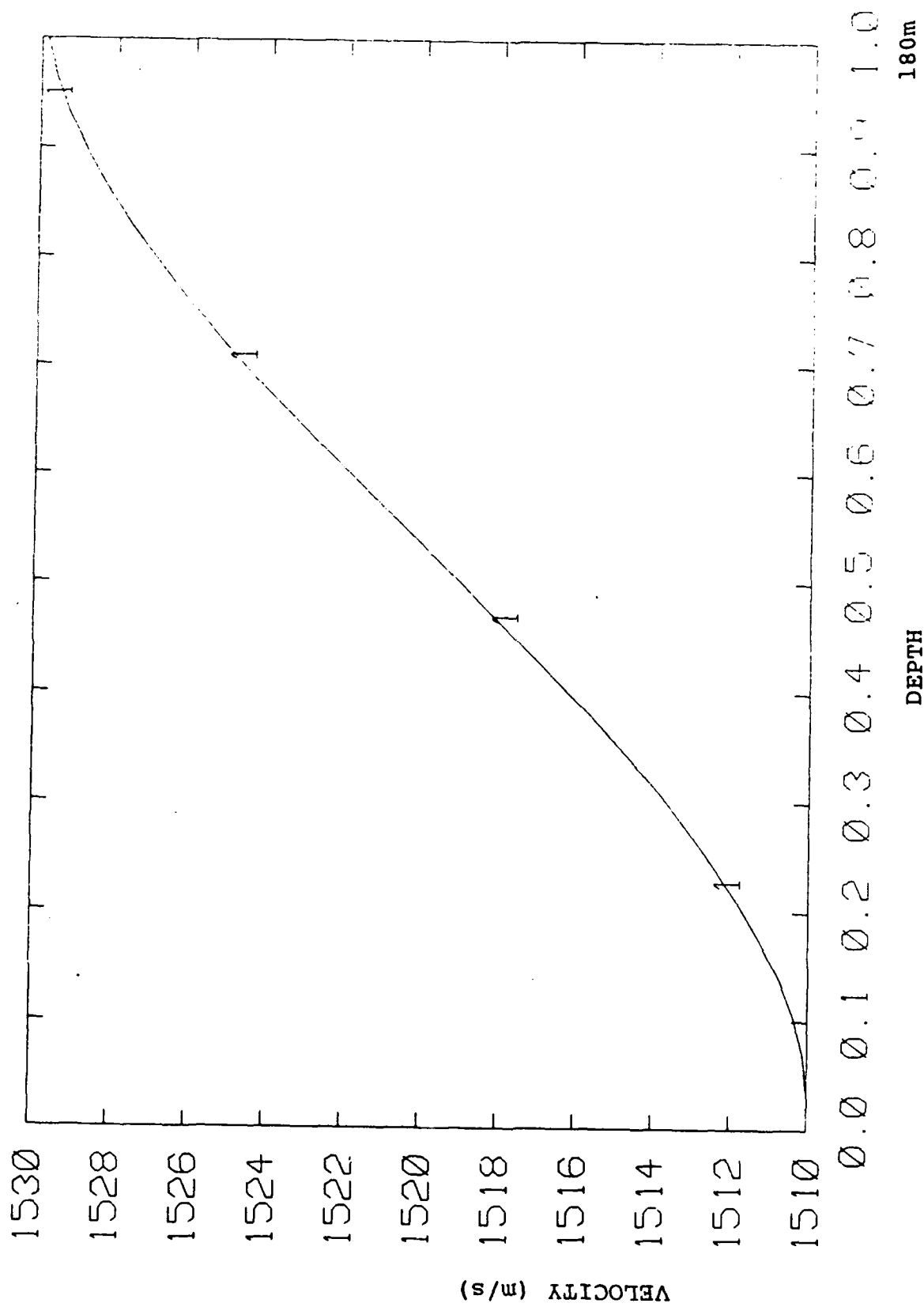
Figure 10: Stickler Profile
$c_0 = 1510\text{m/s}$, $c_1 = 1530\text{m/s}$, $L = 180\text{m}$
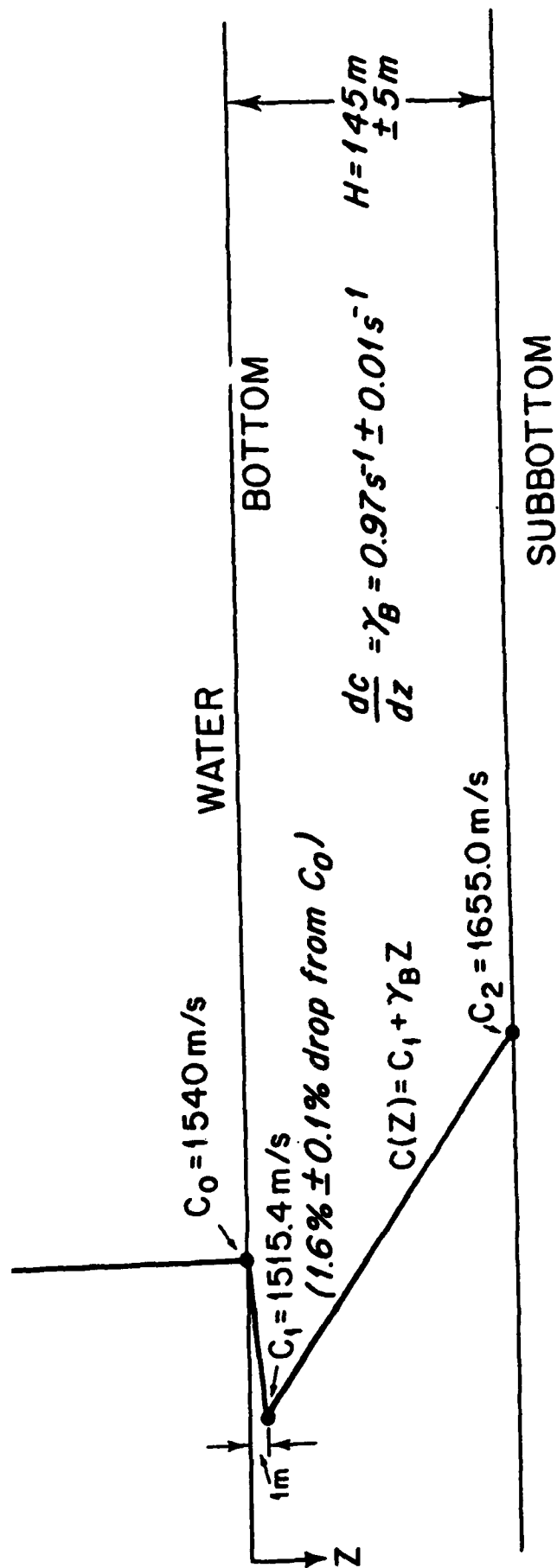
Figure 11: Frisk Profile
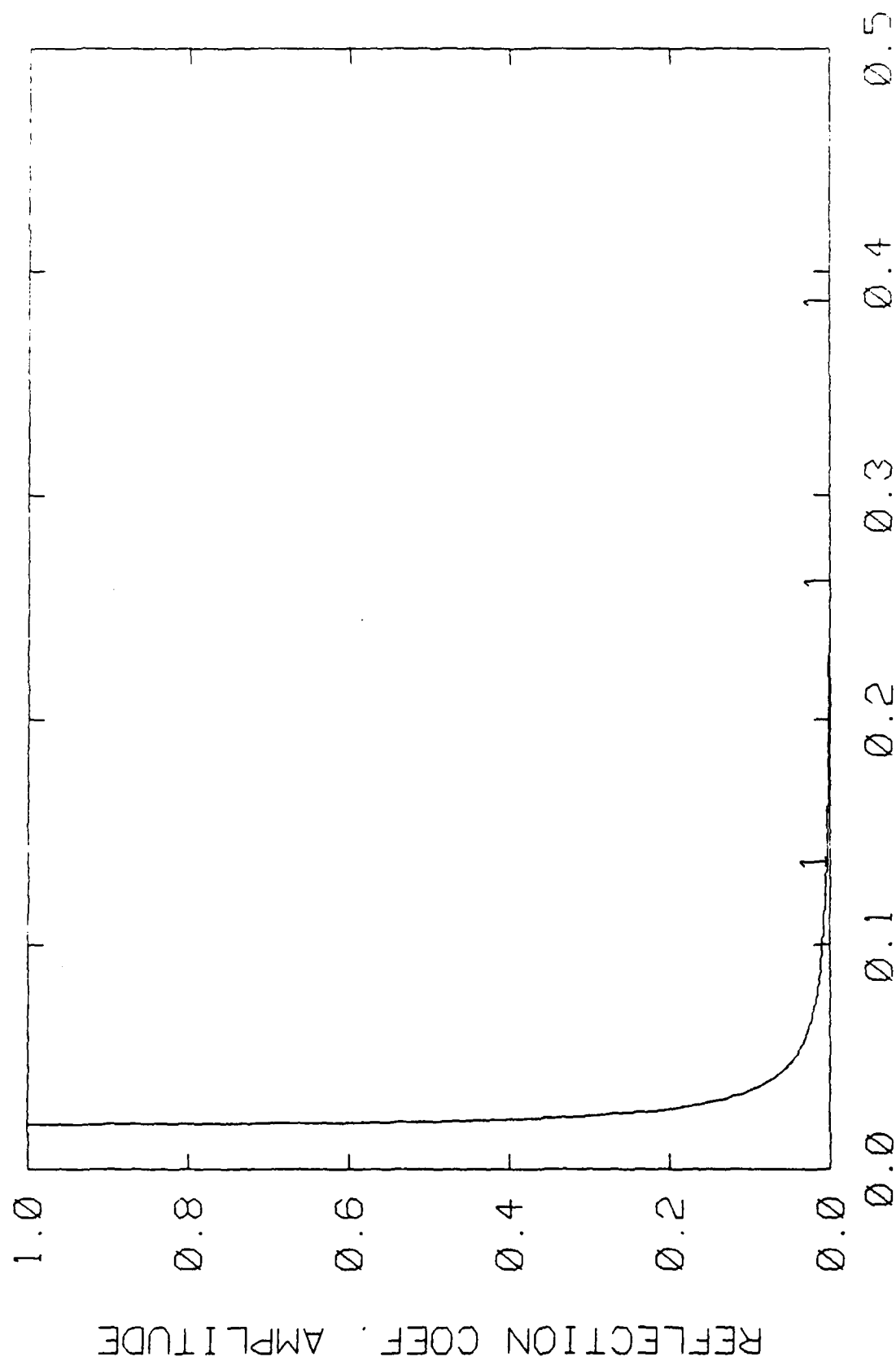
VERTICAL WAVENUMBER

Figure 12a: Reflection Coefficient Amplitude for a Half-Space
f = 25Hz
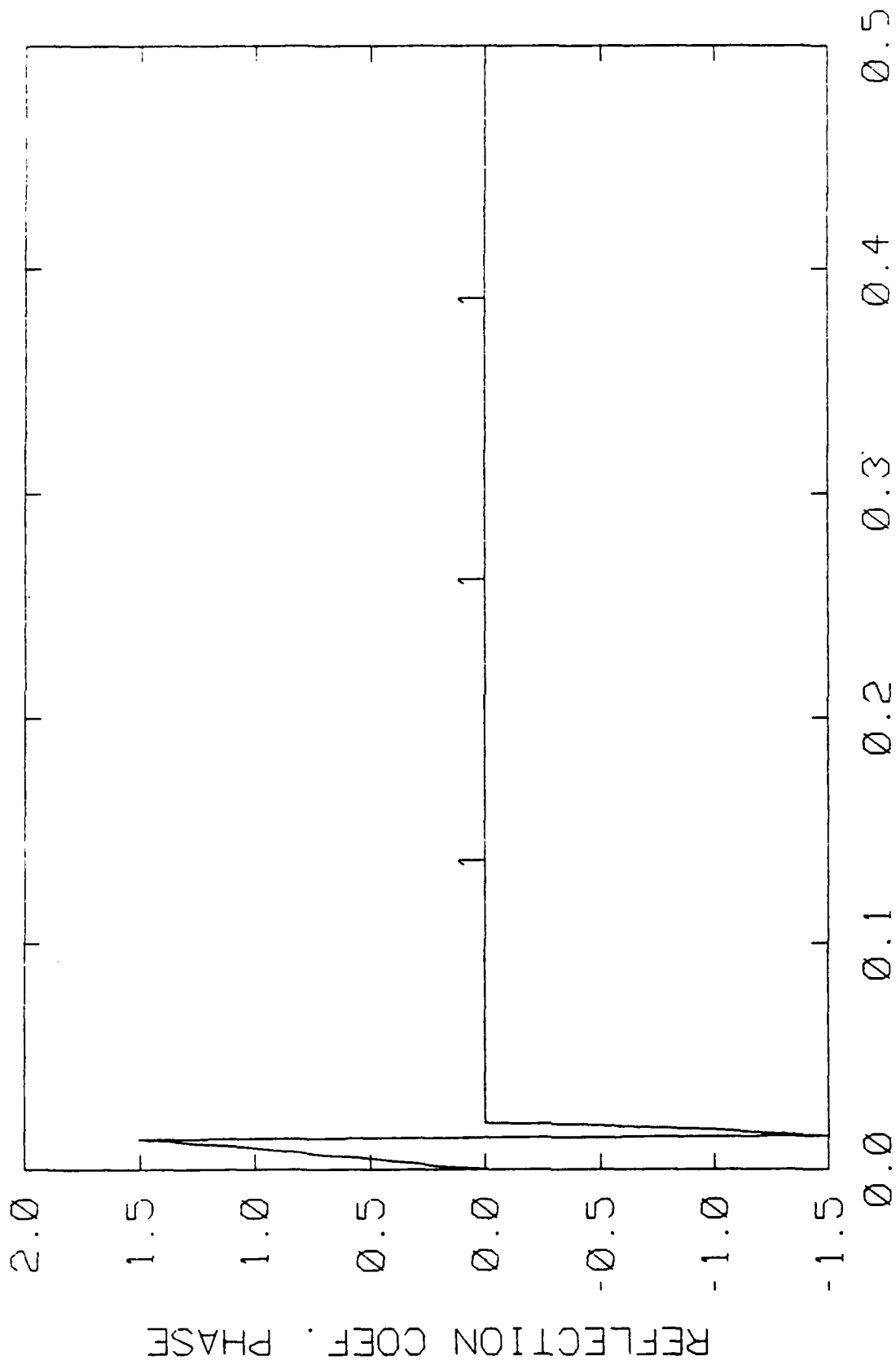
Figure 12b: Reflection Coefficient Phase for a Half-Space (radians)
f = 25Hz
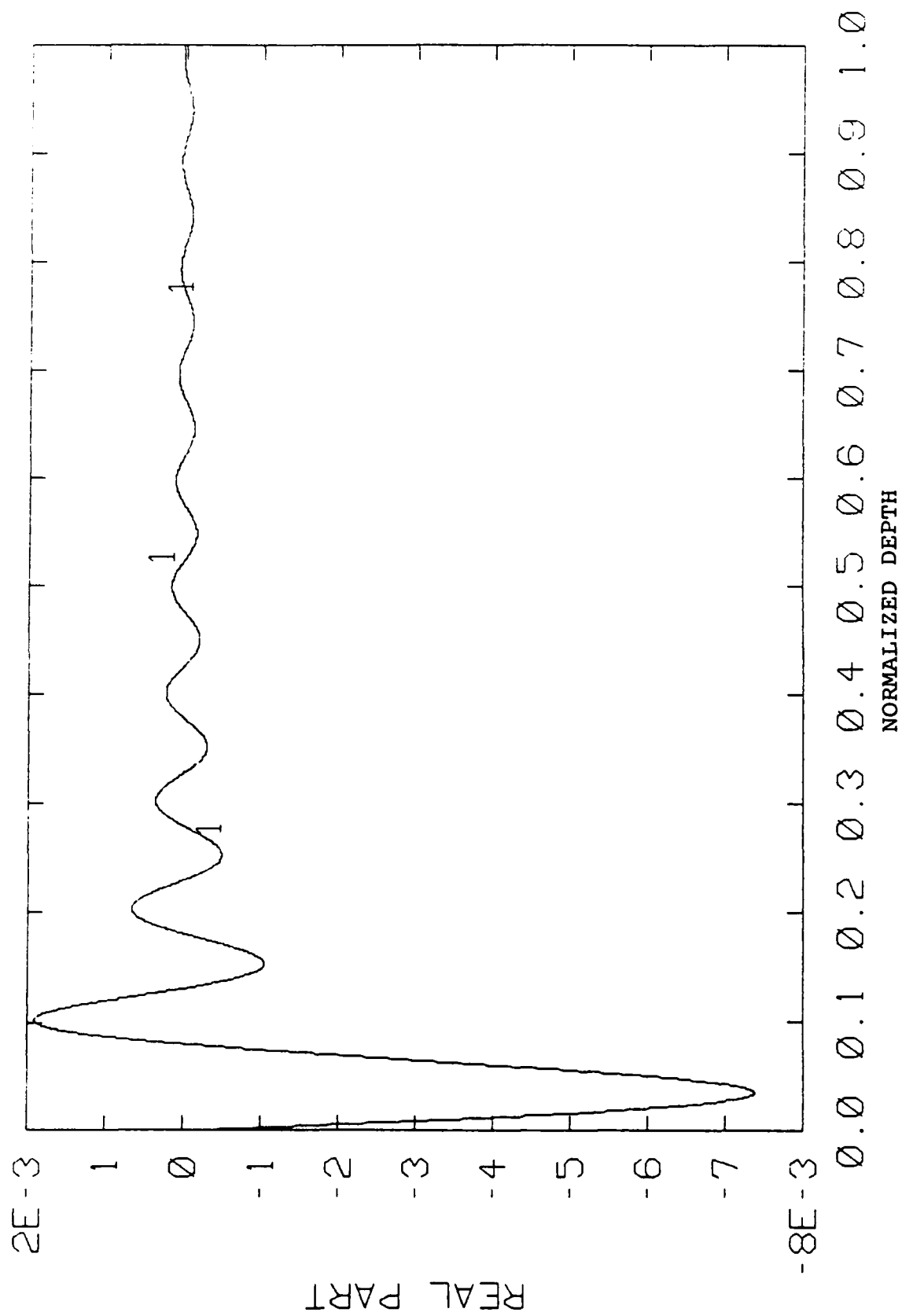
Figure 12c: Fourier Transform of Figure 12(a,b).
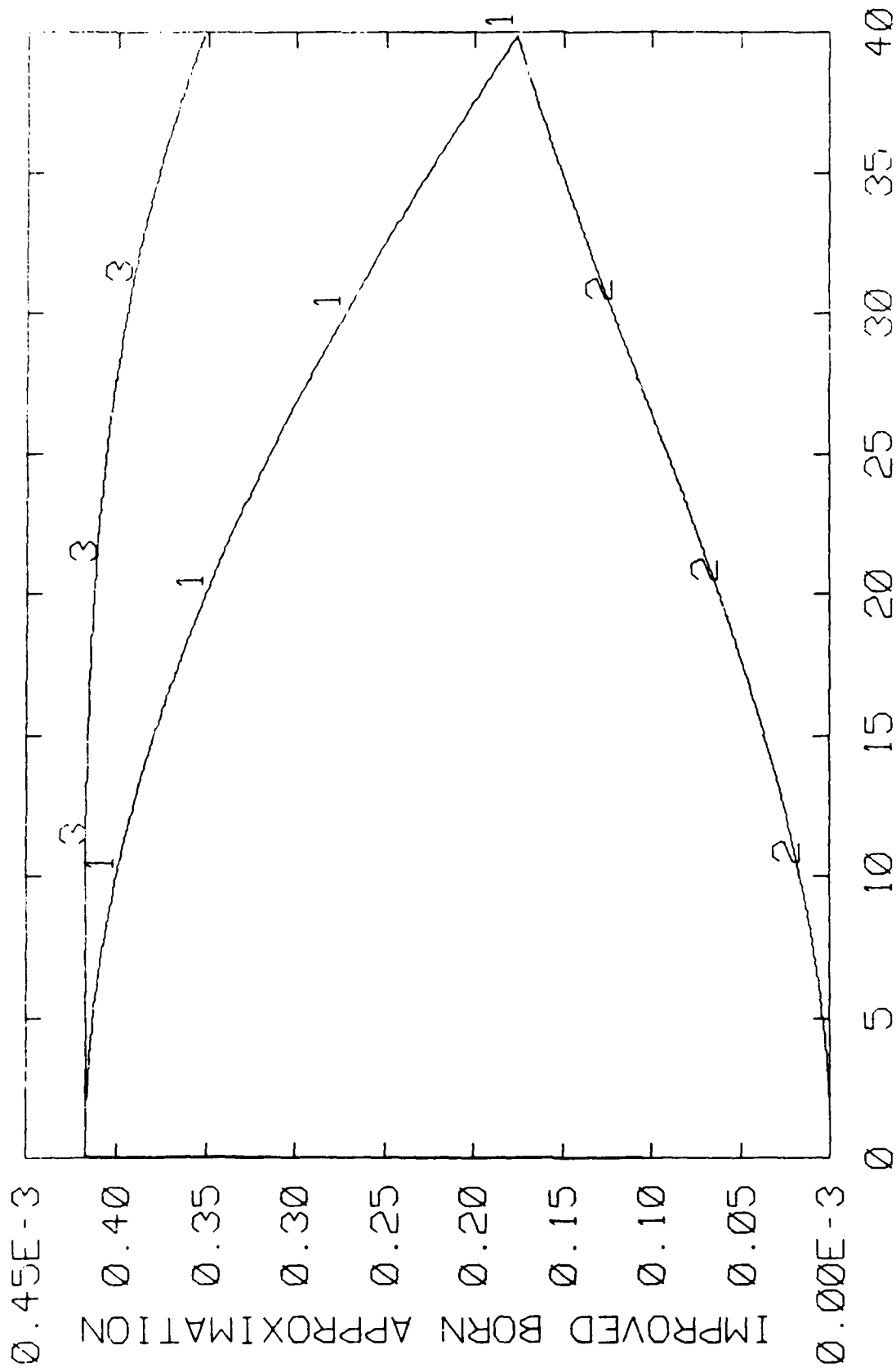
Figure 12d: Half-Space Potential Reconstruction, $c_0 = 1510 m/s$,
$c_1 = 1540 m/s$, 1:Born, 2:Correction, 3:Improved Born = (1)+(2)
$f = 25Hz$
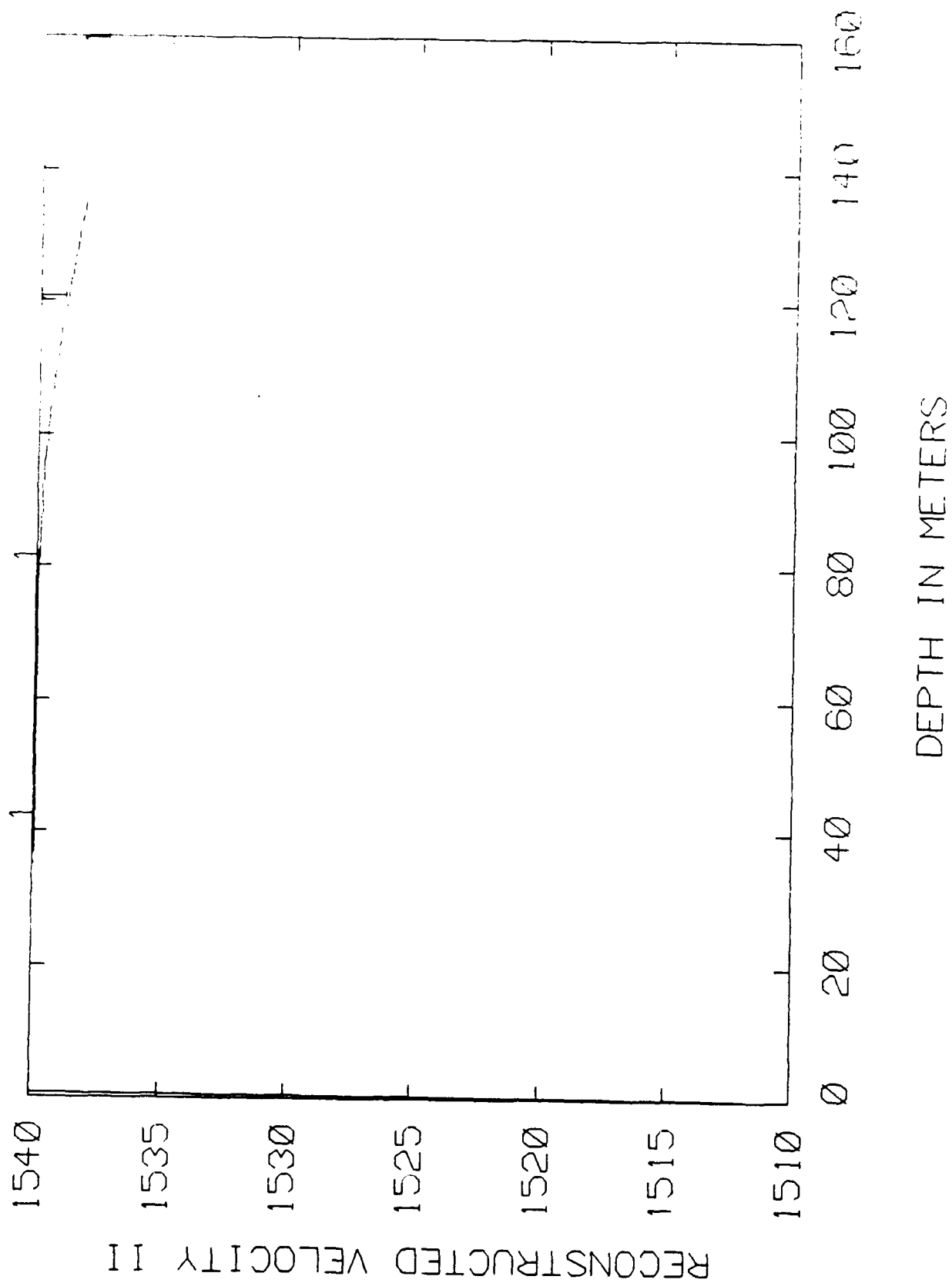
Figure 13: Velocity Reconstruction for a Half-Space (m/s) R(z) obtained from analytic expression - $\Delta z = 0.767$m
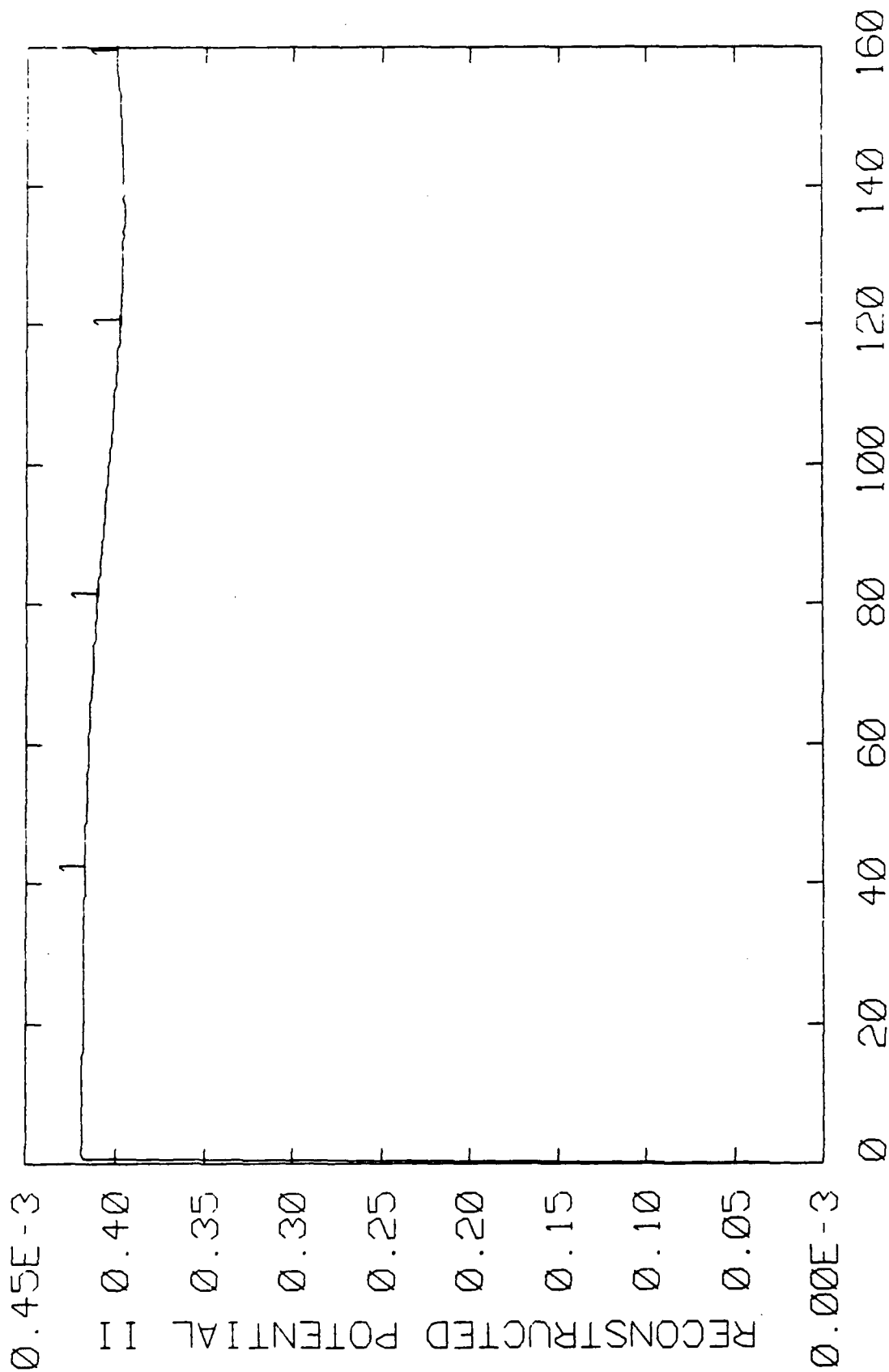
Figure 14a: Reconstruction for a Half-Space (Potential)
$\Delta z = 0.767m$, $f = 25Hz$
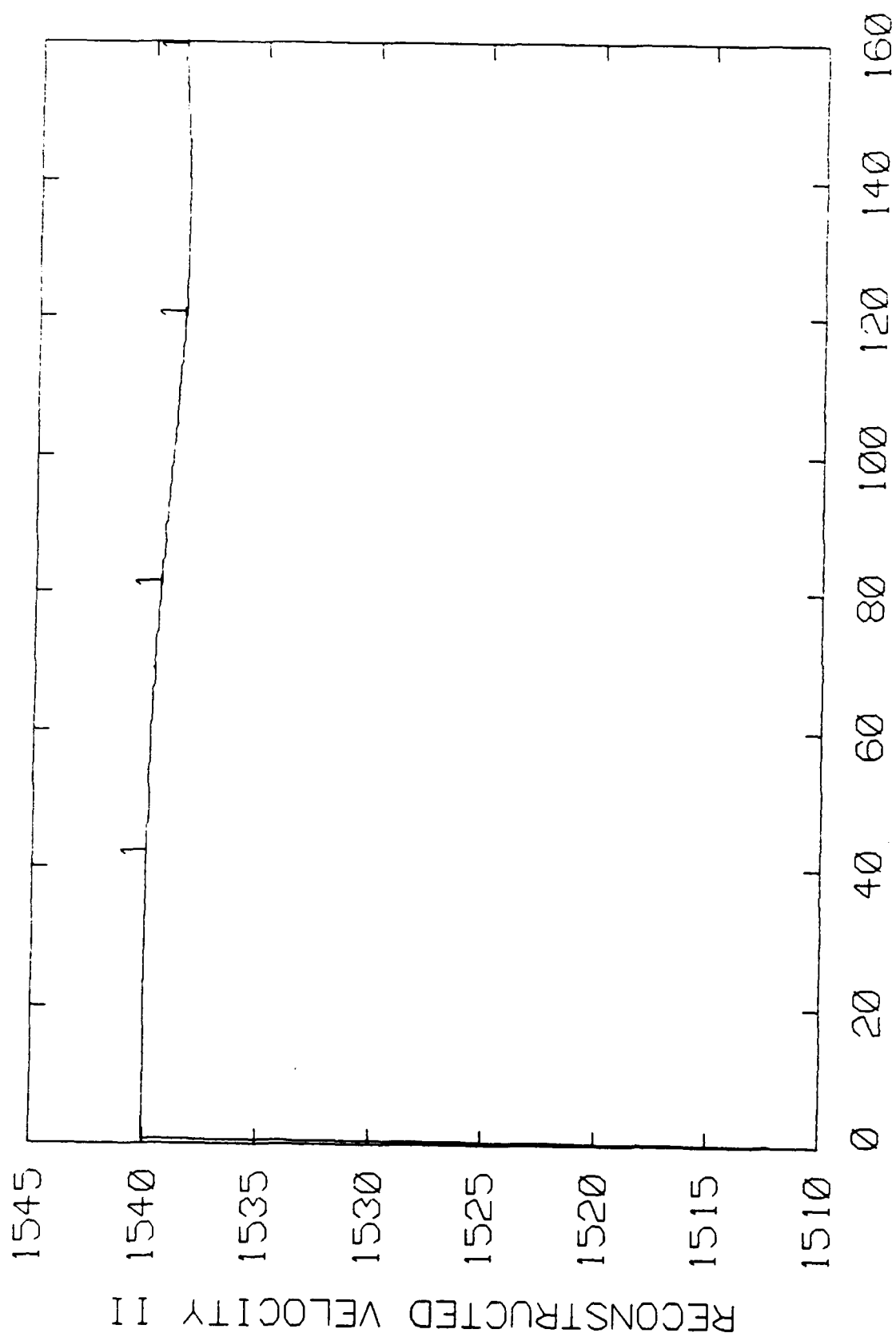
Figure 14b: Velocity Reconstruction for a Half-Space (m/s). R(z) obtained numerically. Δz = 0.767m
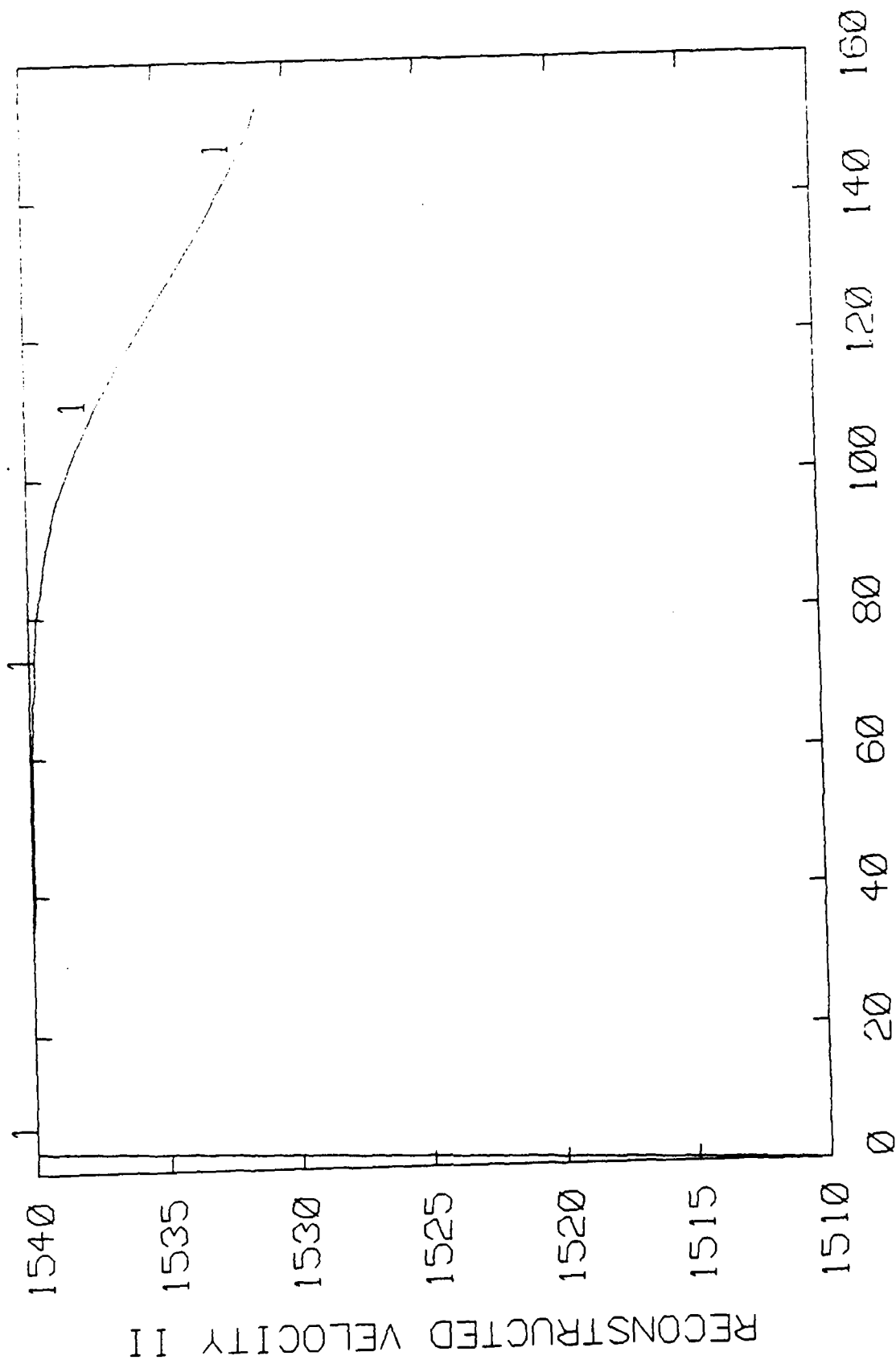
Figure 15: Velocity Reconstruction for a Half-Space (m/s)
$\Delta z = 3.06m$, $f = 25Hz$, $k_z = 10^{-3}$
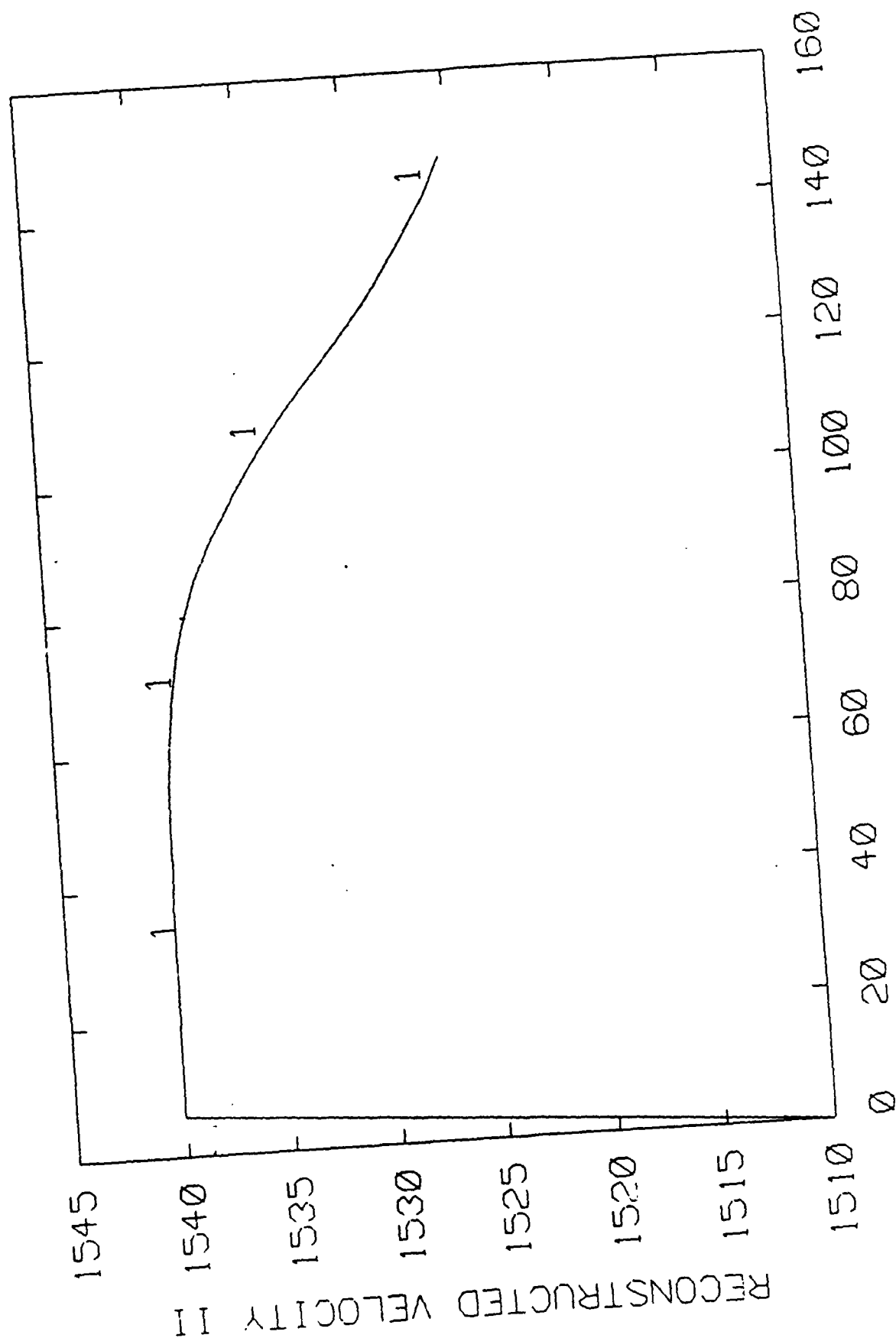
Figure 16: Velocity Reconstruction for a Half-Space (c_0 = 1510m/s, c_1 = 1540 m/s). Δz = 6.135m, F = 25Hz
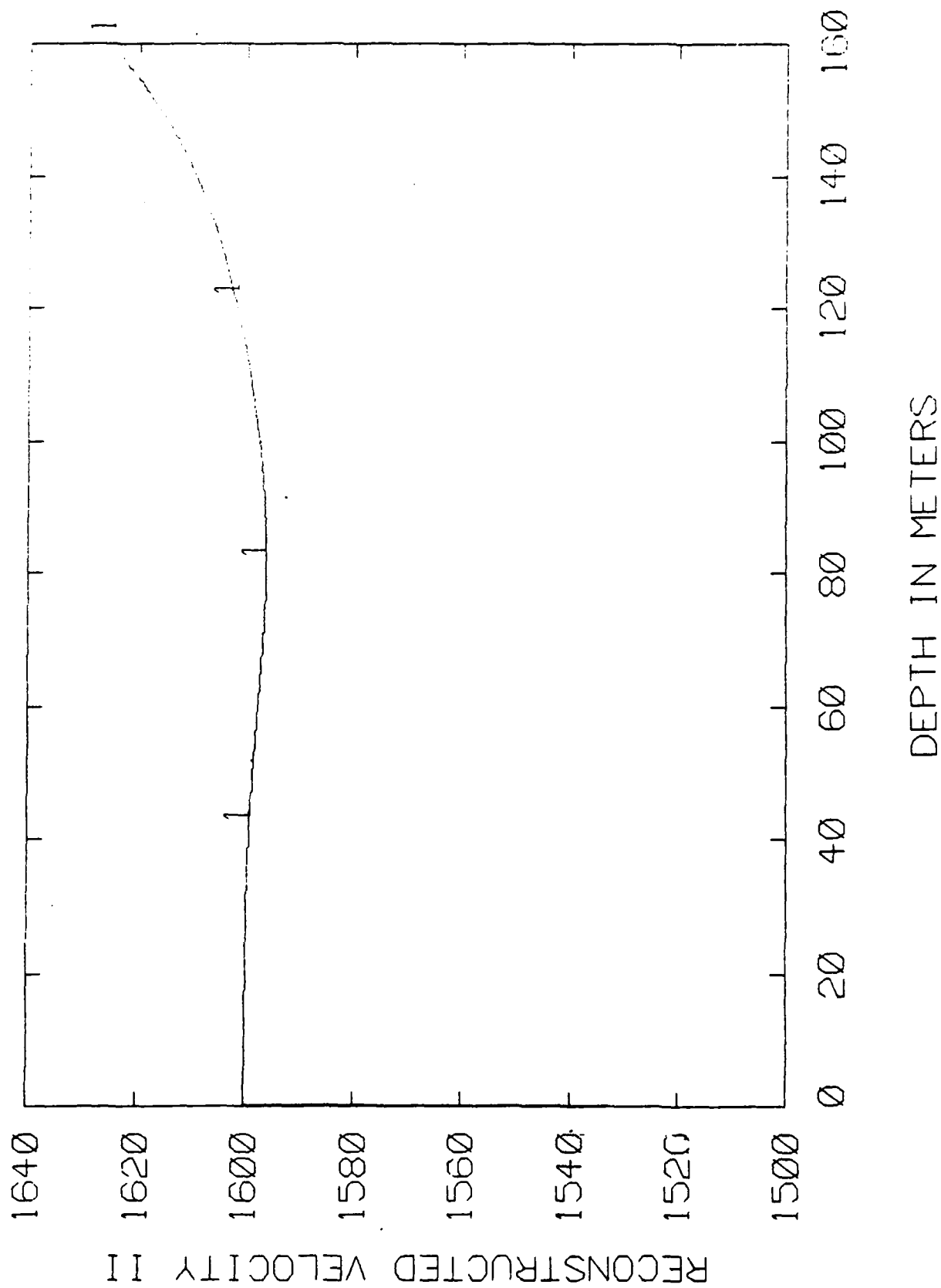
Figure 17a: Velocity Reconstruction for a Half-Space.
c_0 = 1500m/s, c_1 = 1600m/s). Δz = 0.3125m, f = 25Hz
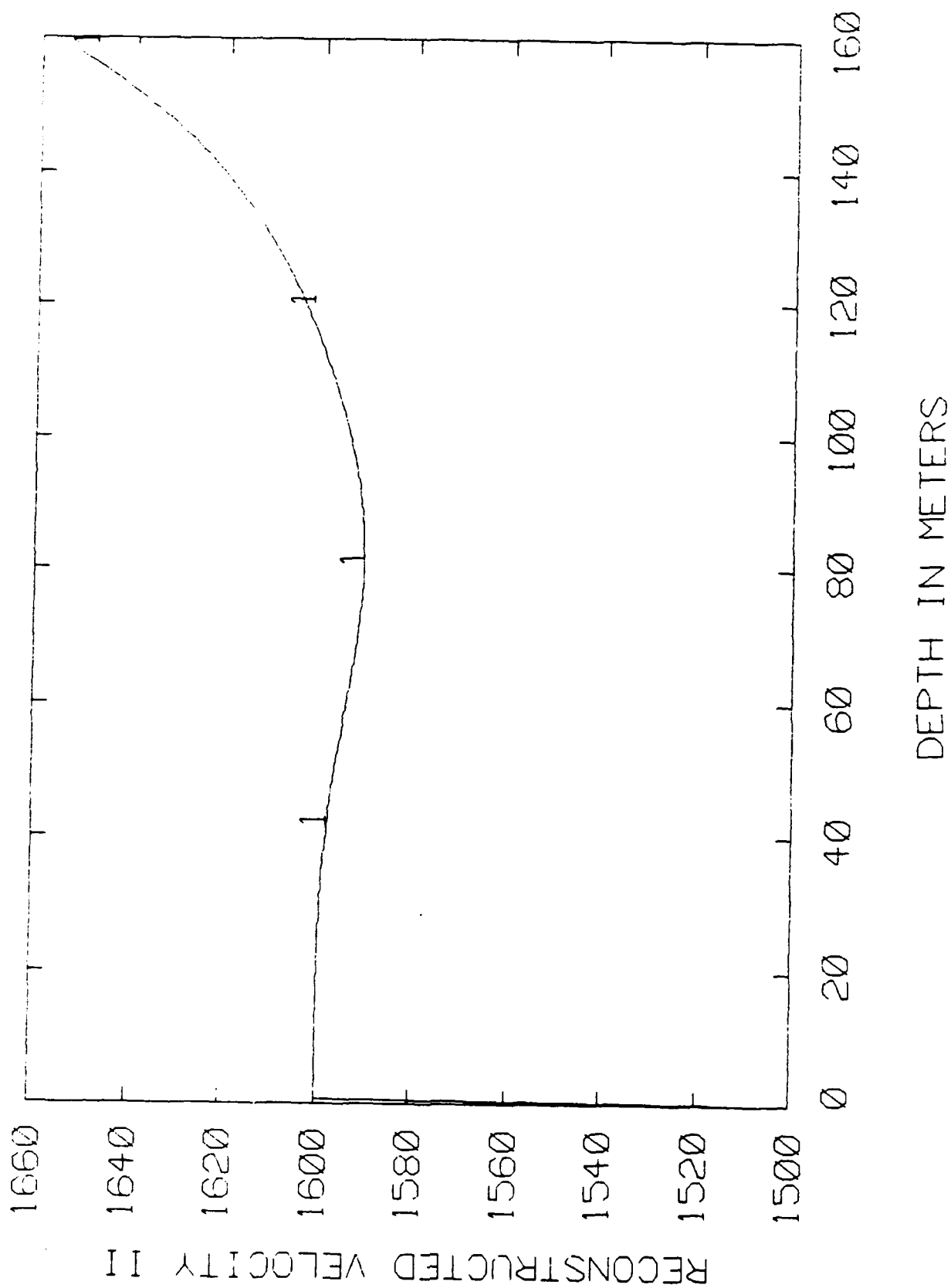
Figure 17b: Velocity Reconstruction for Half-Space.
(c_0 = 1500m/s, c_1 = 1600m/s).
Δz = 0.767m, f = 25Hz.
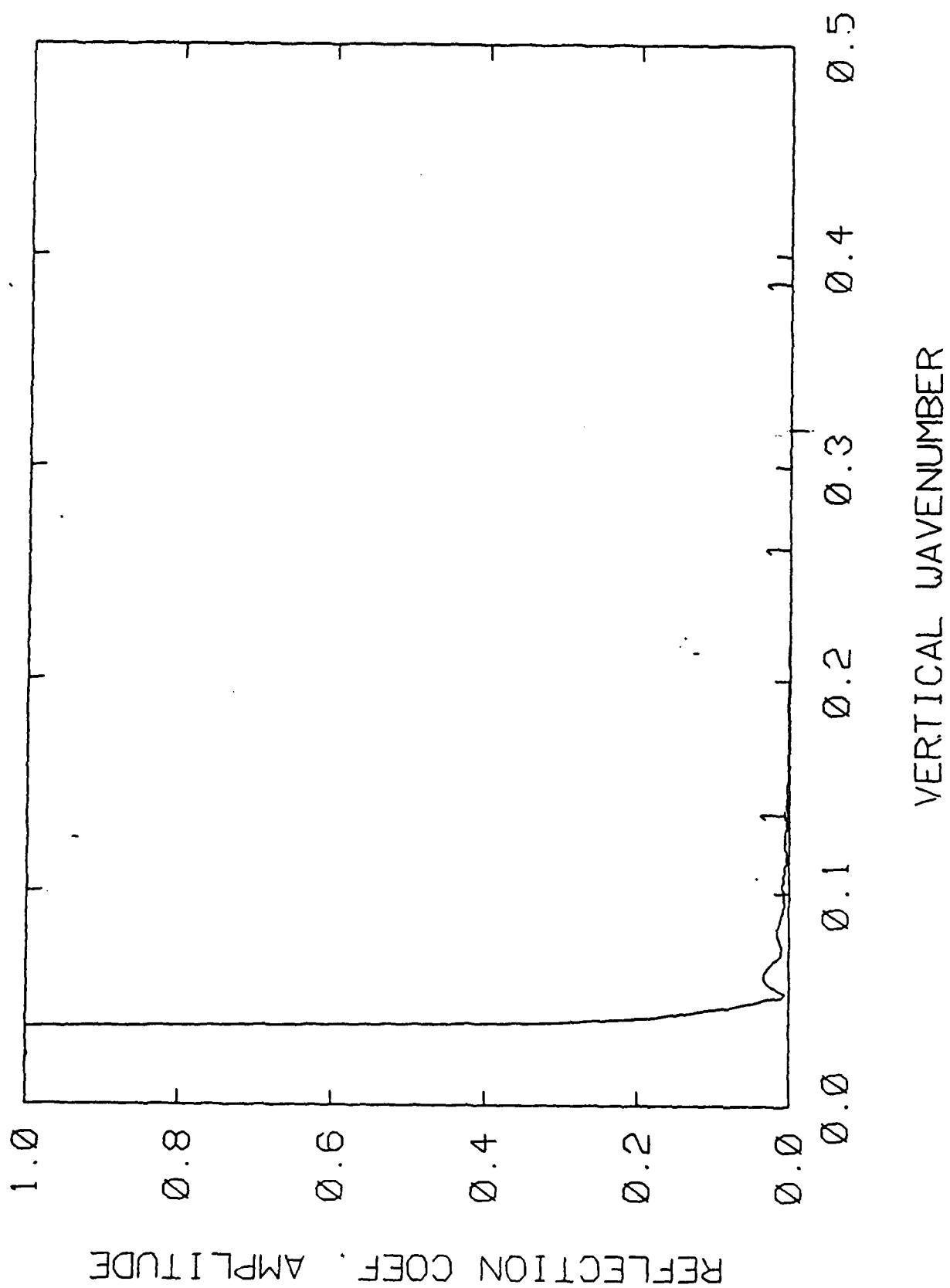
Figure 18a: Reflection Coefficient Amplitude. Frisk Profile
$k_0 = 0.1$, $f = 25$Hz.
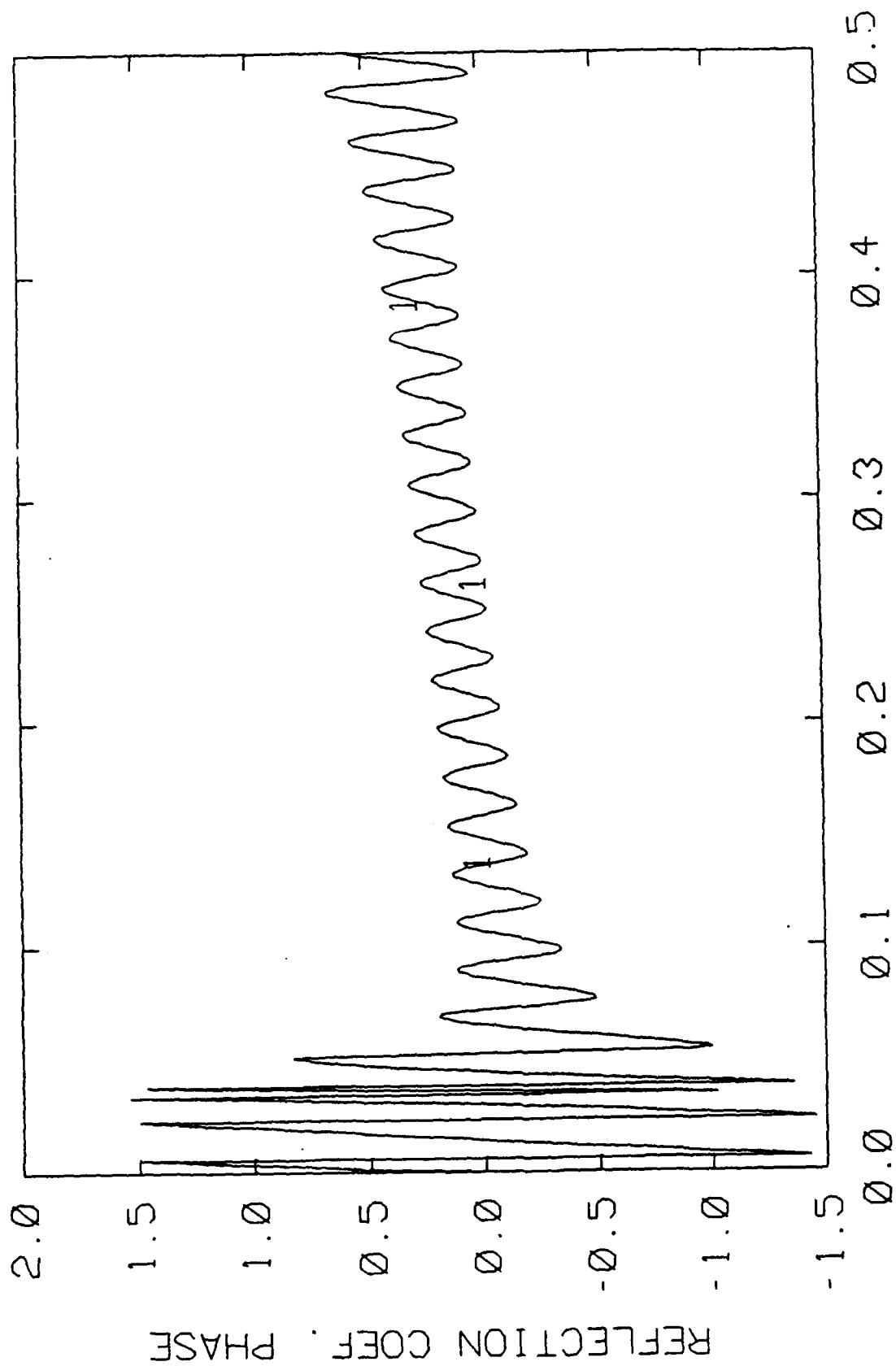
Figure 18b: Reflection Coefficient Phase - Frisk Profile. f = 25Hz
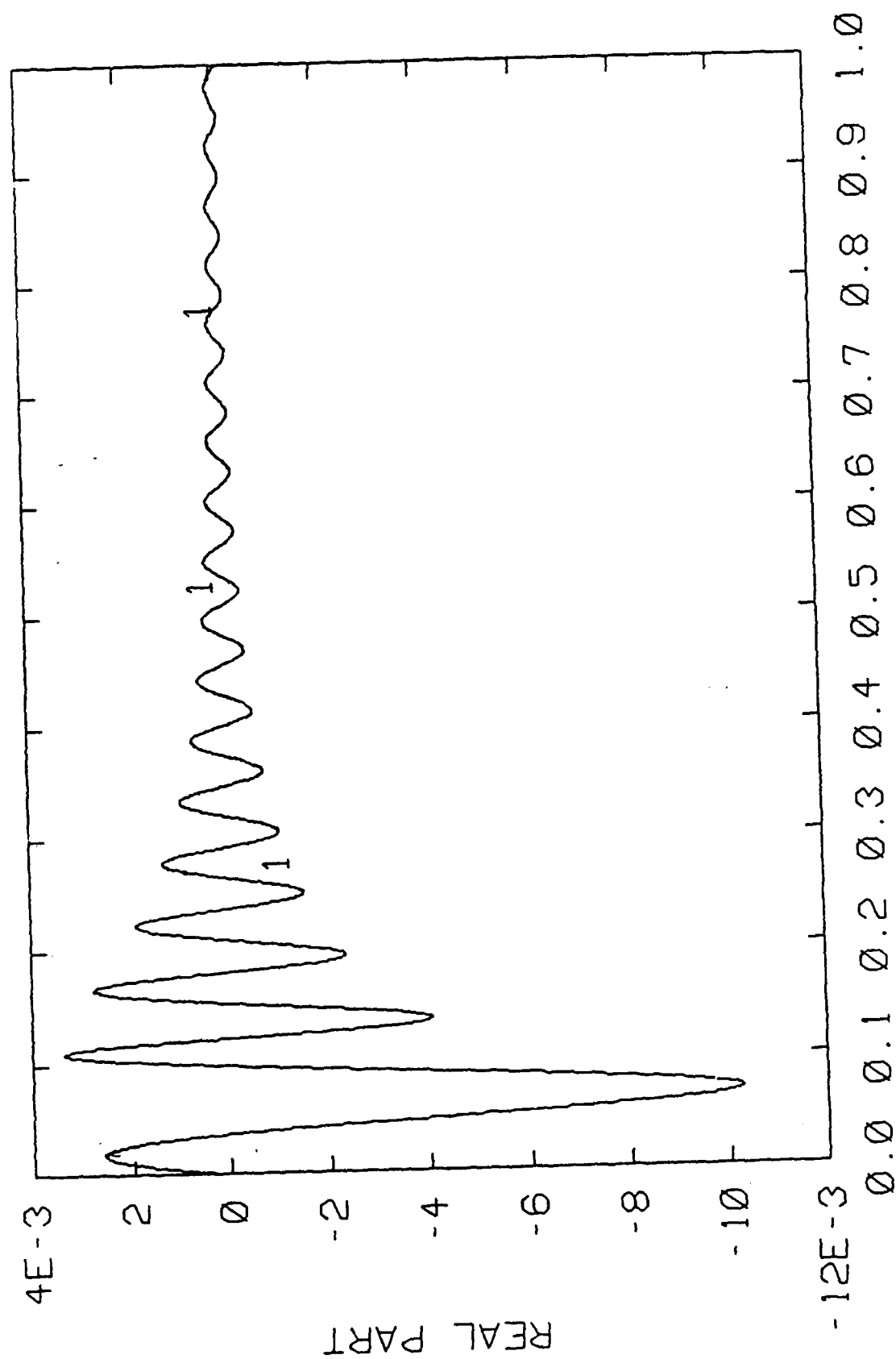
Figure 18c: R(z), Fourier Transform of Figure 18(a,b)

Figure 18d: Frisk Profile Reconstruction - N_g Iteration -
$\Delta z = 0.767m$, $f = 25Hz$; $\Delta k_z = 10^{-3}$
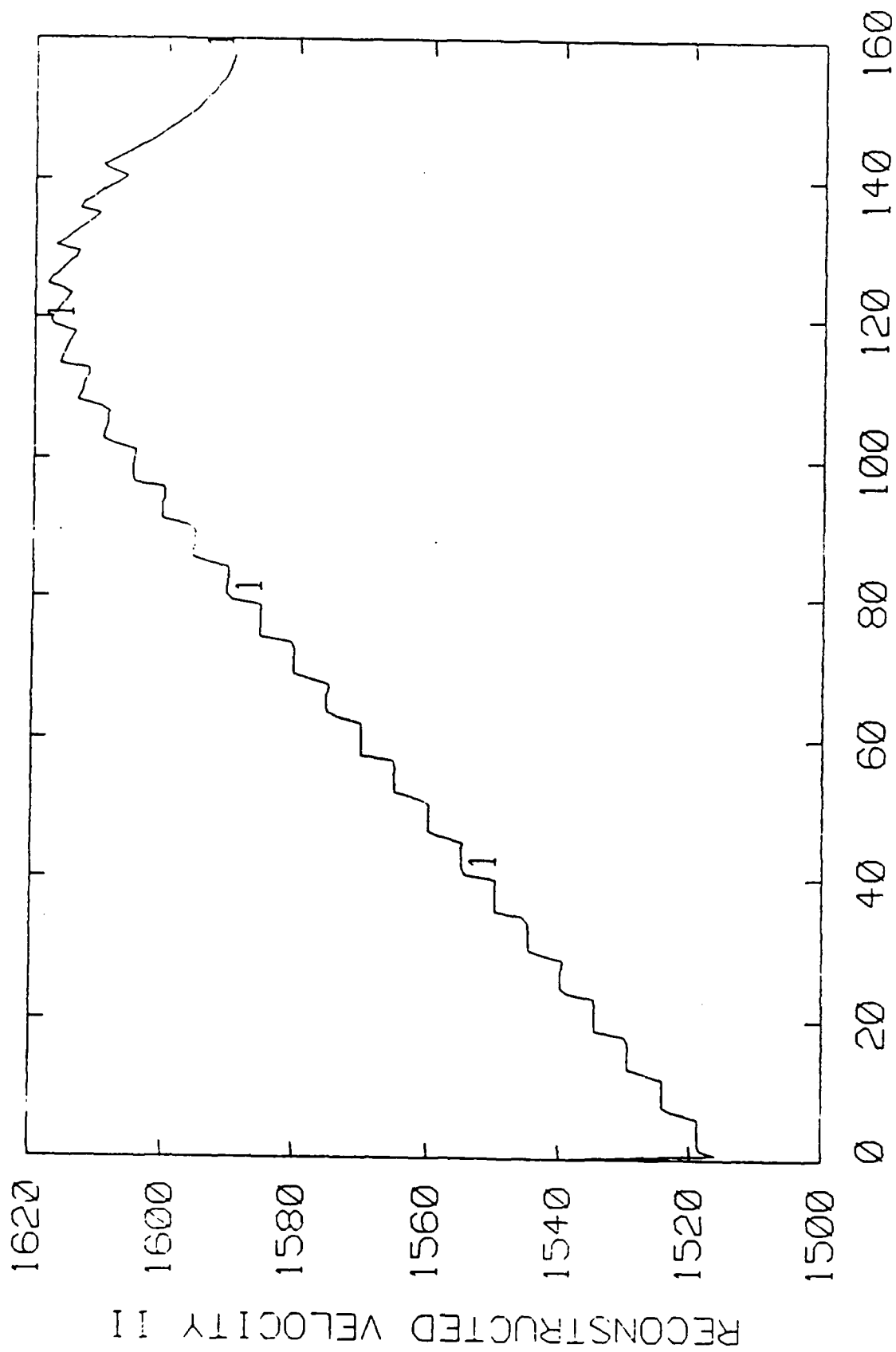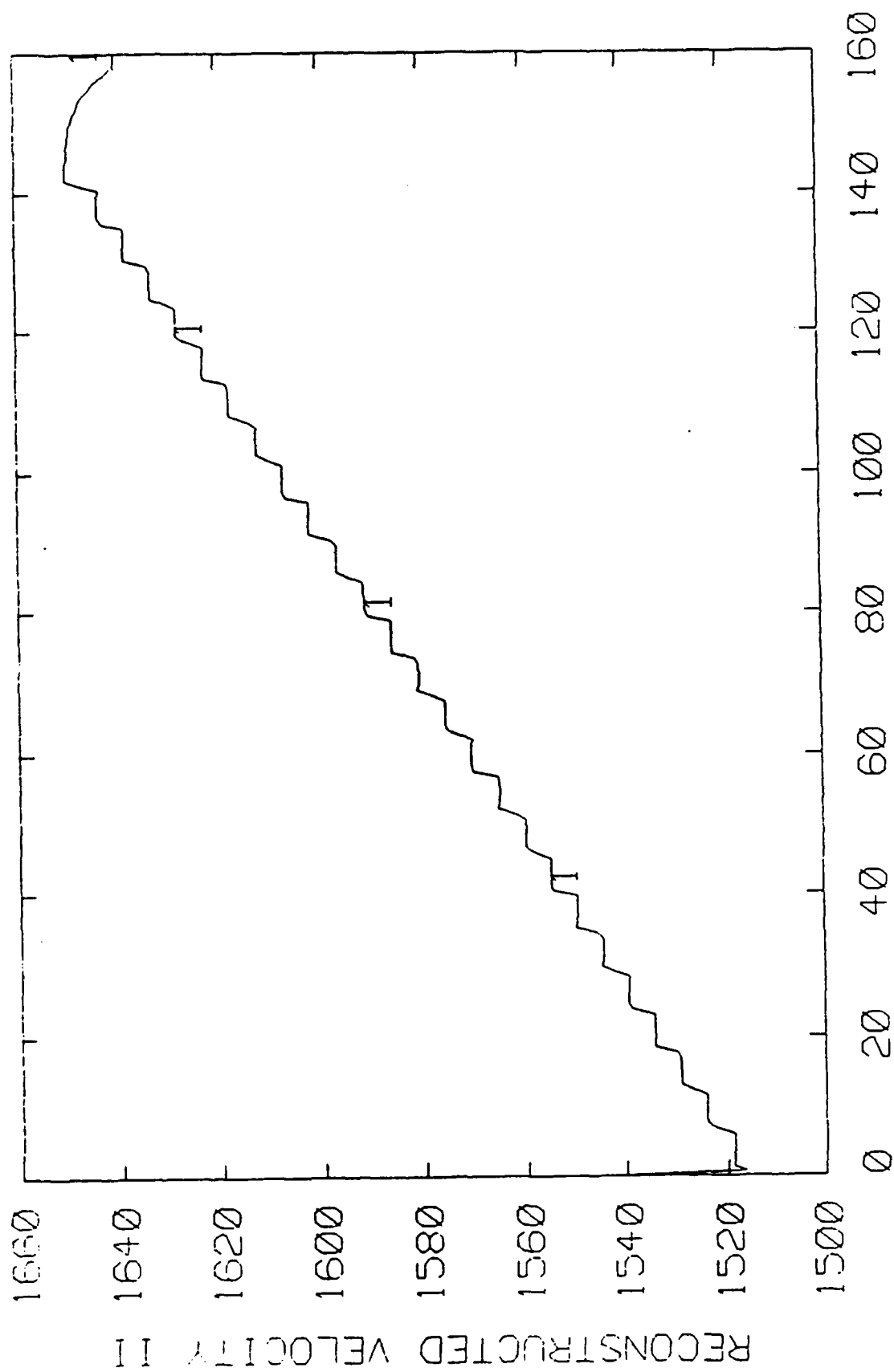
DEPTH IN METERS

Figure 18e: Frisk Profile Reconstruction – 20 Iterations
$\Delta z = 0.767m$, $f = 25Hz$

Figure 18f: Frisk Profile Reconstruction - 40 Iterations
$\Delta z = 0.767m$, $f = 25Hz$

Figure 18g: Velocity Reconstruction - Frisk Profile - (Detail)
$\Delta z = 0.767m$, $f = 25Hz$

VERTICAL WAVENUMBER
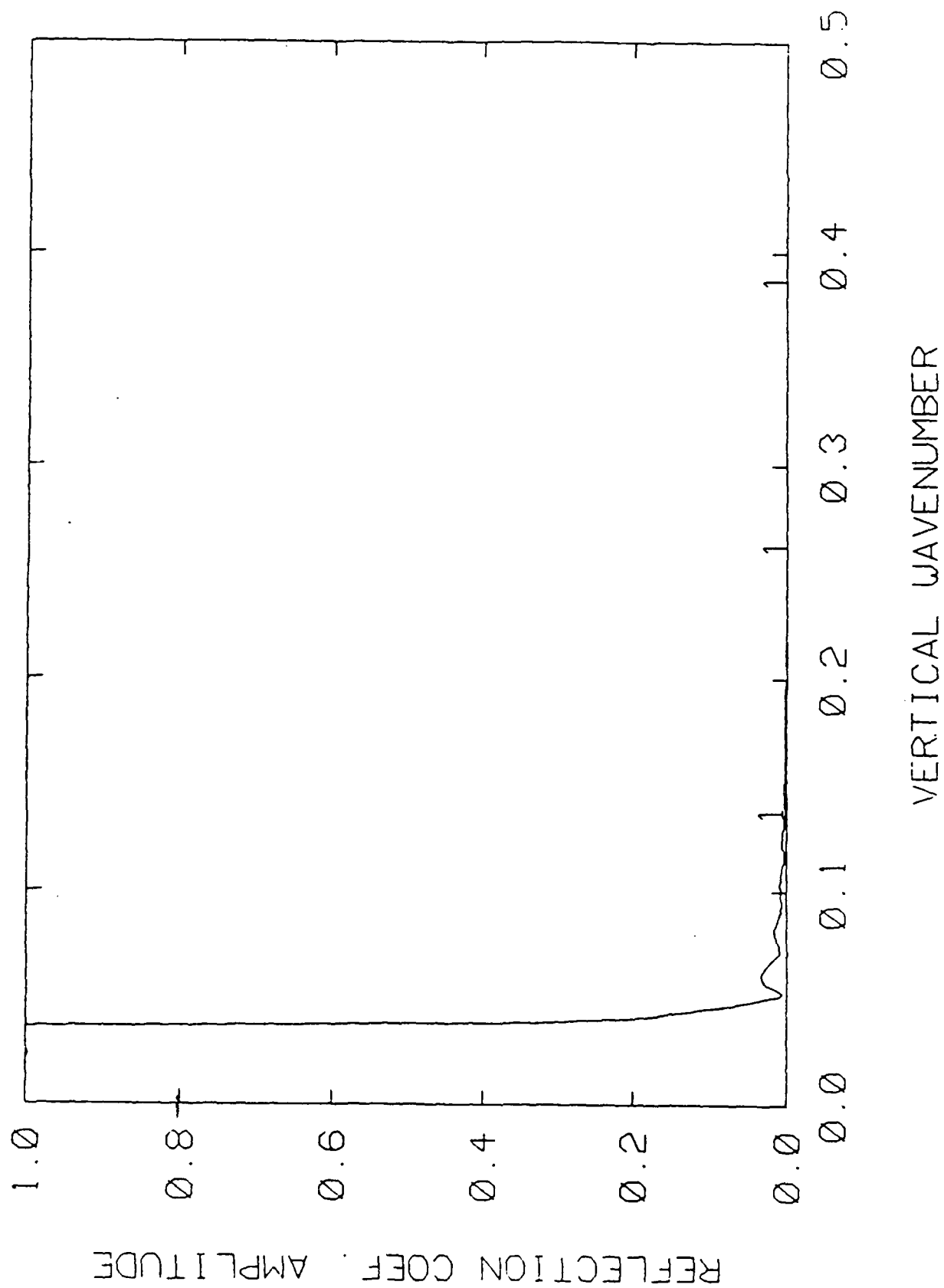
Figure 19a: Reflection Coefficient Amplitude. Frisk Profile
Limited Range, $K_{zmax} = 0.512$, $f = 25Hz$

REFLECTION COEF. AMPLITUDE
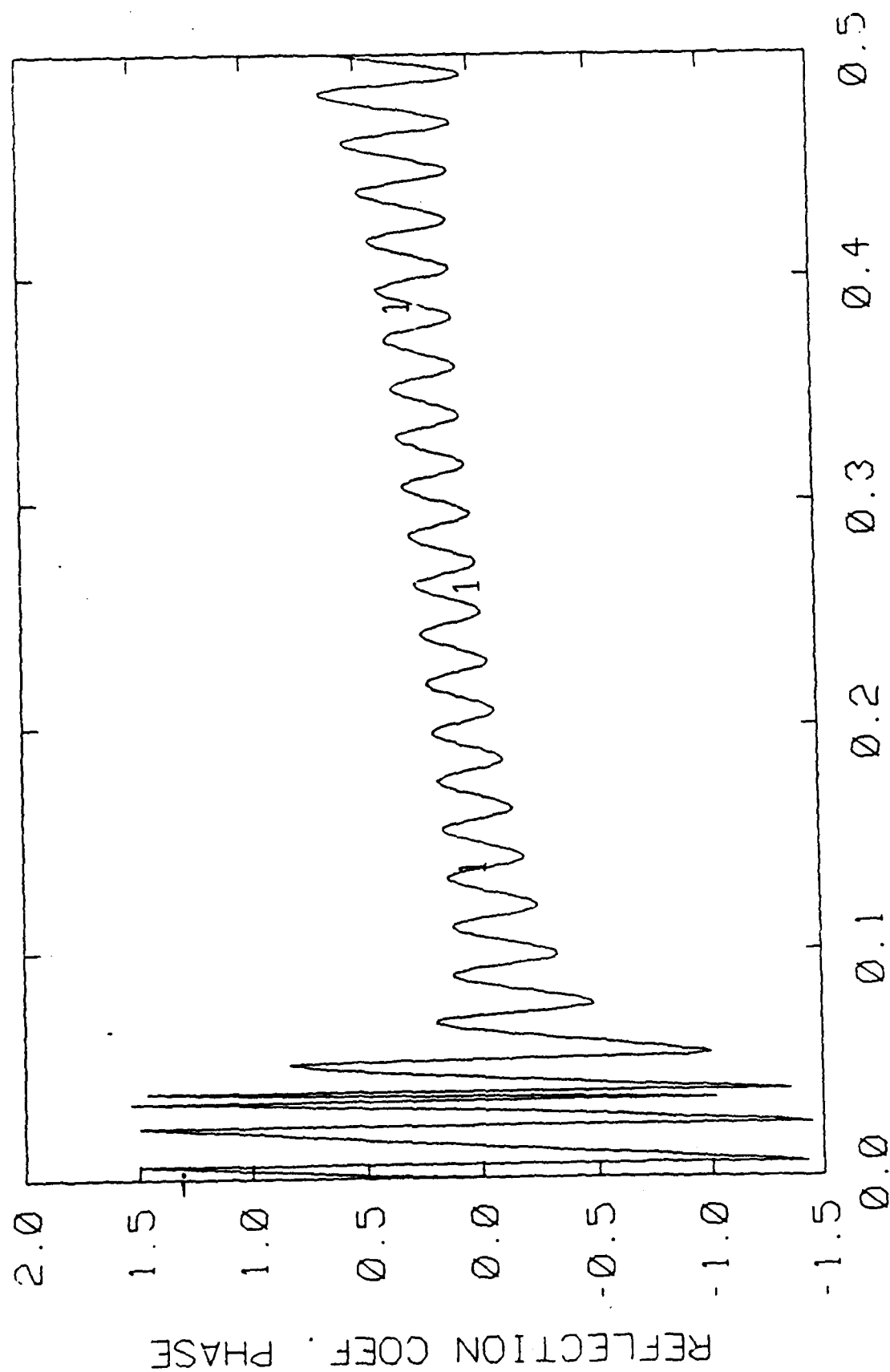
Figure 19b: Reflection Coefficient Phase - Firsk Profile
Limited Range, $K_{zmax} = 0.512$, f = 25Hz
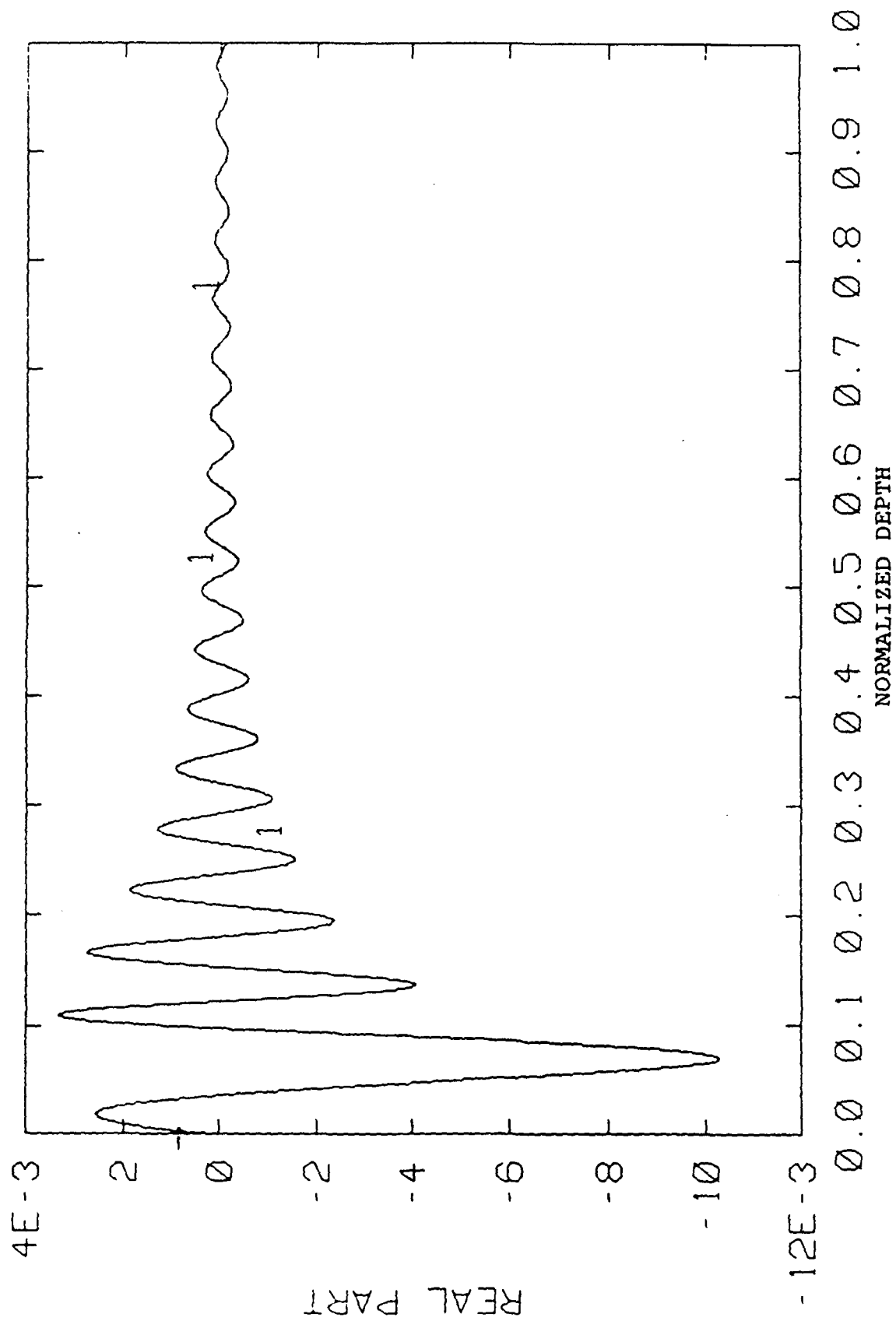
Figure 19c: Fourier Transform of Figure 19 (a,b)
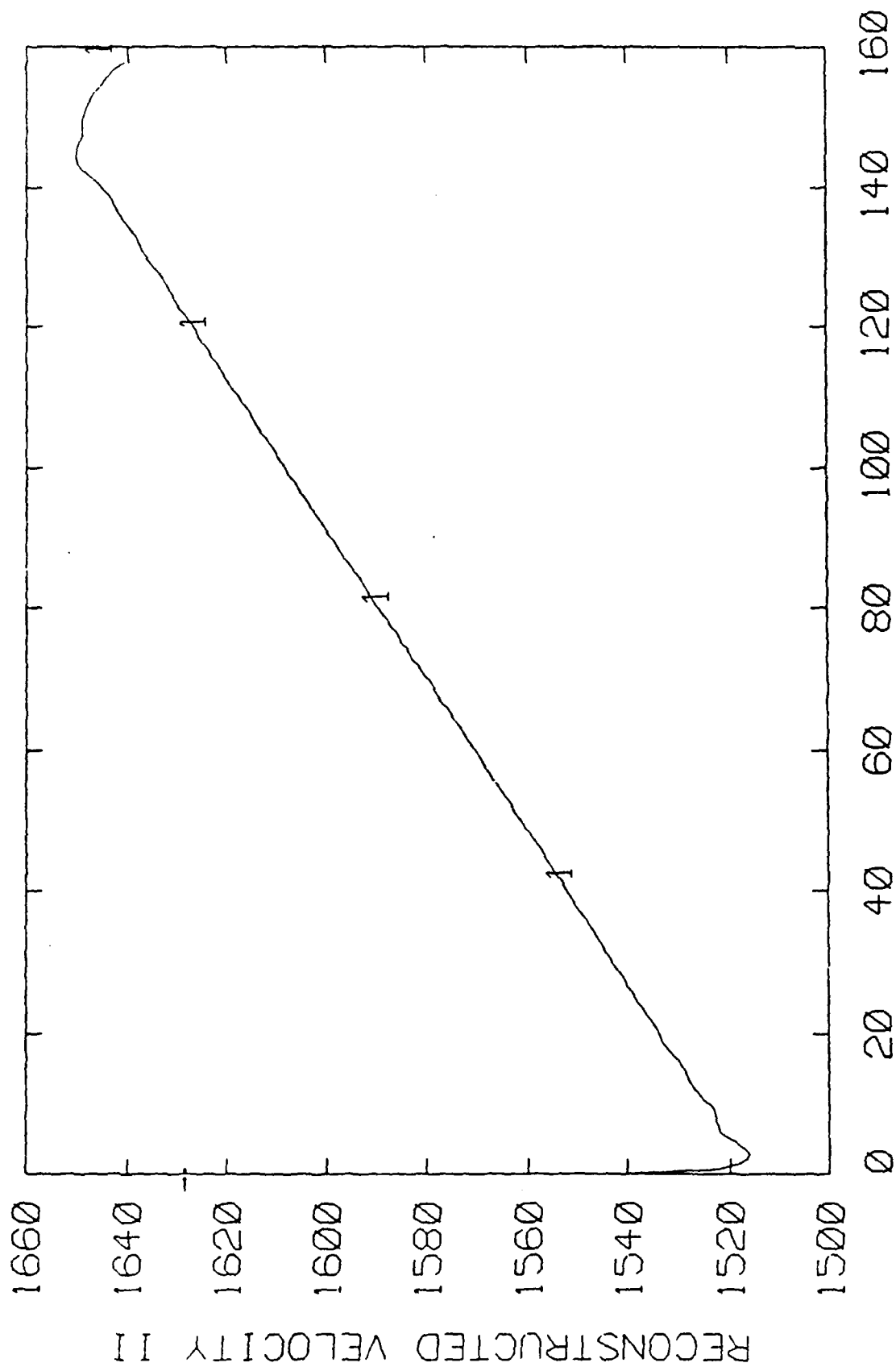
Figure 19d: Reconstructed Velocity - Frisk Profile - 20 Iterations
Limited Range K_{zmax} = 0.512, f = 25Hz
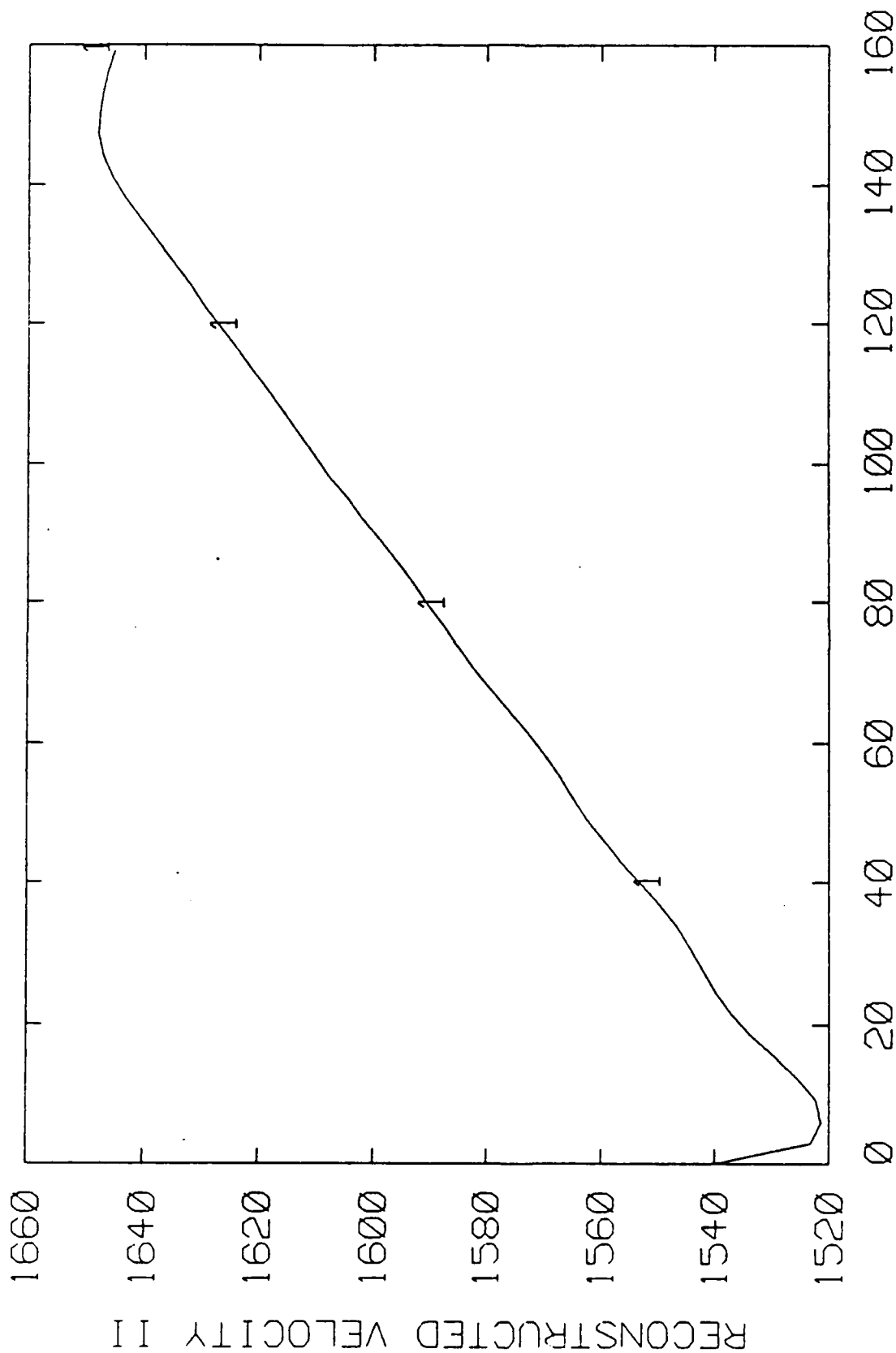
Figure 20: Frisk Profile Reconstruction. 50 Iterations
$\Delta K_z = 0.0005$, $\Delta z = 3.06m$, $K_{zmax} = 0.125$
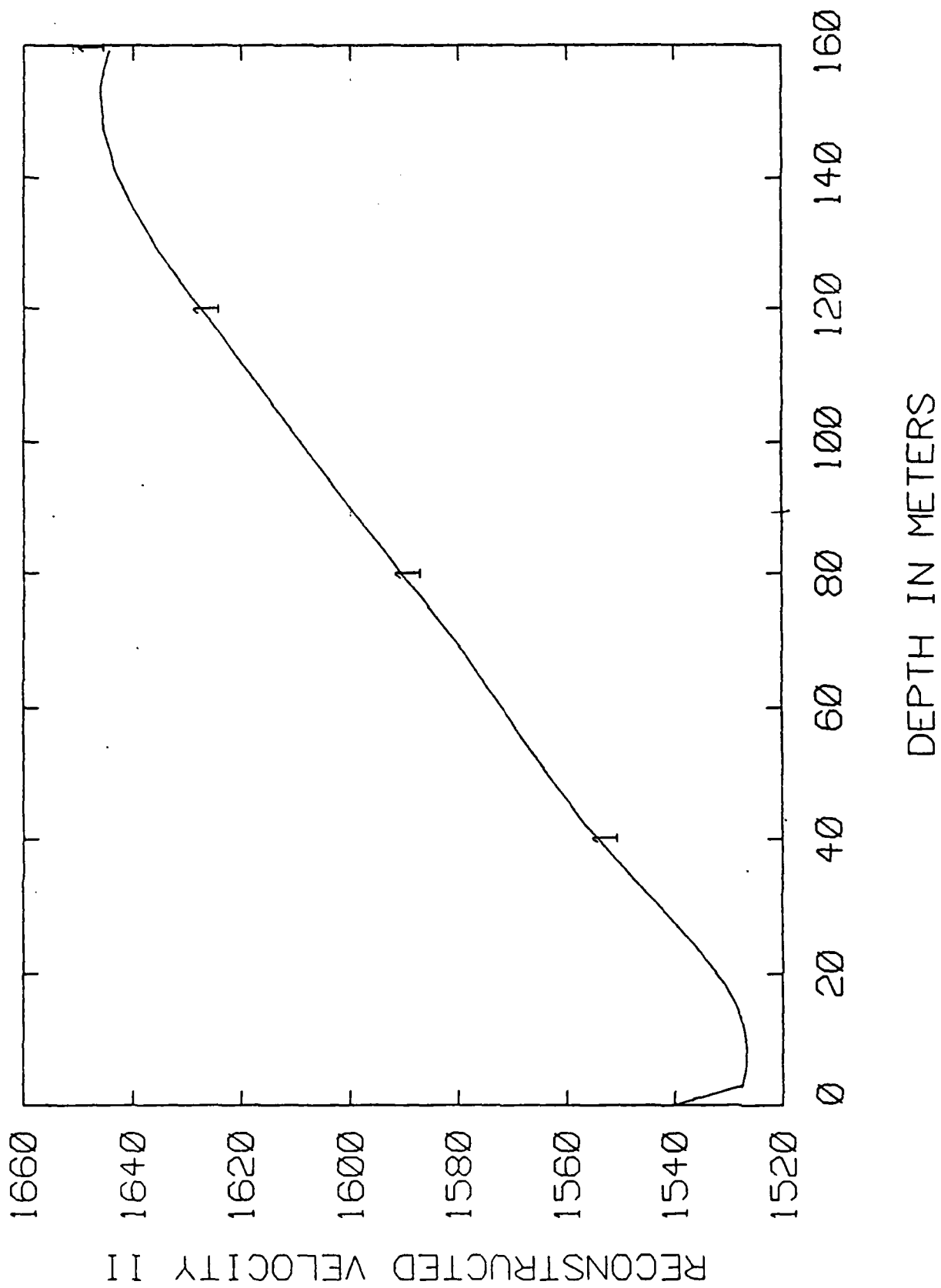
Figure 21: Frisk Profile Reconstruction. 40 Iterations
Limited Range $K_{zmax} = 0.064$ - $\Delta z = 3.06m$
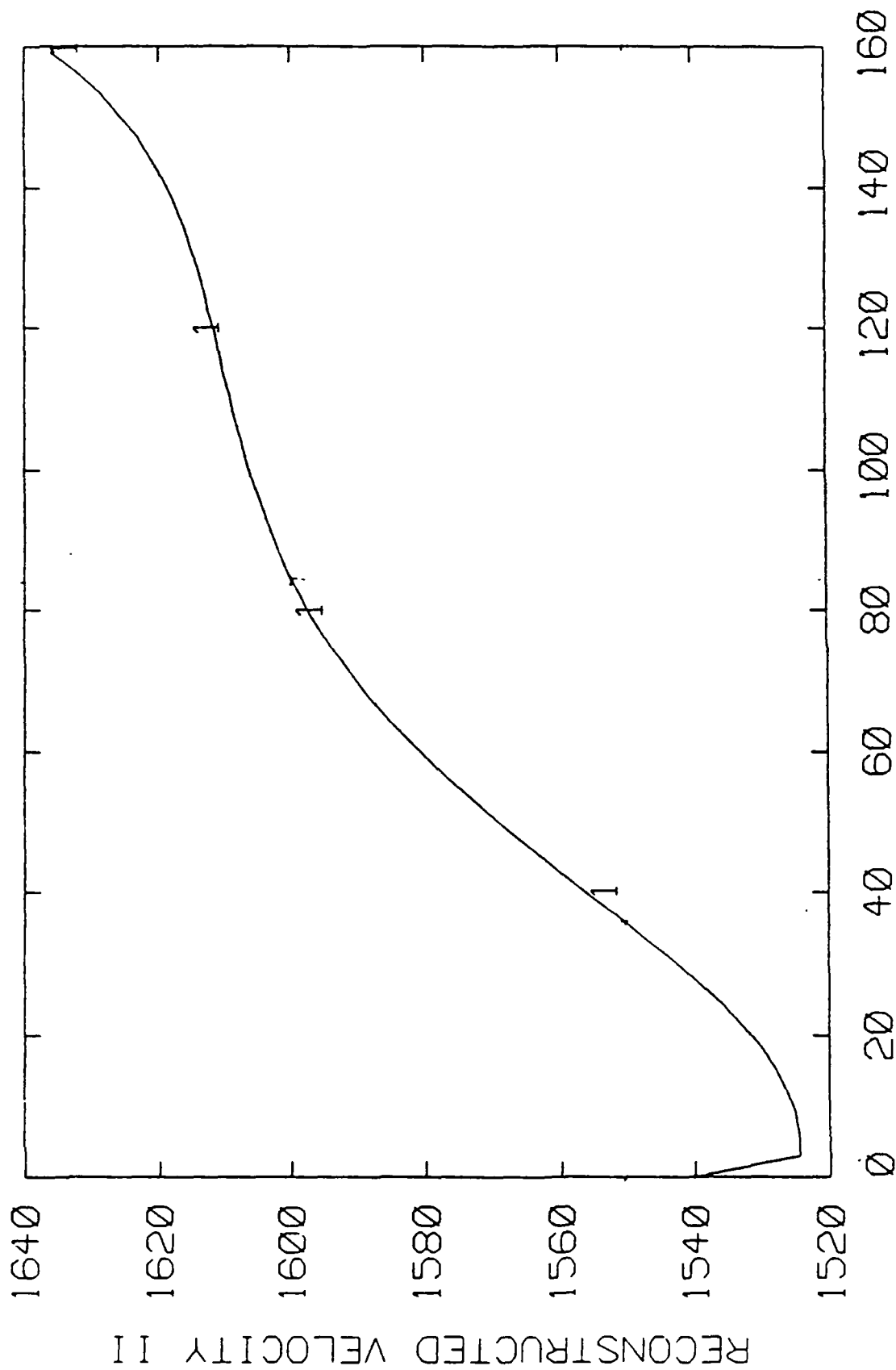
Figure 22: Frisk Profile Reconstruction. 40 Iterations
Limited Range $K_{zmax} = 0.032$. $\Delta z = 3.06m$
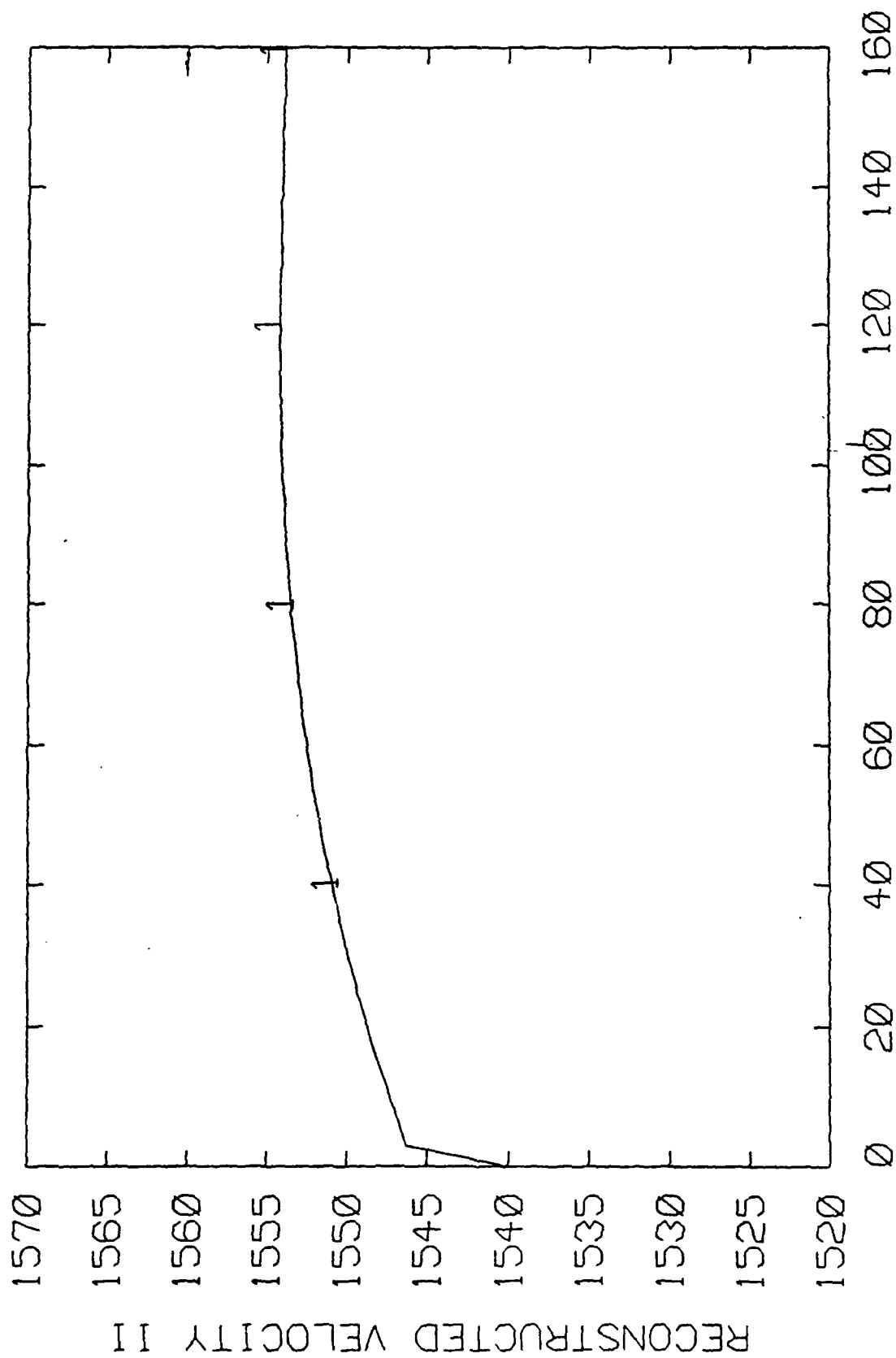
Figure 23: Frisk Profile Reconstruction.
Limited Range $K_{zmax} = 0.016$, $\Delta z = 3.06m$
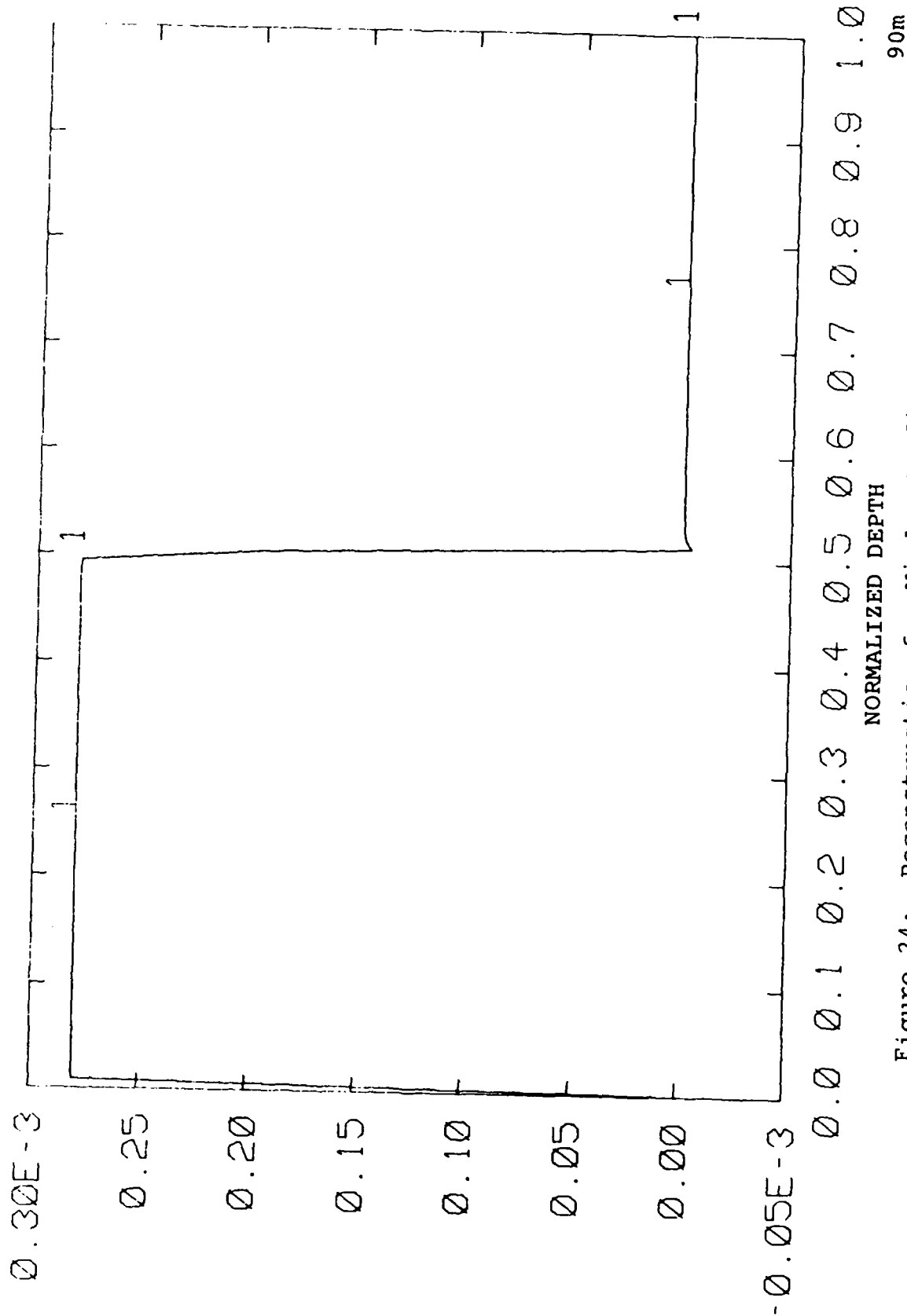
Figure 24: Reconstruction for Window Profile (Potential)

$\Delta z = 0.767m, \quad f = 25Hz$

90m
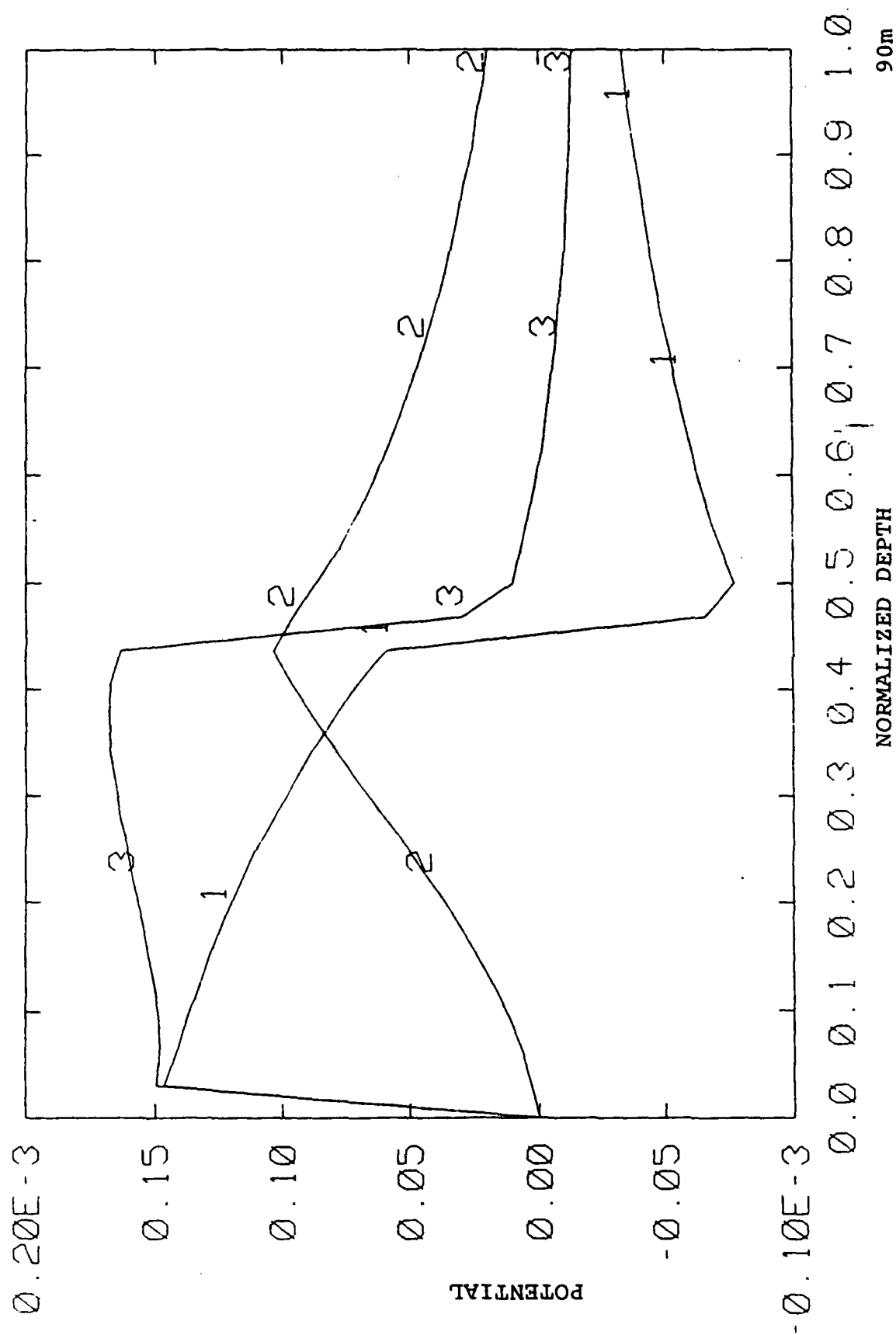
Figure 25a: Lossy Window Profile Reconstruction (W = 45m) α = 0.001dB/m
1: Born, 2: Correction, 3: Improved Born. f = 25Hz
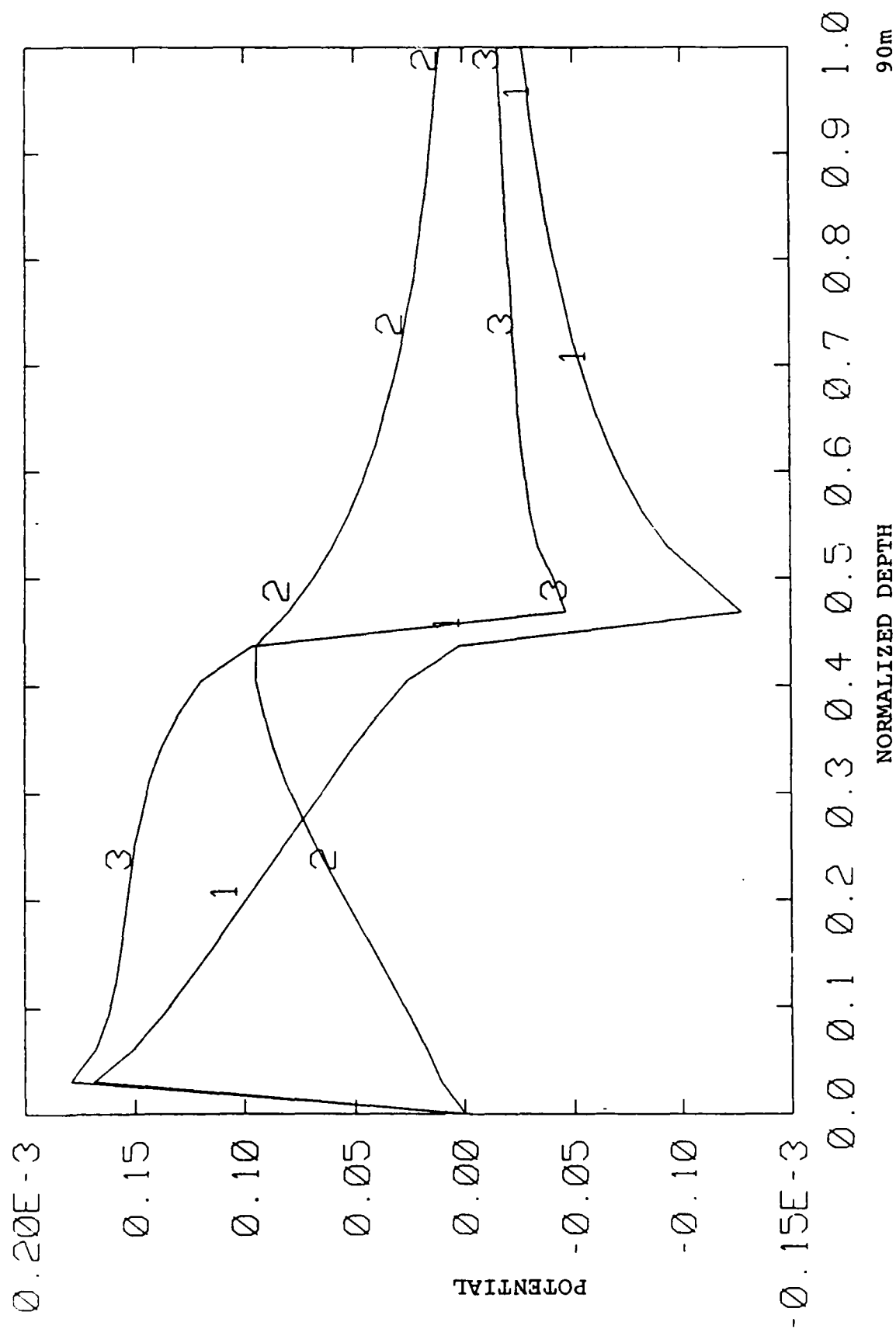
Figure 25b: Lossy Window Profile Reconstruction (W = 45m), α = 0.005db/m
1: Born, 2: Correction, 3: Improved Born. f = 25Hz

90m

- 172 -
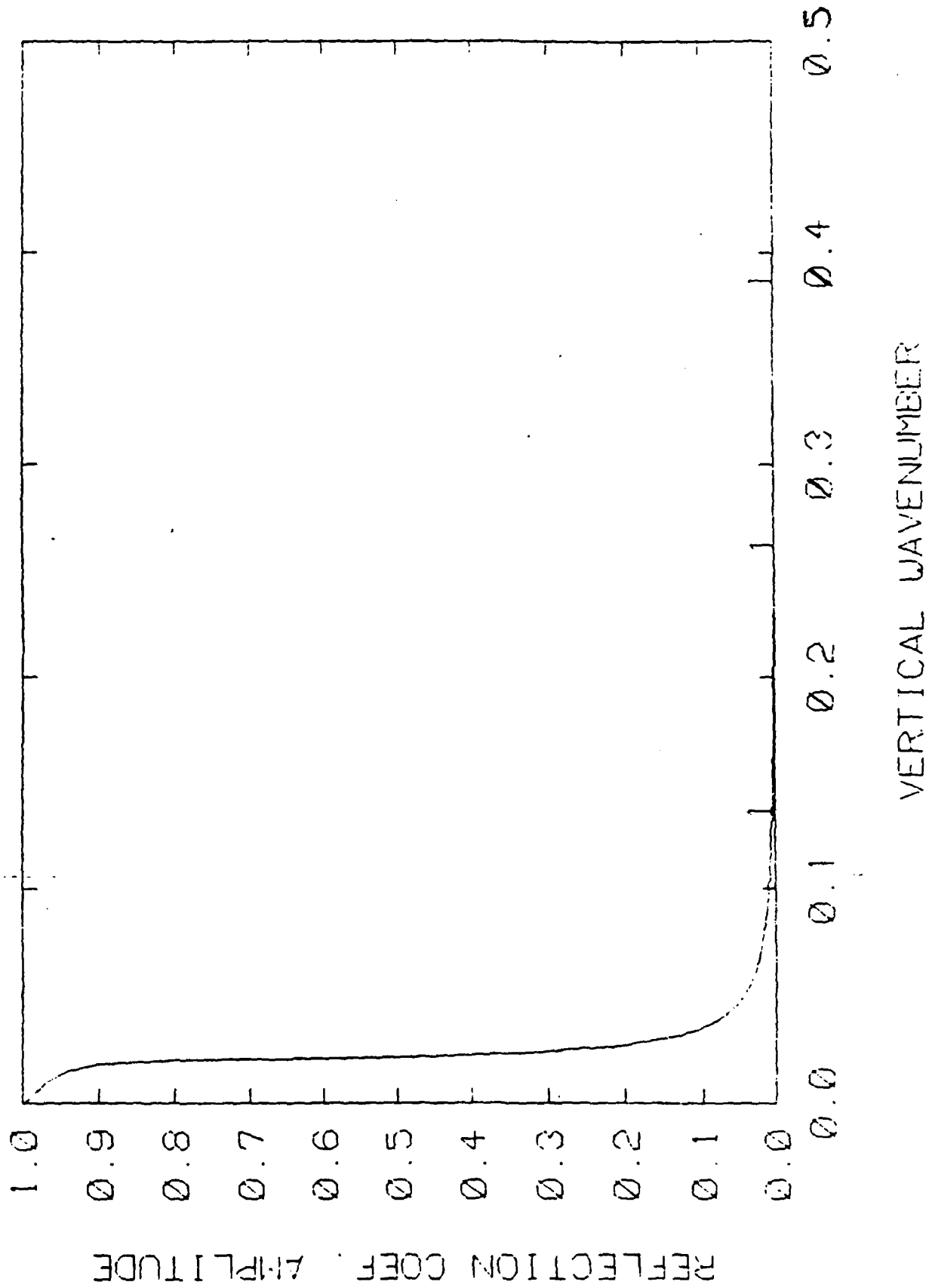
Figure 26a: Reflection Coefficient Amplitude.   f = 25Hz
              Lossy Half Space,   α = 0.0001dB/m
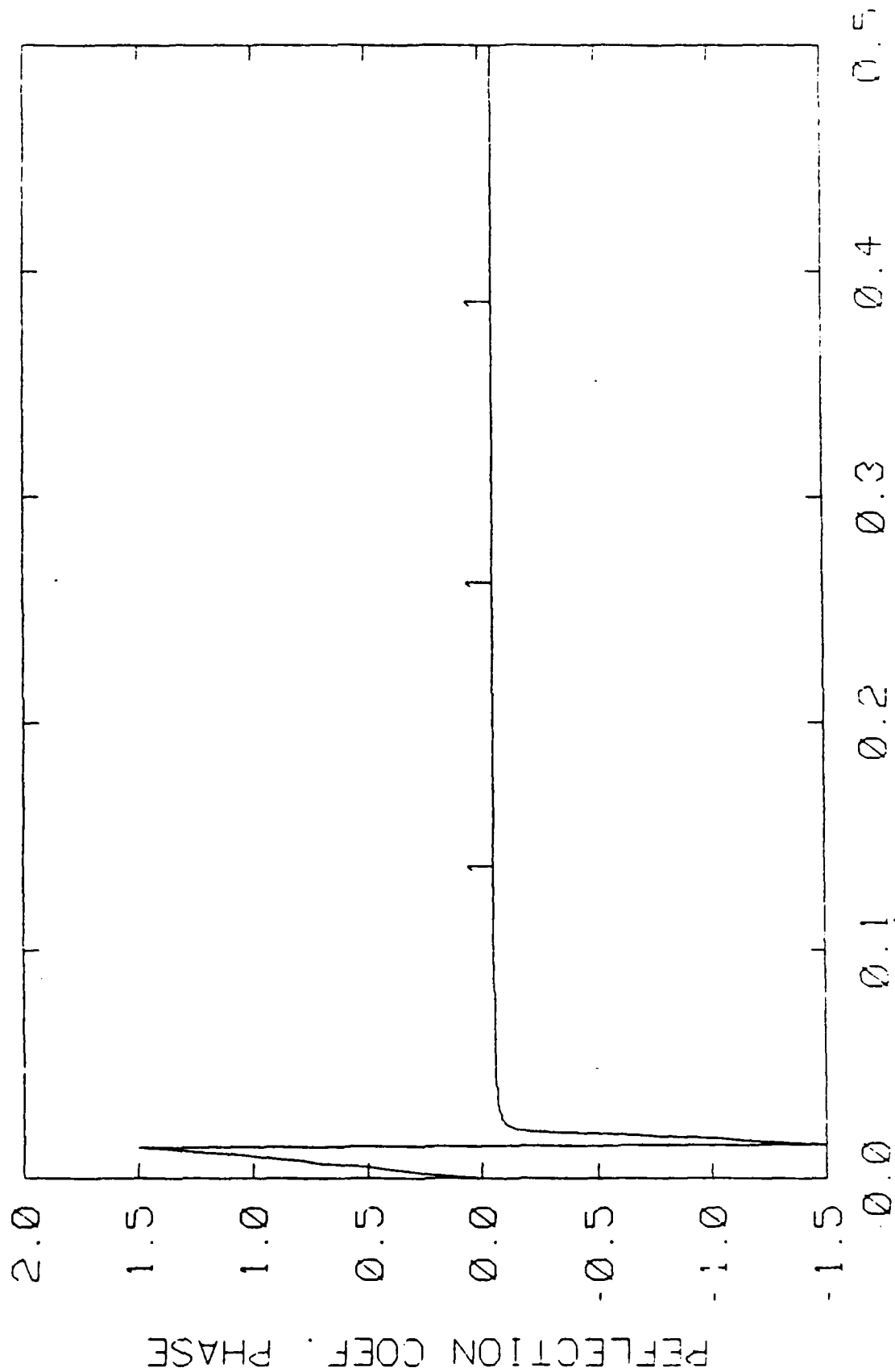
Figure 26b: Reflection Coefficient Phase, f = 25Hz
Lossy Half-Space, α = 0.001dB/m
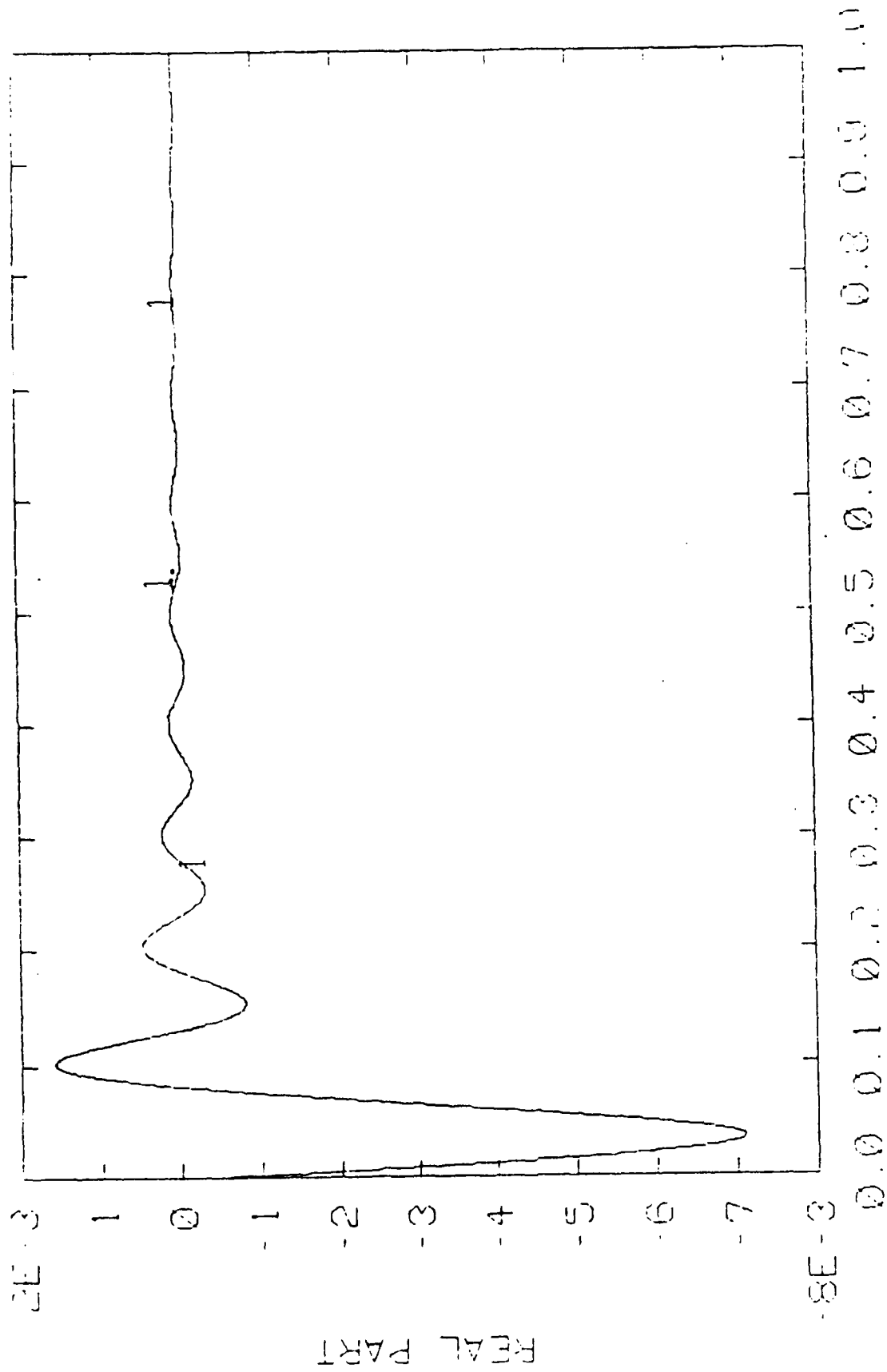
Figure 26c: Fourier Transform of Figure 26(a,b)
Lossy Half-Space, α = 0.001dB/m
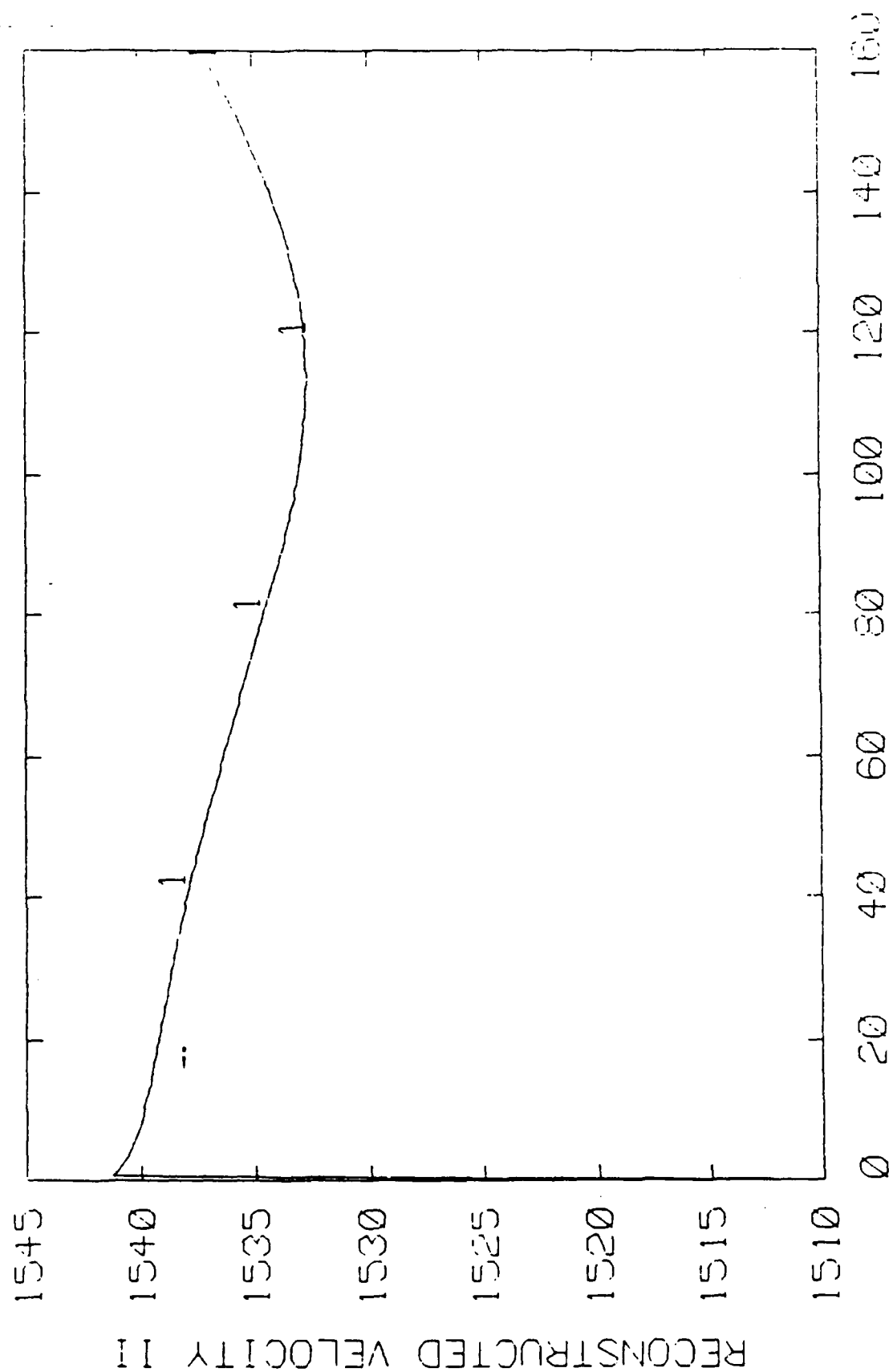
Figure 26d: Lossy Half-Space Reconstruction, α = 0.001dB/m
Δz = 0.767m, f = 25Hz

VERTICAL WAVENUMBER
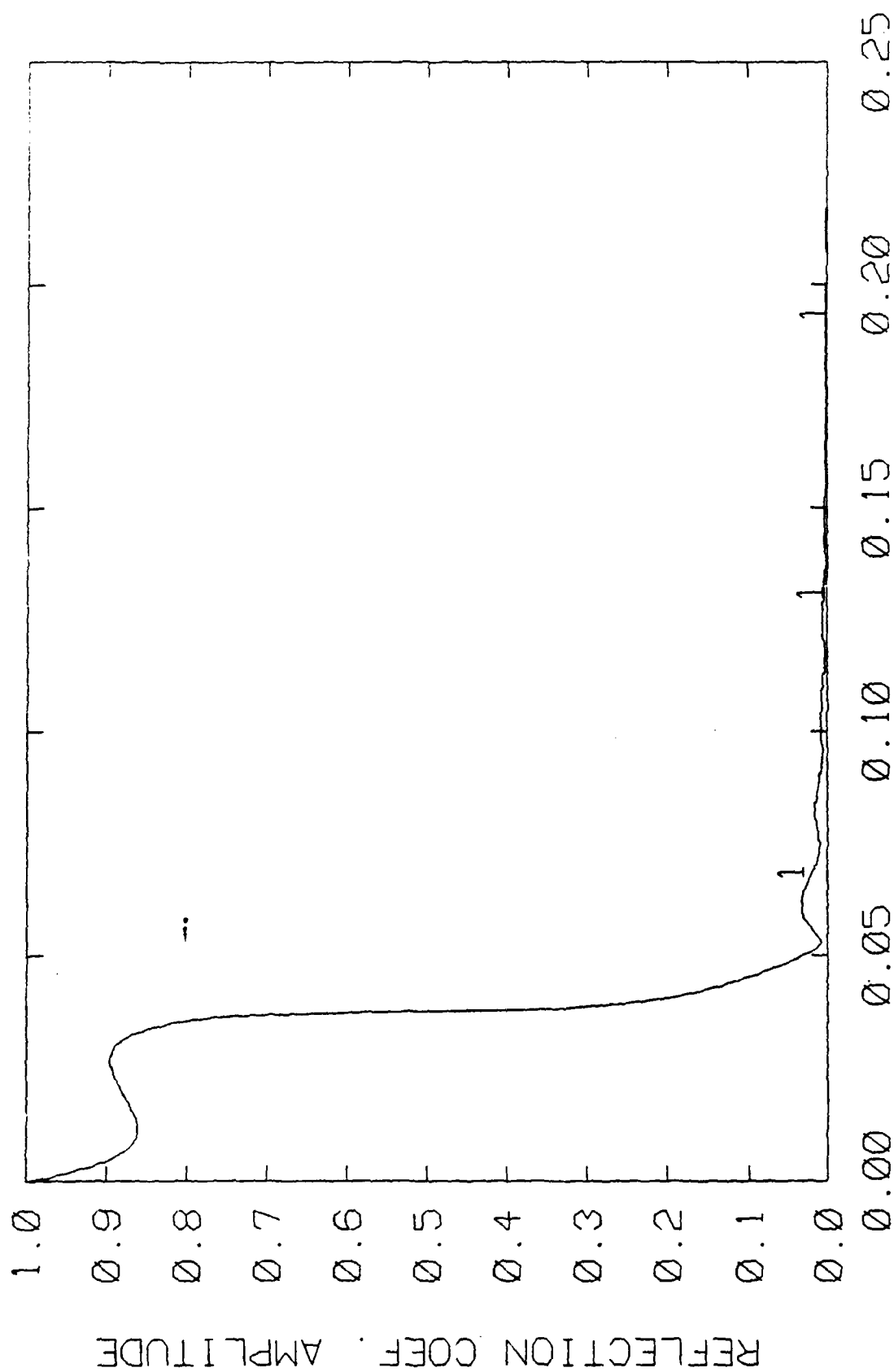
Figure 27a: Reflection Coefficient Amplitude, f = 25Hz
Lossy Frisk Profile,   α= 0.005dB/m
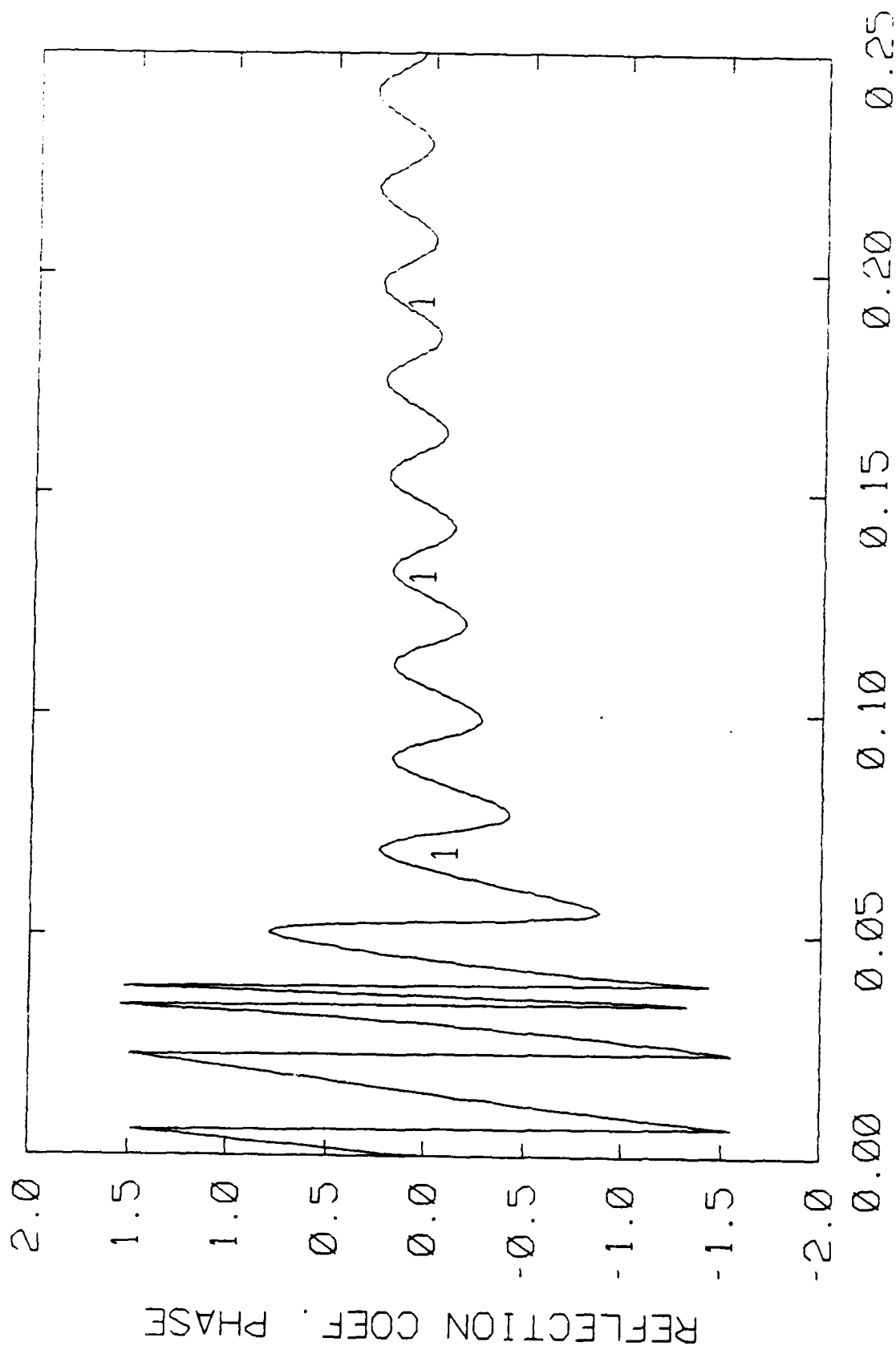
Figure 27b: Reflection Coefficient Phase, f = 25Hz
Lossy Frisk Profile, α= 0.005dB/m

NORMALIZED DEPTH
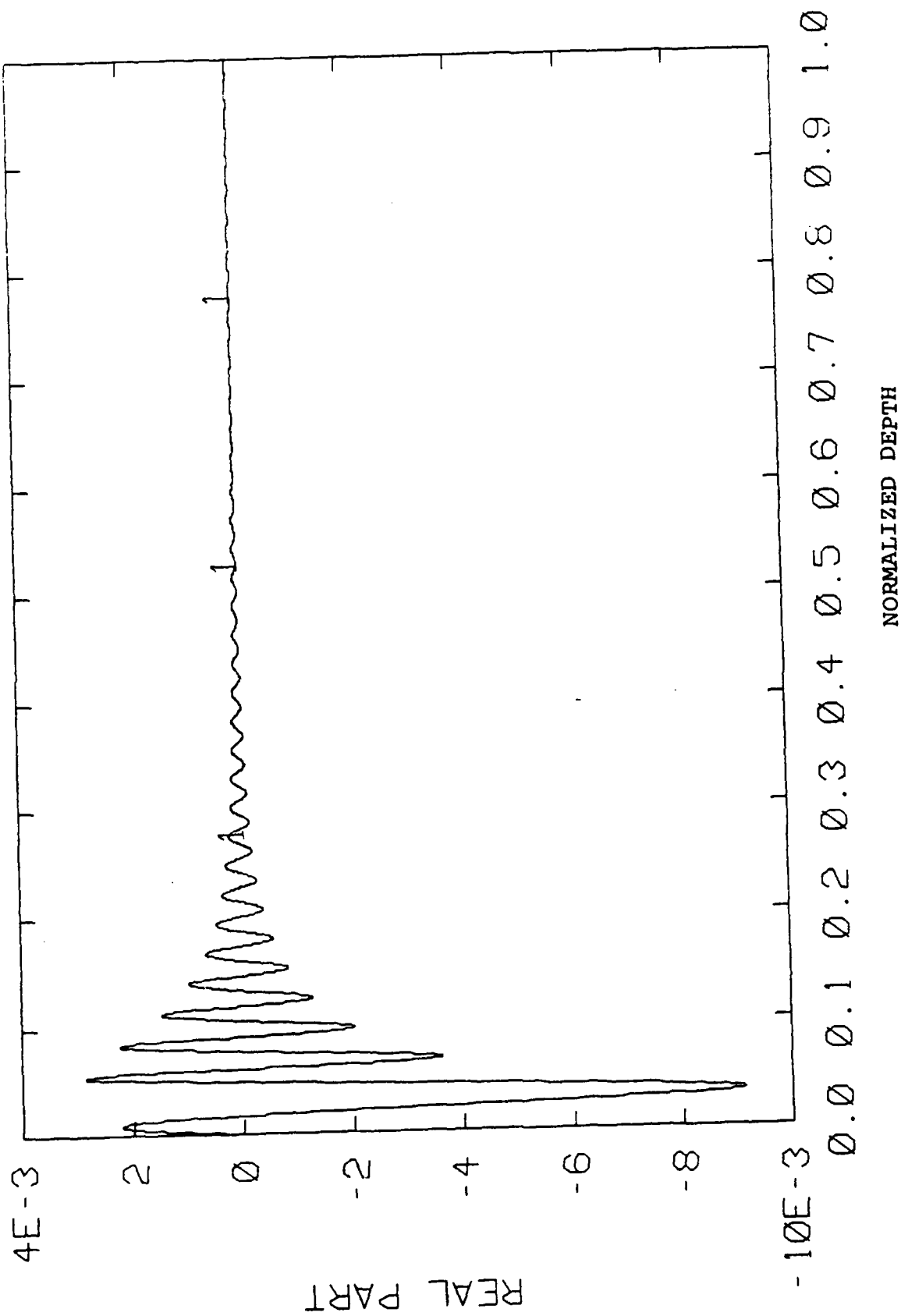
Figure 27c: Fourier Transform of Figure 27 (a,b)
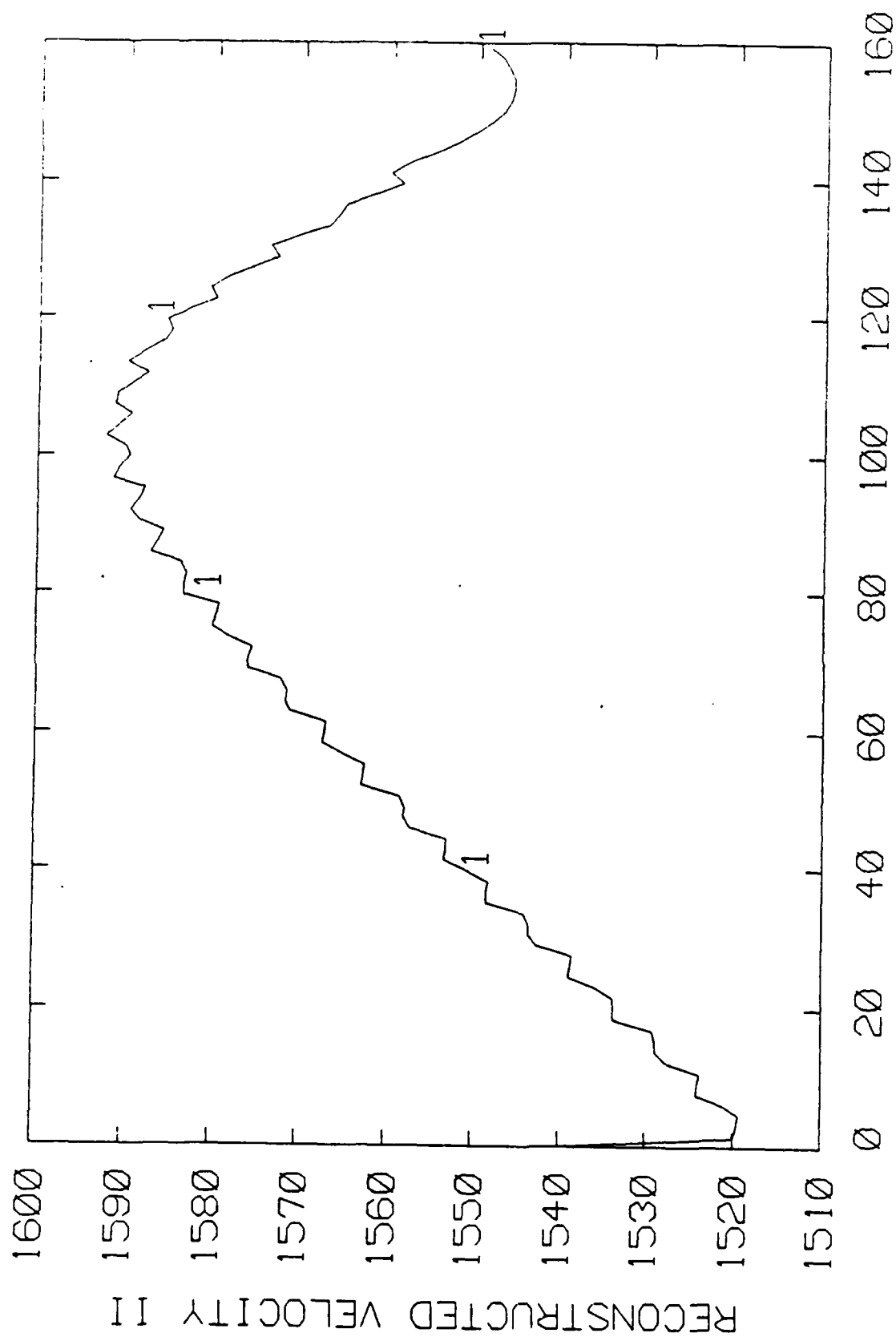
Figure 27d: Velocity Reconstruction, f = 25Hz
Lossy Frisk Profile,   α= 0.005dB/m
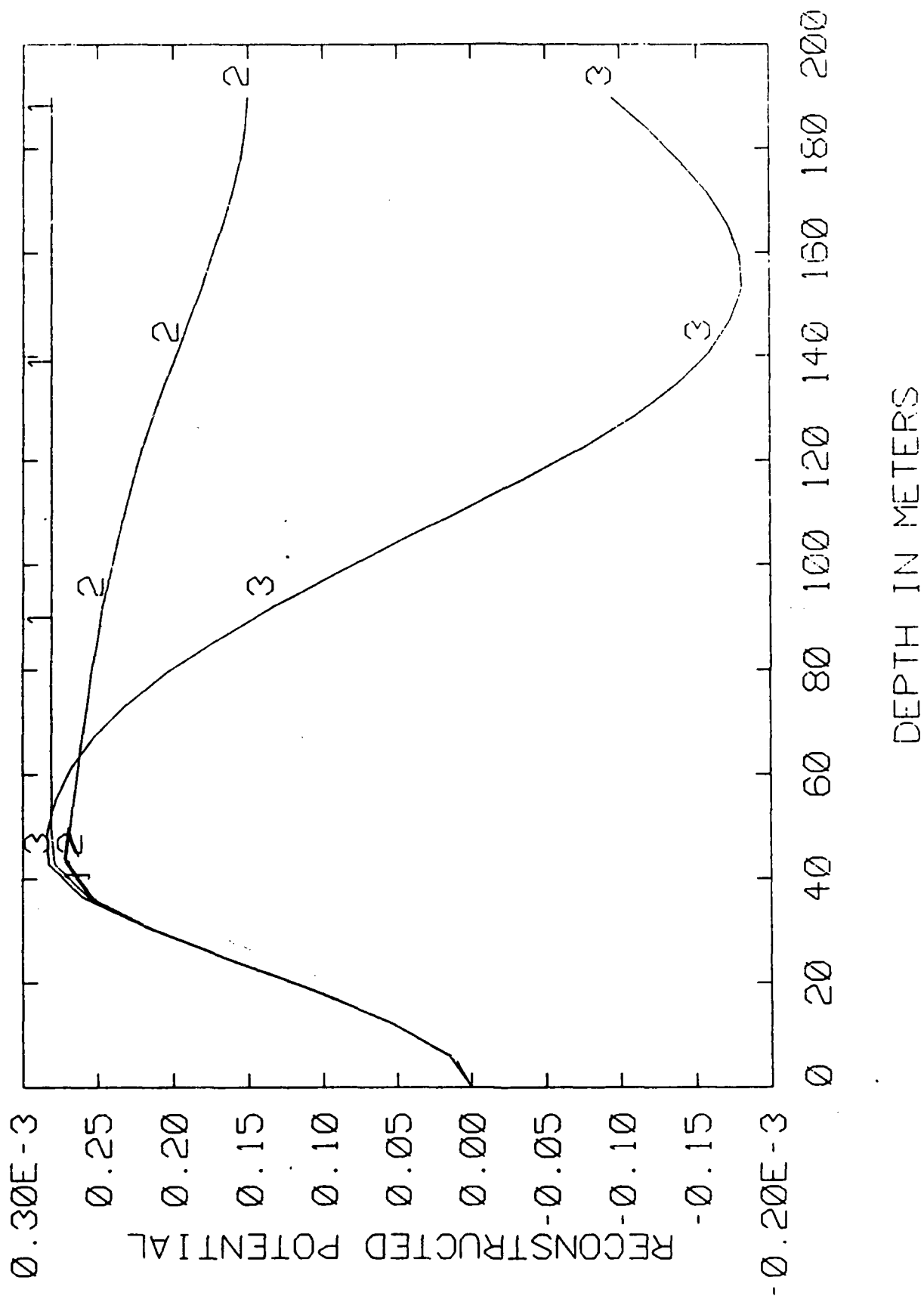
Figure 28: Stickler Profile Reconstruction. $\Delta z = 6.03m$, $L = 40m$, $f = 25Hz$; 1: Original Profile, 2: Finite Difference, 3: Improved Born
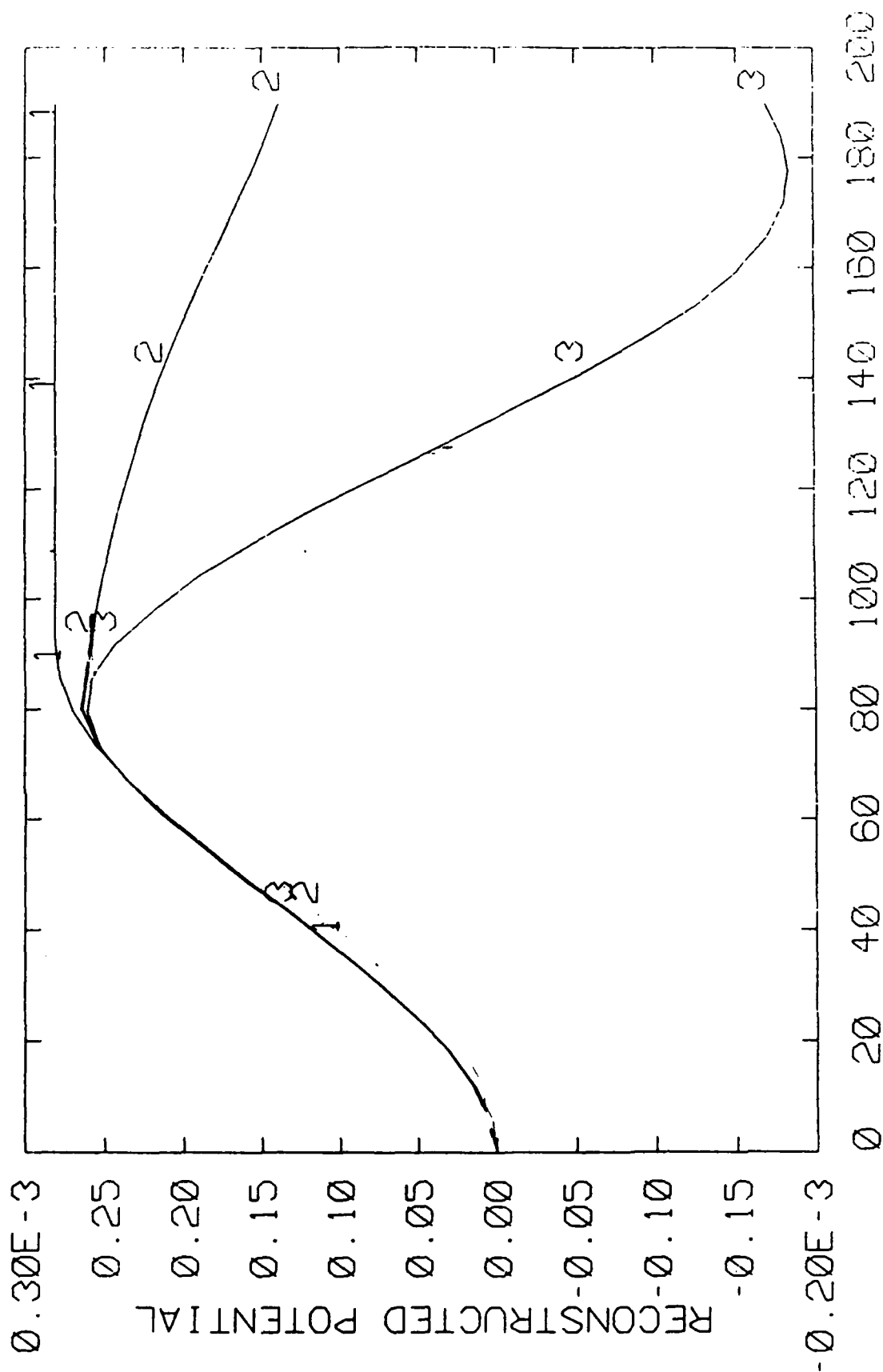
Figure 29: Stickler Profile Reconstruction. $\Delta z = 6m$, $L = 90.6m$
1: orginal profile, 2: Finite Difference, 3: Improved Born
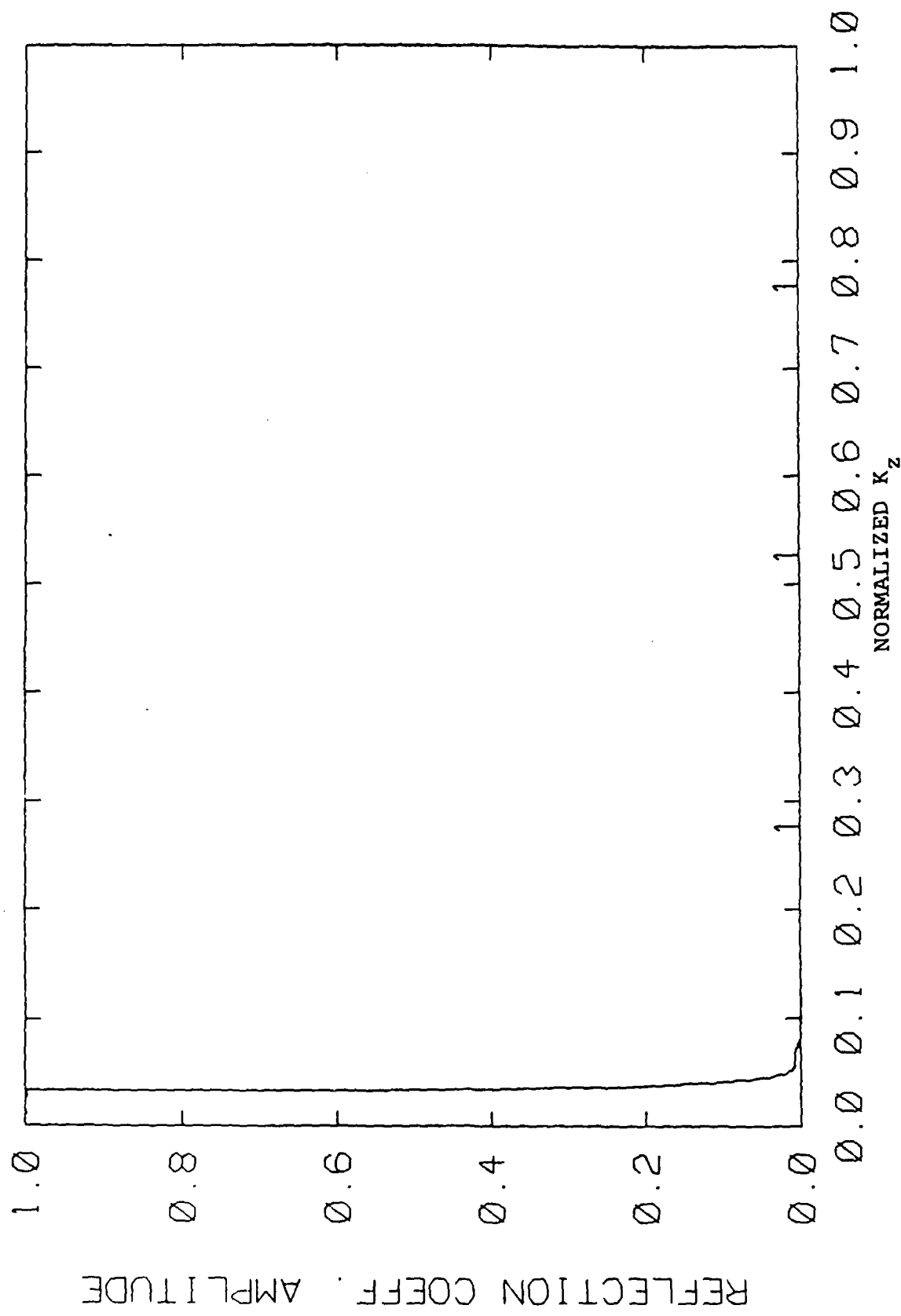
Figure 30a: Reflection Amplitude - Stickler Profile
Density $\rho(z) = c(2)/1000$, $f = 25Hz$
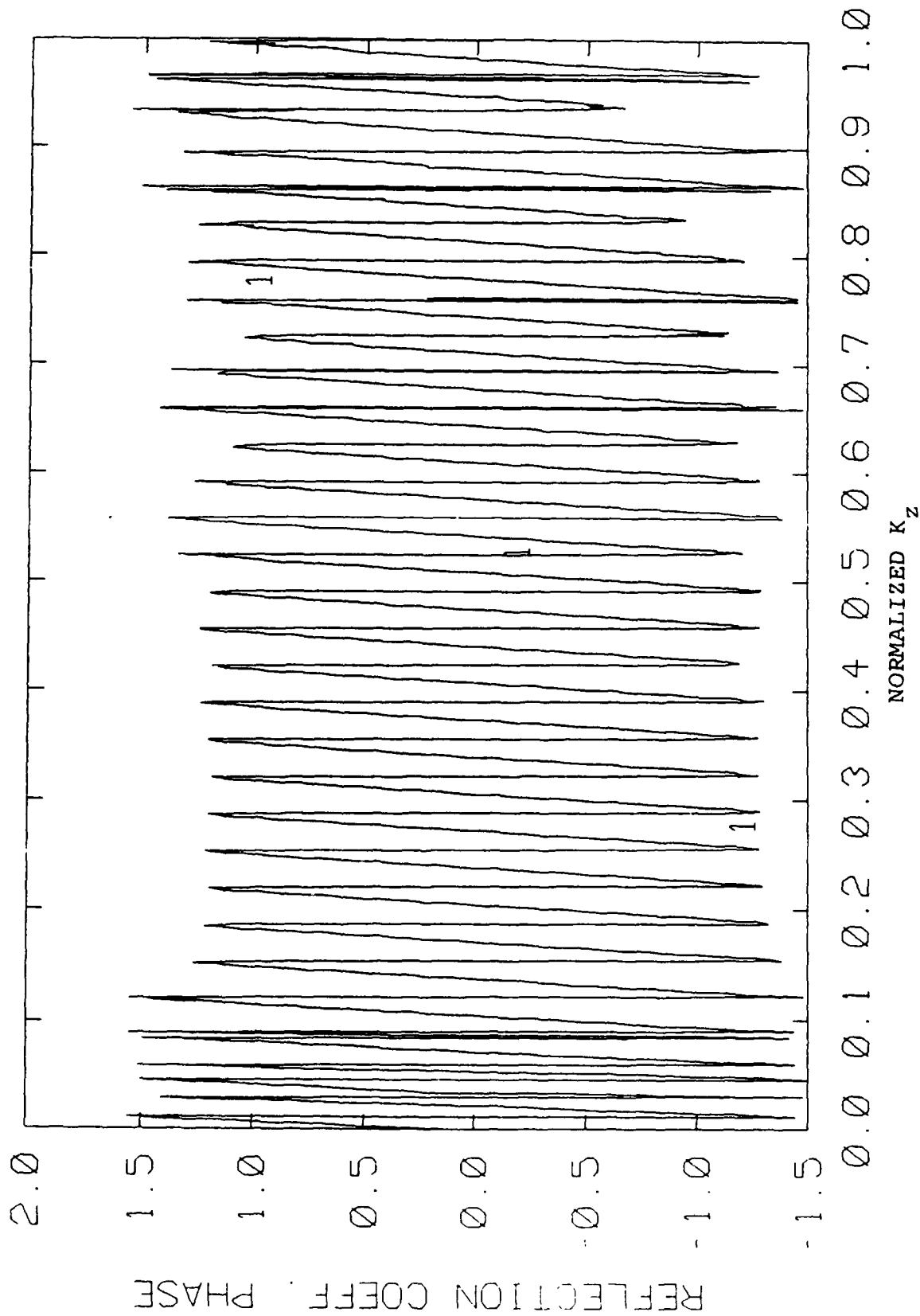
Figure 30b: Reflection Phase Stickler Profile
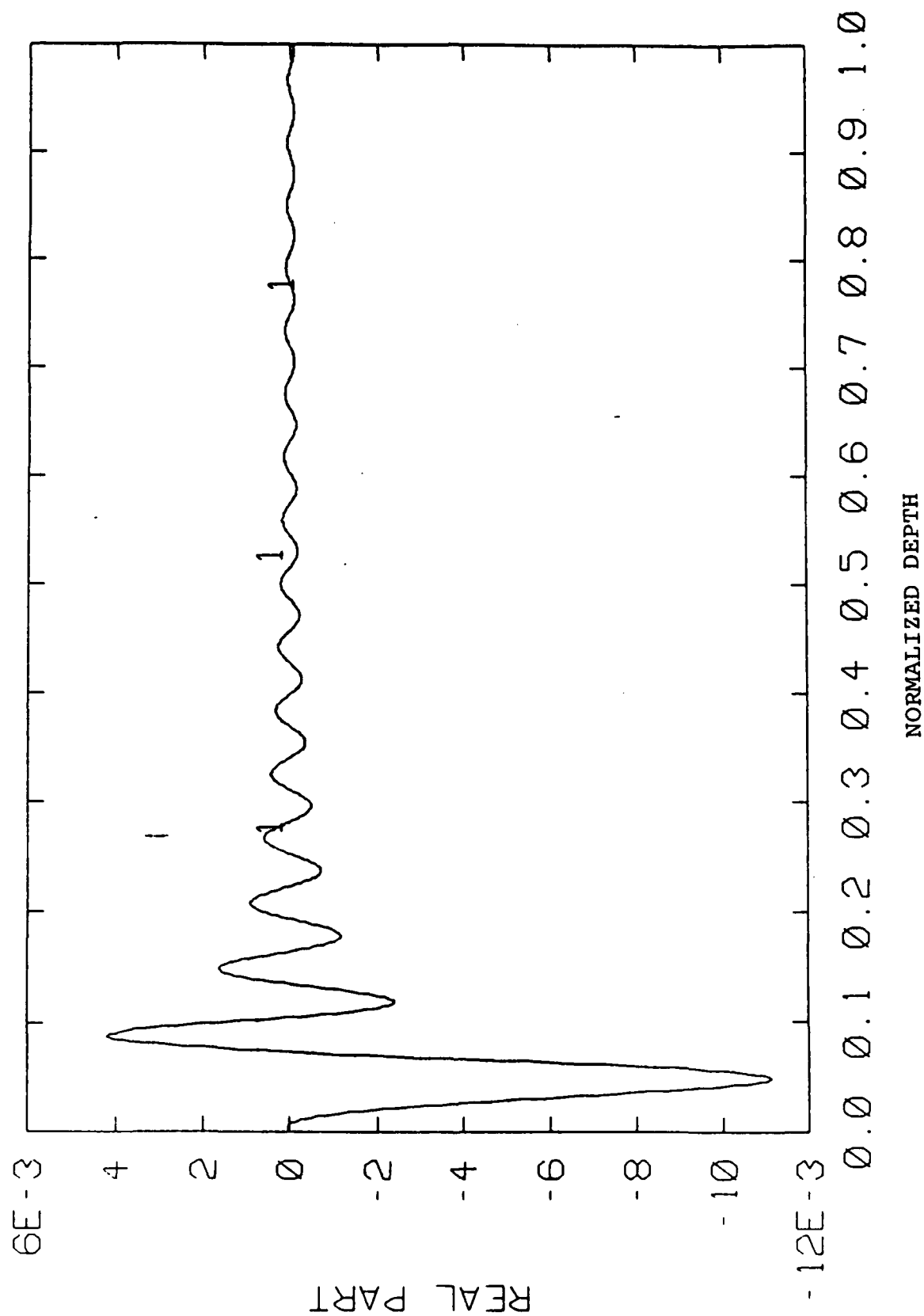Density $\rho(z) = c(z)/1000$, $f = 25Hz$

Figure 30c: Fourier Transform of Figure 30 (a,b)

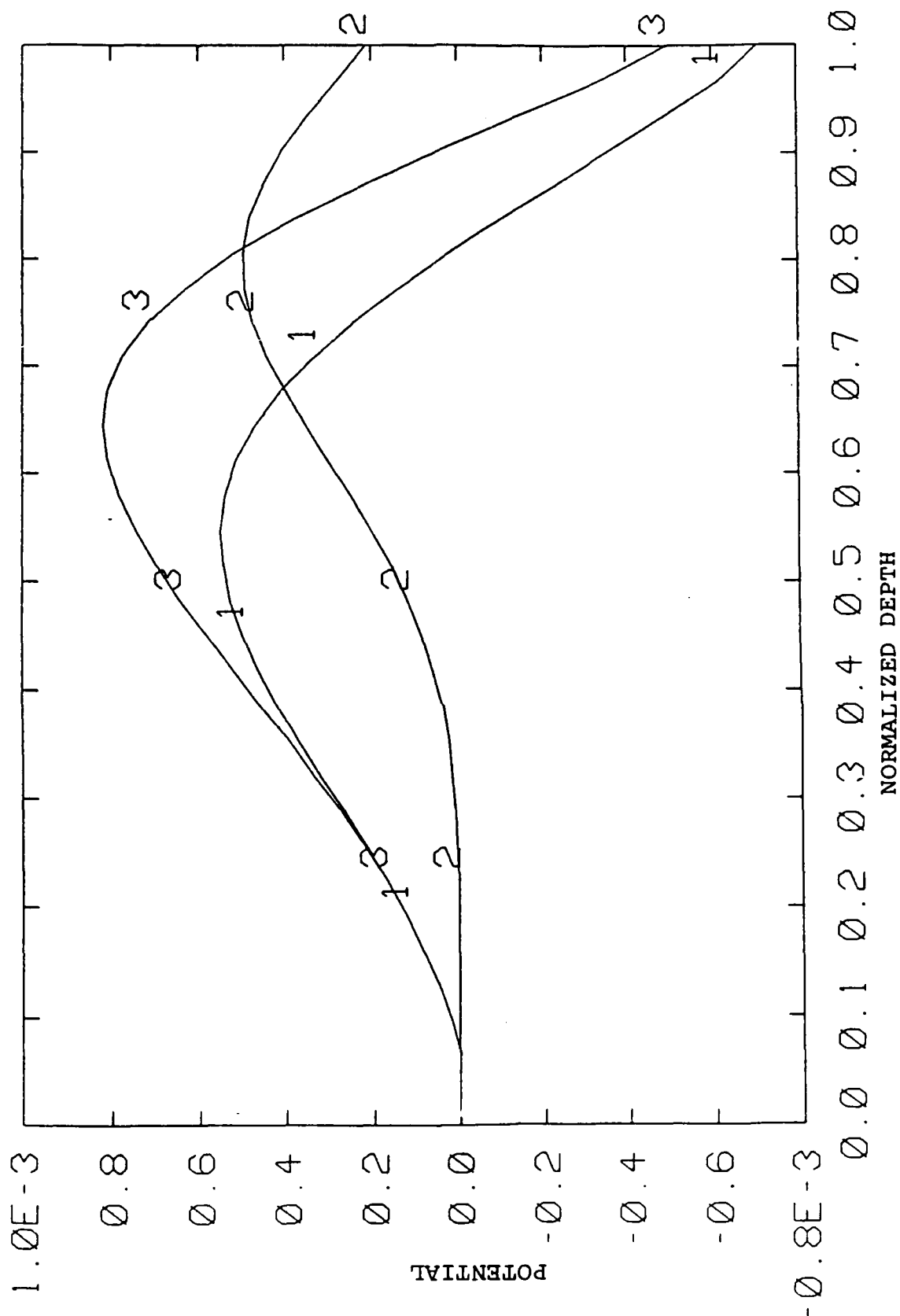Figure 30d: Density-Dependent Potential Reconstruction $V_1'(z)$
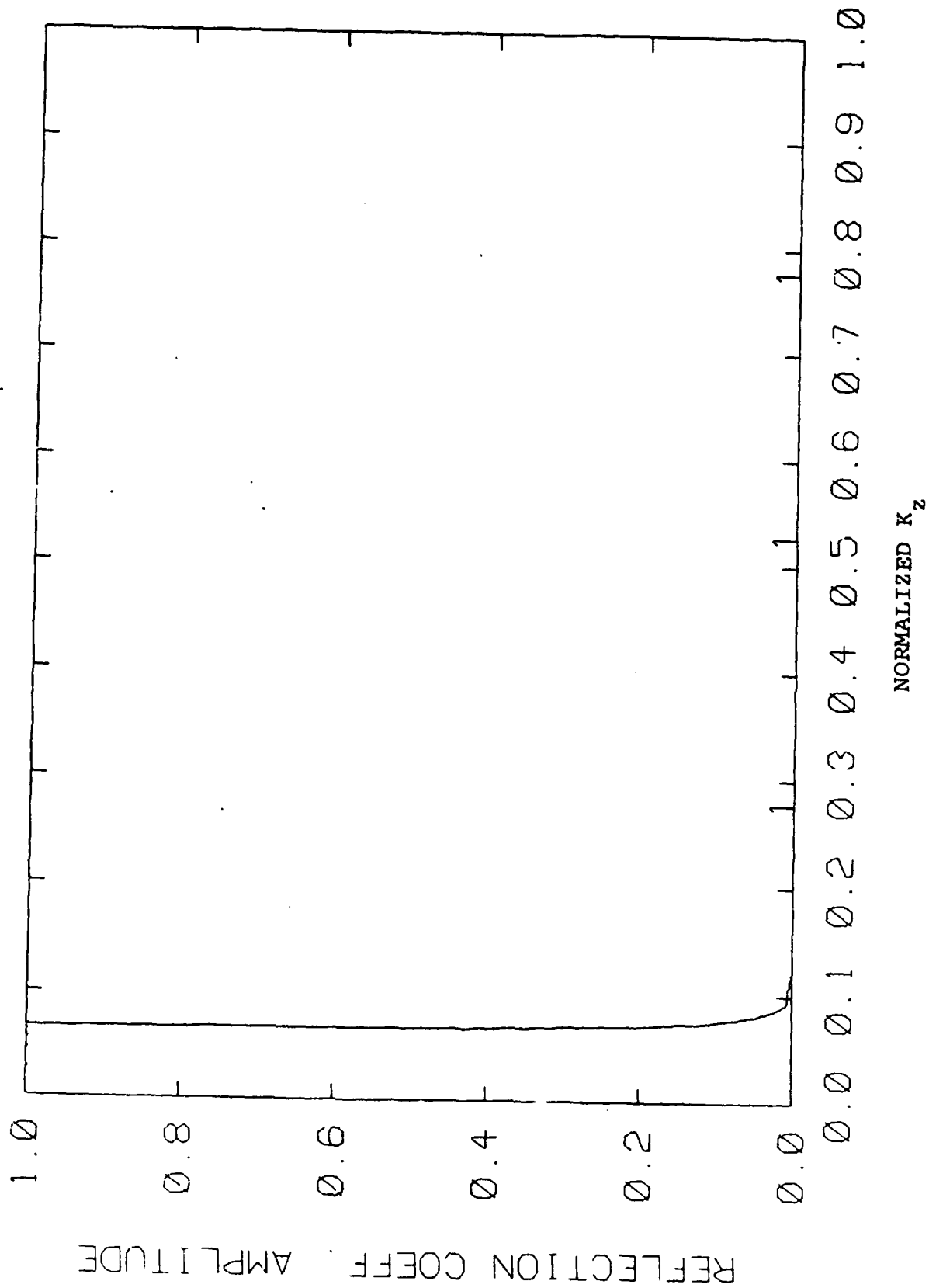Born: 1, Correction: 2, Improved Born: 3
$f = 25Hz$, $\rho(z) = c(z)/1000$

NORMALIZED K_z

Figure 30e: Reflection Amplitude. Stickler Profile
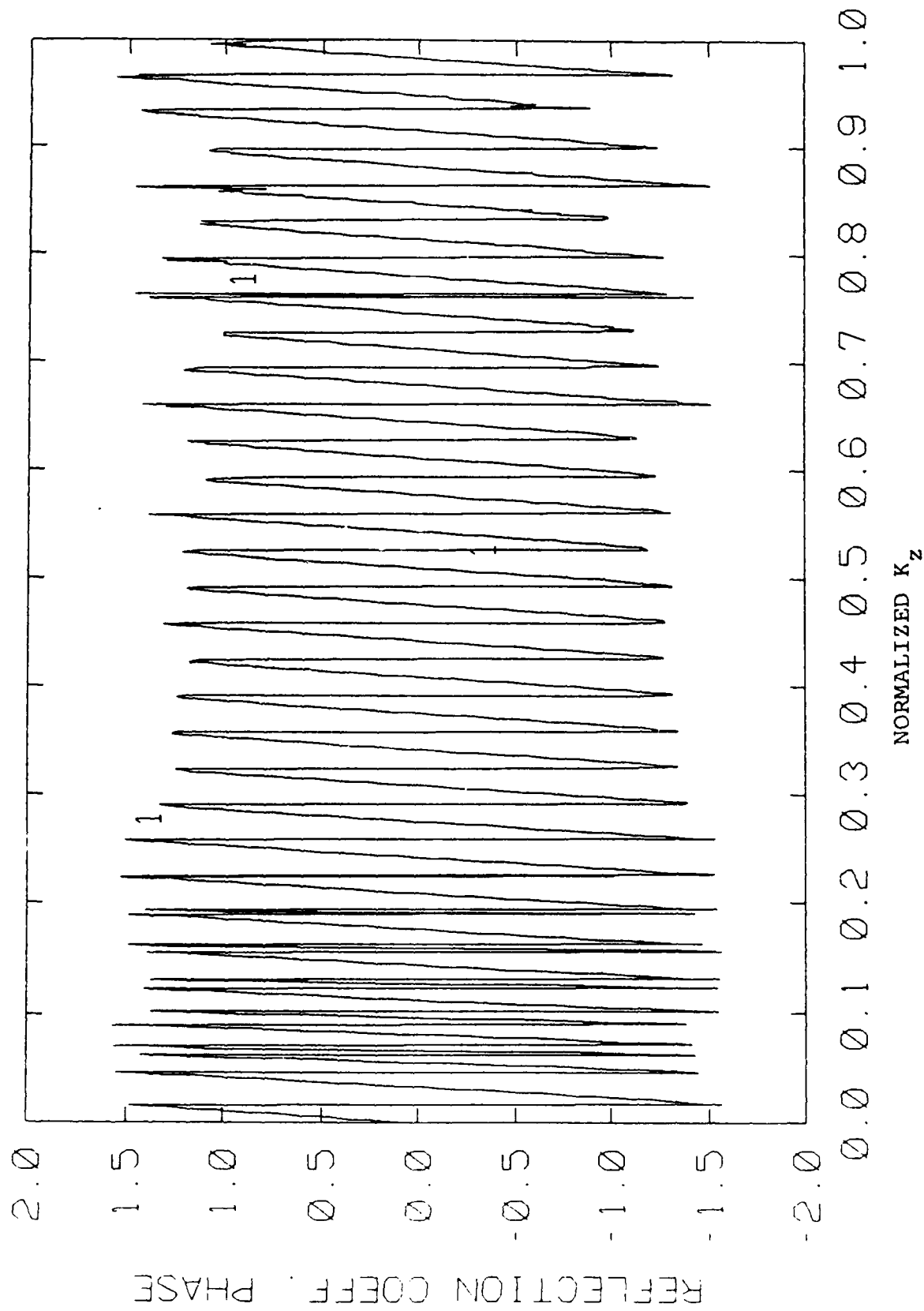f = 50Hz, Density $\rho(z) = c(z)/1000$

Figure 30f: Reflection Phase. Stickler Profile
f = 50Hz, $\rho(z) = c(z)/1000$

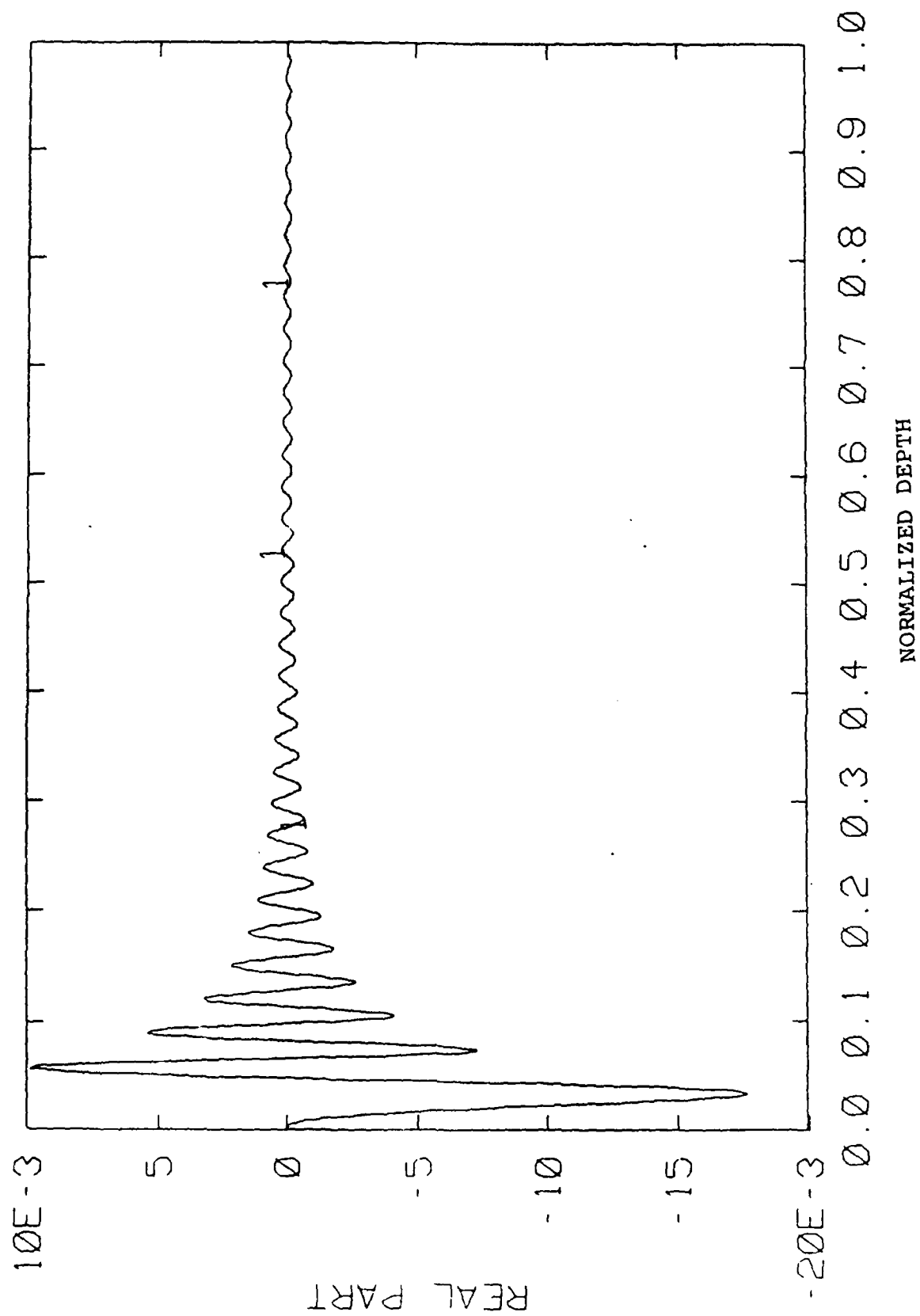NORMALIZED K_z

REFLECTION COEFF. PHASE
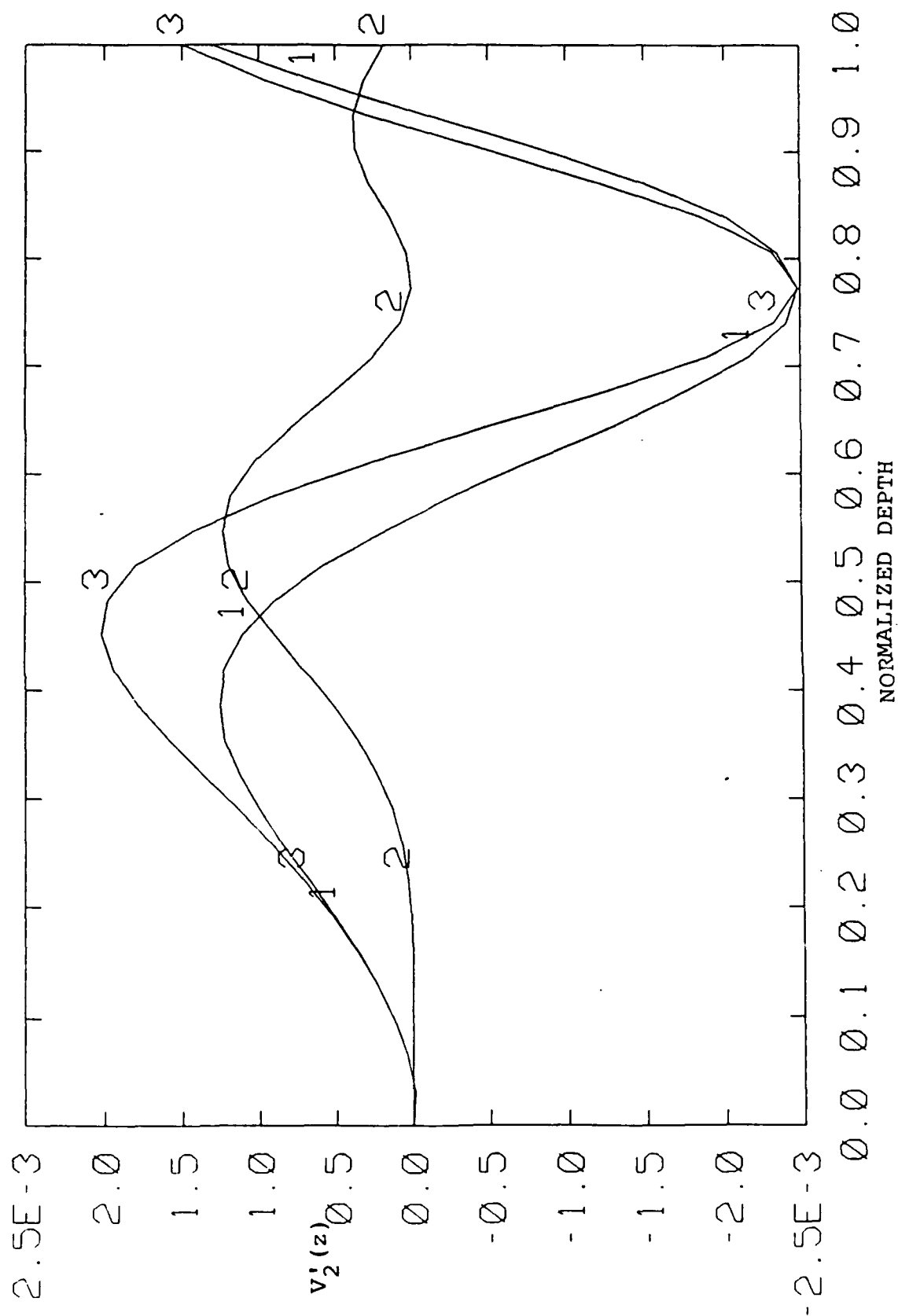
NORMALIZED DEPTH

Figure 30g: Fourier Transform of Figure 30 (e,f)

Figure 30h: Density-Dependent Potential Reconstruction $V_2'(z)$
Born:1, Correction: 2, Improved Born: 3
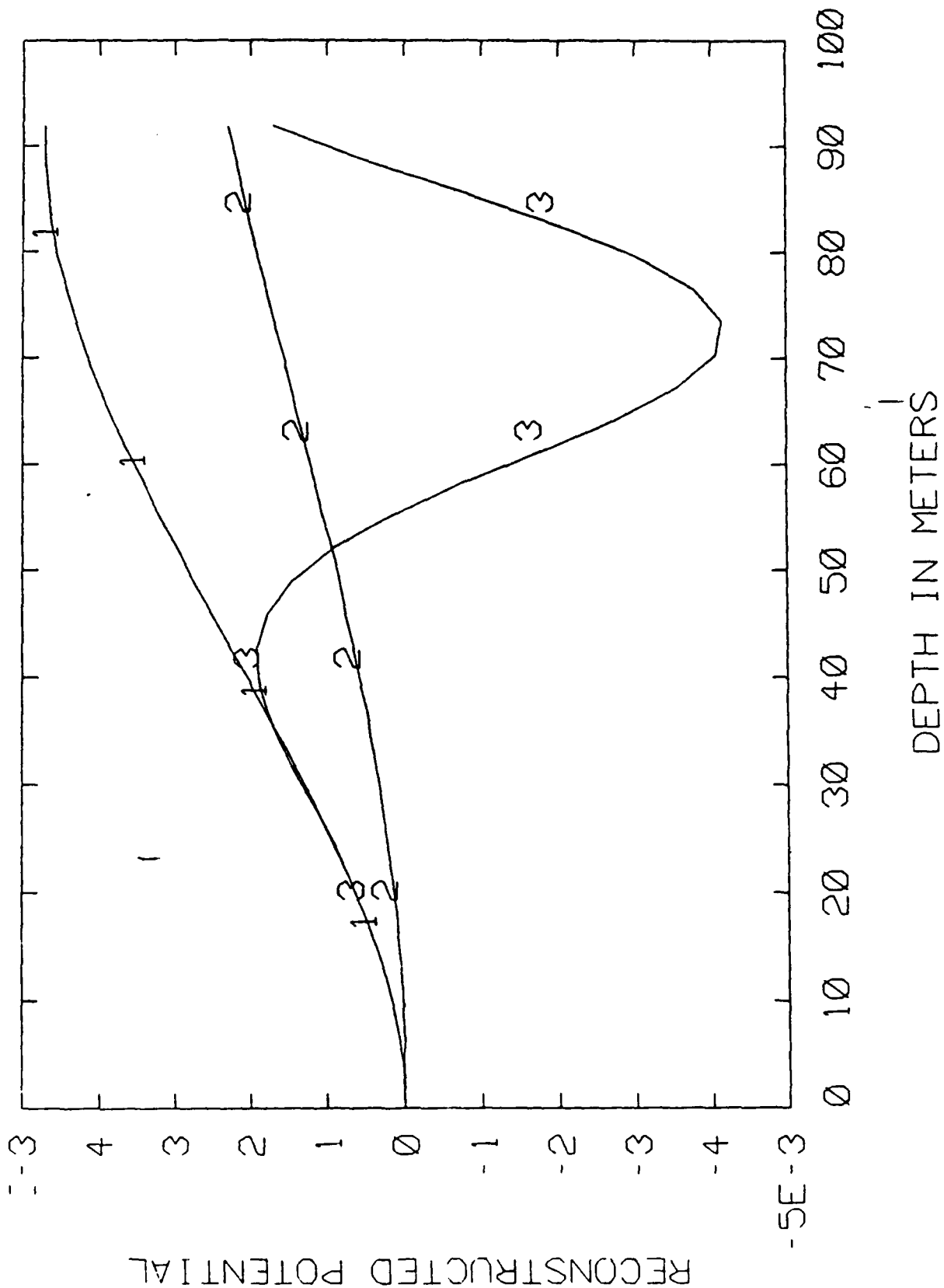f=50Hz, Density $\rho(z) = c(z)/1000$

Figure 30i: Reconstructed Velocity Potential $V(z) - \rho(z) = c(z)/1000$
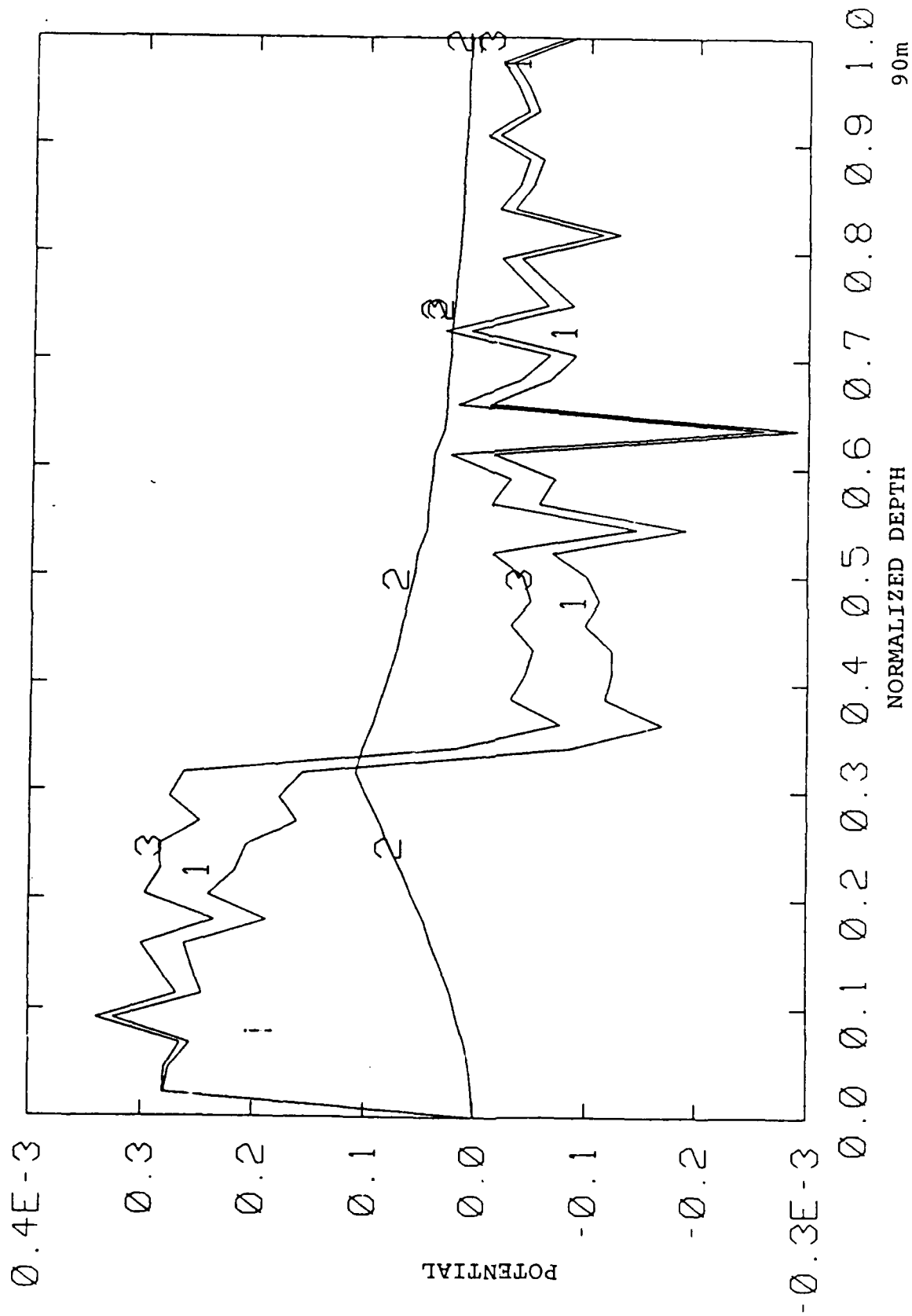1: Original Stickler Profile, 3: Improved Born

Figure 31: Improved Born Reconstruction of Window Profile (W = 45m) Noisy Reflection Coefficient (Zero-Mean Gaussian, $\sigma = 0.1$)

BIBLIOGRAPHY

1. S.R. Santaniello, F.R. diNapoli, R.K. Dullea, and
    P.D. Herstein, NUSC Technical Document 5337, 1976.

2. G.V. Frisk, J. Doutt, and E. Hays, "Bottom Interaction
    of Low-Frequency Acoustic Signals at Small Grazing
    Angles in the Deep Ocean", J. Acoust. Soc. Am., 69,
    84-94 (1981).

3. G.V. Frisk, D.R. Mook, J.A. Doutt, E.E. Hays, M.S.
    Wengrovitz, and A.V. Oppenheim, "The Application to
    Experimental Data of a Technique for Measuring the
    Plane-Wave Reflection Coefficient of the Ocean
    Bottom", to be submitted to J. Acoust. Soc., Am.

4. G.V. Frisk, J. Doutt, and E. Hays, "Geoacoustic Models
    for the Icelandic Basin", J. Acoust. Soc. Am., 80,
    591-600 (1986).

5. G.V. Frisk, A.V. Oppenheim, and D. Martinez, "A
    Technique for Measuring the Plane-Wave Reflection
    Coefficient of the Ocean Bottom", J. Acoust. Soc.
    Am., 68, 602-612 (1980).

6A. G.V. Frisk, D.R. Mook, J.A. Doutt, E.E. Hays, and A.V.
    Oppenheim, "The Application to Real Data of a
    Technique for Measuring the Plane-Wave Reflection
    Coefficient of the Ocean Bottom", J. Acoust. Soc.
    Am., 72, (S1) S97(a) (1982).

6B. D.R. Mook, G.V. Frisk, and A.V. Oppenheim, "A Hybrid
    Numerical/Analytic Technique for the Computation of
    Wave Fields in Stratified Media Based on the Hankel
    Transform", J. Acoust. Soc. Am., 76, 222-243
    (1984).

7. D.C. Stickler, "Inverse Scattering in a Stratified
    Medium", J. Acoust. Soc. Am., 74, 994-1005 (1983).

8. G.J. Fryer, "Reflectivity of Ocean Bottom at Low
    Frequency", J. Acoust. Soc. Am., 63, 35-43 (1978)

9. P.J. Vidmar and T.L. Foreman, "A Plane Wave Reflection
    Loss Model Including Sediment Rigidity", J. Acost.
    Soc. Am., 66, 1830-1835 (1979).

10. G.J. Fryer, "Compressional-Shear Wave Coupling Induced
    by Velocity Gradients in Marine Sediments",
    J. Acoust. Soc. Am., 69, 647-659 (1981).

BIBLIOGRAPHY (Continued)

11. L.M. Brekhovskikh, Waves in Layered Media, (Academic, New York, 1960).

12. R.G. Newton, "Inversion of Reflection Data for Layered Media: a Review of Exact Methods", Geophys. J.R. Astr. Soc., 65, 191-215 (1981).

13. R. Newton, "Note on Inversion of Reflection Data for Layered Media", Geophys, J.R. Soc, 69, 571-572 (1982).

14. I.M. Gelfand and B.M. Levitan, "On the Determination of a Differential Equation from its Spectral Function", Amer. Math. Soc. Trans., Series 2, Vol. 1, 253-304 (1955).

15. Z.S. Agranovich and V.A. Marchenko, The Inverse Problem of Scattering Theory, (Gordon and Breach, New York, 1963).

16A. L.D. Faddeyev, "The Inverse Problem in the Quantrum Theory of Scattering", translated by B. Seckler, J. Math. Phys., 4, 72-104 (1963).

16B. L.D. Faddeyev, "Properties of the S Matrix of the One-Dimensional Schrödinger Equation", Am. Math. Soc. Trans., Series 2, 65, 139-166 (1964).

17. K. Chadan and P.C. Sabatier, Inverse Problems in Quantum Scattering Theory, (Springer, New York, 1977).

18. R. Burridge, "The Gelfand-Levitan, the Marchenko, and the Gopinath-Sondhi Integral Equations of Inverse Scattering Theory, Regarded in the Context of Inverse Impulse-Response Problems", Wave Motion, 2, 305-324 (1980)

19. I. Kay, "The Inverse Scattering Problem for Transmission Lines" in Mathematics of Profile Inversion, L. Colin, Editor, NASA TM X-62, 150, 6-2 to 6-17 (1972).

20. H.E. Moses and G.M. deRidder, Properties of Dielectrics from Reflection Coefficients in One Dimension, Lincoln Lab. Tech. Rep. 322 (1963).

BIBLIOGRAPHY (Continued)

21. J.A. Ware and K. Aki, "Continuous and Discrete Inverse
     Scattering Problems in a Stratified Elastic
     Medium", J. Acoust. Soc. Am., $\underline{45}$, 911-921 (1969).

22. J.F. Claerbout, Fundamentals of Geophysical Data
     Processing, (Mc Graw-Hill, New York, 1976).

23. A.K. Jordan and S. Ahn, "Inverse Scattering Theory and
     Profile Reconstruction", Proc. Inst. Elec. Eng.,
     $\underline{126}$, 945-950 (1979).

24. M.H. Reilly and A.K. Jordan, "The applicability of an
     Inverse Method for Reconstruction of Electron
     Density Profiles", IEEE Trans. Antennas
     Propagation, $\underline{29}$, 245-253 (1981).

25. A.K. Jordan and H.N. Kritikos, "An Application of One-
     Dimensional Inverse Scattering Theory for
     Inhomogeneous Regions", IEEE Trans. Antennas
     Propagation, $\underline{21}$, 909-911 (1973).

26A. J.G. Berryman and R.R. Greene, "Discrete Inverse Methods
     for Elastic Waves in Layered Media", Geophysics,
     $\underline{45}$, 213-234 (1980)

26B. J.G. Berryman and R.R. Greene, "Discrete Inverse
     Scattering Theory and the Continuum Limit", Phys.
     Letters, $\underline{65A}$, 13-15 (1978)

27. A. Jacobs and R.H. Stolt, "Seismic Inversion in a
     Layered Medium - The Gelfand-Levitan Algorithm",
     Stanford Explor. Project Rep., No. 24, 109-134
     (1980).

28. R. Carroll and F. Santosa, "On Complete Recovery of
     Geophysical Data, Math. Meth. Appl. Sci. (1982).

29. R. Carroll and F. Santosa, "Stability for the One
     Dimensional Inverse Problem via the Cel'fand-
     Levitan Equation", Appl. Analysis, $\underline{13}$, 271-277
     (1982).

30. F. Santosa, "Numerical Scheme for the Inversion of
     Acoustical Impedance Profile Based on the Gelfand-
     Levitan Method", Geophys. J.R. Astr. Soc., $\underline{70}$,
     229-243 (1982).

BIBLIOGRAPHY (Continued)

31. B. Gopinath and M.M. Sondhi, "Determination of the Shape
       of the Human Vocal Tract from Acoustical Measure-
       ments", Bell System Tech. J., 49, 1195-1214 (1970).

32. S. Coen, "Inverse Scattering of a Layered and
       Dispersionless Dielectric Half-Space, Part I:
       Reflection Data from Plane Waves at Normal
       Incidence", 29, 726-732 (1981).

33. S. Coen, "Density and Compressibility Profiles of a
       Layered Acoustic Medium from Precritical Incidence
       Data", Geophysics, 46, 1244-1246 (1981).

34. S. Coen, "Velocity and Density Profiles of a Layered
       Acoustic Medium from Common Source - Point Data",
       Geophysics, 47, 898-905 (1982).

35. D.H. Schaubert and R. Mittra, "A Special Domain Method
       for Remotely Probing Stratified Media", IEEE Trans.
       Antennas Propagat., 25, 261-265 (1977)

36. A. Roger, "Determination of the Index Profile of a
       Dielectric Plate from Scattering Data", Applied
       Inverse Problems, (Springer, New York, 1978).

37. P. Deift and E. Trubowitz, "Inverse Scattering on the
       Line", Comm. Pure Appl. Math., 23, 121-251 (1979).

38. A. Yagle and B. Levy, "The Schur Algorithm and its
       Applications, Tech. Report, Laboratory for
       Information and Decision Systems", MIT, Cambridge
       (1983).

39. A. Yagle and B. Levy, "Application of the Schur
       Algorithm to the Inverse Problem for a Layered
       Acoustic Medium", Tech. Report, Laboratory for
       Information and Decision Systems, MIT, Cambridge
       (1983).

40. A. Nilsen and B. Gjevik, "Inversion of Reflection Data",
       Geophys. Prosp., 26, 421-432 (1978).

41. H.E. Moses, "Calculation of the Scattering Potential
       from Reflection Coefficients", Phys. Rev., 102,
       559-567 (1956).

BIBLIOGRAPHY (Continued)

42. F. Santosa and W. Symes, "The Determination of a Layered
    Acoustic Medium Via Multiple Impedance Profile
    Inversions from Plane Wave Responses", Geophys.
    J.R. Soc., 81, 175-195 (1985).

43. F. Santosa and H. Schwetlick, "The Inversion of
    Acoustical Impedance Profile by Methods of
    Characteristics", Wave Motion, 4, 99-110 (1982).

44. D.P. Klemer and C.B. Sharpe, "An Integral Equation
    Associated with the Inverse Problem for Nonuniform
    Transmission Lines with Terminal Discontinuities",
    IEEE Trans. Antennas Propagation, 34, 546-553
    (1986).

45. J.K. Cohen and N. Bleistein, "An Inverse Method for
    Determining Small Variations in Propagation Speed",
    SIAM J. Appl. Math., 32, 784-799 (1977).

46. J.K. Cohen and N. Bleistein, "Velocity Inversion
    Procedure for Acoustic Waves", Geophysics, 44,
    1077-1085 (1979).

47. S.H. Gray, J.K. Cohen, and N. Bleistein, "Velocity
    Inversion in a Stratified Medium with Separated
    Source and Receiver", J. Acoust. Soc. Am., 68,
    24-240 (1980).

48. S. Raz, "Direct Reconstruction of Velocity and Density
    Profiles from Scattered Field Data", Geophysics,
    46, 832-836 (1981).

49. M. Razavy, "Determination of the Wave Velocity in an
    Inhomogenous Medium from the Reflection Coeffi-
    cient", J. Acoust. Soc. Am., 58, 956-963 (1975).

50. M.A. Hooshayar and M. Razavy, "A Method for Constructing
    Wave Velocity and Density Profiles from the Angular
    Dependence of the Reflection Coefficient,
    J. Acoust. Soc. Am., 73, 19-23 (1983).

51. A.B. Weglein and S.H. Gray, "The Sensitivity of Born
    Inversion to the Choice of Reference Velocity: A
    Simple Example", Geophysics, 48, 36-38, (1983).

52. S. Gray, "The Relationship Between 'Direct, Discrete'
    and 'Iterative, Continuous' One-Dimensional Inverse
    Methods", Geophysics, 49, 54-59 (1984).

BIBLIOGRAPHY (Continued)

53. J. Cohen and F. Hagin, "Velocity Inversion Using a Stratified Reference", Geophysics, 50, 1689-1700 (1985).

54. N. Bleistein and J. Cohen, "The Velocity Inversion Problem-Present Status, New Direction", Geophysics, 47, 1479-1511 (1982).

55. C. Rorres, J. Bai, P.C. Pedersen, and O.J. Tretiak, "Inverse Acoustic Scattering for One-Dimensional Lossy Media", J. Acoust. Soc. AM., 78, 1851-1858, (1985).

56. A. Gersztenkorn, J. Bednar, and L. Lines, "Robust Iterative Inversion for the One-Dimensional Acoustic Wave Equation, Geophysics, 51, 357-368 (1986).

57. S.M. Candel, F. Defillippi, and A. Lannay, "Determination of the Inhomogenous Structure of a Medium from its Plane Wave Reflection Response, Part II: A Numerical Approximation", J. Sound Vib, 68, 583-595 (1980).

58. J.A. Kong Theory of Electromagnetic Waves, (John Wiley, New York, 1975).

59. V. Bargmann, "On the Number of Bound States in a Central Field of Force", Proc. Nat. Acad. Sci. USA, 38, 961-966 (1952).

60. E.L. Hamilton, "Geoacoustic Modeling of the Sea Floor", J. Acoust. Soc. Am., 68 1313-1339 (1980).

61. S.G. Mikhlin, Integral Equations (Pergamon Press, New York, 1957).

62. H.N. Kritikos, D.L. Jaggard, and D.B. Ge, "Numerical Reconstruction of Smooth Dielectric Profiles", Proc. IEEE, 70, 295-297 (1982).

63. D.B. Ge, D.L. Jaggard, and H.N. Kritikos, "Perturbational and High Frequency Profile Inversion", IEEE Trans. Antennas Propagation, 31, 804-808 (1983).

BIBLIOGRAPHY (Continued)

64. D.R. Mook, "The Numerical Synthesis and Inversion of Acoustic Fields Using the Hankel Transform with Application to the Estimation of the Plan Wave Reflection Coefficient of the Ocean Bottom", Sc.D. Thesis MIT/WHOI Joint Program, Cambridge, MA, and Woods Hole, MA (1983).

65. M. Abramowitz and I.A. Stegun, Handbook of Mathematical Functions, (NBS, Washington, DC, 1970).

66. A.V. Oppenheim and R.W. Schafer, Digital Signal Processing (Prentice Hall, Englewood Cliffs, 1975).

67A. S.D. Rajan and G.V. Frisk, "An Inverse Method for Obtaining the Attenuation Profile and Small Variations in the Sound Speed and Density Profiles of the Ocean Bottom", in Proceedings of the I.C.A.Congress, Symposium on Underwater Acoustics (Halifax, Nova Scotia, Canada, 16-18 July 1986).

67B. S.D. Rajan and G.V. Frisk, "An Inverse Method for Obtaining the Attenuation Profile and Small Variations in the Sound Speed and Density Profiles of the Ocean Bottom", to be submitted to J. Acoust. Soc. Am.

68. S.D. Rajan, "An Inverse Method for Obtaining the Attenuation Profile and Small Variations in the Sound Speed and Density Profiles of the Ocean Bottom", Ph.D. Thesis, MIT/WHOI Joint Program, Cambridge, MA, and Woods Hole, MA (1983).

69. M. Jaulent, "Inverse Scattering Problems in Absorbing Media", J. Math. Phys., 17, 1351-1360 (1976).

70. A. Bruckstein, B. Levy, and T. Kailath, "Differential Methods in Inverse Scatter", SIAM J. Appl. Math. (1984).

71. K.P. Bube and R. Burridge, "The One-Dimensional Inverse Problem of Reflection Seismology", SIAM Review, 25, 497-559 (1983).

72. P.C. Sabatier, "Theoretical Considerations for Inverse Scattering, Radio Science, 18, 1-18 (1983).

BIBLIOGRAPHY (Concluded)

73. D.C. Stickler, "Application of the Trace Method for
     Inverse Scattering to a Medium Which Supports
     N-Wave Types", unpublished report.

74. W. Symes, "Stable Solution of the Inverse Reflection
     Problem for a Smoothly Stratified Elastic Medium,
     SIAM J. Math. Anal., 12, 421-453 (1980).

75. A.B. Weglein, "The Inverse Scattering Concept and its
     Seismic Application", in Fitch, A.A., Ed.,
     Developments in Geophysical Methods, 6 (Elsevier
     Science, 1985).

76. R.H. Stolt and A.B. Weglein, "Migration and Inversion of
     Seismic Data", Geophysics, 50, 2458-2472 (1985).

50272-101

REPORT DOCUMENTATION PAGE	1. REPORT NO. WHOI-88-12	2.	3. Recipient's Accession No.

4. Title and Subtitle

Exact Reconstruction of Ocean Bottom Velocity Profiles from Monochromatic Scattering Data

5. Report Date
January 1987

6.

7. Author(s)
Andre A. Merab

8. Performing Organization Rept. No.
WHOI-88-12

9. Performing Organization Name and Address
The Woods Hole Oceanographic Institution
Woods Hole, Massachusetts 02543
and
The Massachusetts Institute of Technology
Cambridge, Massachusetts 02139

10. Project/Task/Work Unit No.

11. Contract(C) or Grant(G) No.
(C)
(G) N00014-82-C-0152

12. Sponsoring Organization Name and Address
The Office of Naval Research
Environmental Sciences Directorate
Arlington, Virginia 22217

13. Type of Report & Period Covered
Sc.D. Thesis

14.

15. Supplementary Notes

This thesis should be cited as: Andre A. Merab, 1988. Exact Reconstruction of Ocean Bottom Velocity Profiles from Monochromatic Scattering Data. MIT/WHOI, WHOI-88-12.

16. Abstract (Limit: 200 words)

This thesis presents the theoretical and computational underpinnings of a novel approach to the determination of the acoustic parameters of the ocean bottom using a monochromatic source. The problem is converted to that of the direct reconstruction of the potential in a Schrodinger equation from the plane-wave reflection coefficient given for all real and imaginary angles of incidence. The problem is solved by extending the Gelfand-Levitan algorithm of inverse scattering theory to the case where basement velocity is higher than water velocity. The reflection coefficient is shown to be integrable, and the neglect of bound states is justified.

The numerical solution of the inverse problem is obtained via three methods: an improved Born approximation, and two finite difference methods based on an efficient solution of the discretized Gelfand-Levitan integral equation. These methods are tested on synthetic data obtained from known geoacoustic models of the ocean bottom. Reconstructions can be very accurate with resolution of less than the water wavelength of the acoustic source. The effects of sampling, finite range of incident angles, density variation, attenuation, and noise are investigated.

17. Document Analysis   a. Descriptors

1. Inverse scattering
2. Bottom acoustics
3. Gelfand-Levitan method

b. Identifiers/Open-Ended Terms

c. COSATI Field/Group

18. Availability Statement	19. Security Class (This Report) UNCLASSIFIED	21. No. of Pages 200
Approved for publication; distribution unlimited.	20. Security Class (This Page)	22. Price

(See ANSI-Z39.18) · *See Instructions on Reverse*

OPTIONAL FORM 272 (4-77)
(Formerly NTIS-35)
Department of Commerce